

NATIONAL BUREAU OF STANDARDS REPORT

9601

Preliminary Report on the Thermodynamic Properties of Selected Light-Element and Some Related Compounds

(The previous reports in this series have the NBS Report Nos. 6297, 6484, 6645, 6928, 7093, 7192, 7437, 7587, 7796, 8033, 8186, 8504, 8628, 8919, 9028, 9389, and 9500.)

1 July 1967



U.S. DEPARTMENT OF COMMERCE
NATIONAL BUREAU OF STANDARDS

This document is subject to special export controls and each transmittal to foreign governments or to foreign nationals may be made only with prior approval of the AFOSR (SRGL).

Qualified requestors may obtain additional copies from the Defense Documentation Center.

THE NATIONAL BUREAU OF STANDARDS

The National Bureau of Standards¹ provides measurement and technical information services essential to the efficiency and effectiveness of the work of the Nation's scientists and engineers. The Bureau serves also as a focal point in the Federal Government for assuring maximum application of the physical and engineering sciences to the advancement of technology in industry and commerce. To accomplish this mission, the Bureau is organized into three institutes covering broad program areas of research and services:

THE INSTITUTE FOR BASIC STANDARDS . . . provides the central basis within the United States for a complete and uniform system of physical measurements, coordinates that system with the measurement systems of other nations, and furnishes essential services leading to accurate and uniform physical measurements throughout the Nation's scientific community, industry, and commerce. This Institute comprises a series of divisions, each serving a classical subject matter area:
—Applied Mathematics—Electricity—Metrology—Mechanics—Heat—Atomic Physics—Physical Chemistry—Radiation Physics—Laboratory Astrophysics²—Radio Standards Laboratory,² which includes Radio Standards Physics and Radio Standards Engineering—Office of Standard Reference Data.

THE INSTITUTE FOR MATERIALS RESEARCH . . . conducts materials research and provides associated materials services, including mainly reference materials and data on the properties of materials. Beyond its direct service to the Nation's scientists and engineers, this Institute yields services which are essential to the advancement of technology in industry and commerce. This Institute is organized primarily by technical fields:
—Analytical Chemistry—Metallurgy—Reactor Radiations—Polymers—Inorganic Materials—Cryogenics²—Office of Standard Reference Materials.

THE INSTITUTE FOR APPLIED TECHNOLOGY . . . provides technical services to promote the use of available technology and facilitate technological innovation in industry and government. The principal elements of this Institute are:
—Building Research—Electronic Instrumentation—Technical Analysis—Center for Computer Sciences and Technology—Textile and Apparel Technology Center—Office of Weights and Measures—Office of Engineering Standards Services—Office of Invention and Innovation—Office of Vehicle Systems Research—Clearinghouse for Federal Scientific and Technical Information³—Materials Evaluation Laboratory—NBS/GSA Testing Laboratory.

¹ Headquarters and Laboratories at Gaithersburg, Maryland, unless otherwise noted; mailing address Washington, D. C., 20234.

² Located at Boulder, Colorado, 80302.

³ Located at 5285 Port Royal Road, Springfield, Virginia 22151.

NATIONAL BUREAU OF STANDARDS REPORT

NBS PROJECT

221-0404
221-0405
221-0426
222-0423
223-0442
223-0513
313-0430

NBS REPORT

9601

1 July 1967

Preliminary Report on the Thermodynamic Properties of Selected Light-Element and Some Related Compounds

(The previous reports in this series have the NBS Report Nos. 6297, 6484, 6645, 6928, 7093, 7192, 7437, 7587, 7796, 8033, 8186, 8504, 8628, 8919, 9028, 9389, and 9500.)

Technical Summary Report
on the Thermodynamic Properties
of Light-Element Compounds

Reference: U.S. Air Force Order No. ISSA 67-6

IMPORTANT NOTICE

NATIONAL BUREAU OF STANDARDS
for use within the Government. Before
and review. For this reason, the report
whole or in part, is not authorized for
Bureau of Standards, Washington, D.C.
the Report has been specifically prepared

Approved for public release by the
director of the National Institute of
Standards and Technology (NIST)
on October 9, 2015

accounting documents intended
subjected to additional evaluation
issuing of this Report, either in
Office of the Director, National
the Government agency for which
copies for its own use.



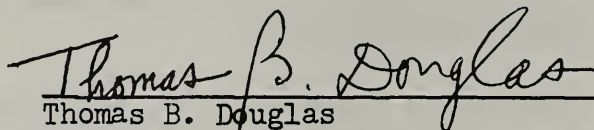
U.S. DEPARTMENT OF COMMERCE
NATIONAL BUREAU OF STANDARDS

ABSTRACT

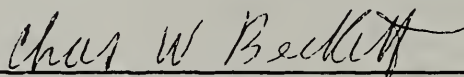
Thermodynamic and related properties of substances important in current high-temperature research and development activities are being investigated under contract with the U. S. Air Force Office of Scientific Research (USAF Order No. ISSA 67-6) and the Advanced Research Projects Agency (ARPA Order No. 20). This research program is a direct contribution to the Interagency Chemical Rocket Propulsion Group (Working Group on Thermochemistry) and, simultaneously, to other organizations oriented toward acquiring the basic information needed to solve not only the technical problems in propulsion but also those associated with ballistics, reentry, and high-strength high-temperature materials. For given substances this needed basic information comprises an ensemble of closely related properties being determined by an extensive array of techniques. Some of these techniques, by relating thermodynamic properties to molecular or crystal structure, make it possible to tabulate these properties over far wider ranges of temperature and pressure than those actually employed in the basic investigations.

This report presents a number of new thermodynamic properties resulting from recent NBS experimental studies and their interpretation, as well as descriptions of improved measuring techniques in two areas. Earlier NBS enthalpy measurements on the compound $\text{BeO} \cdot \text{Al}_2\text{O}_3$ (0° - 1200°K) are extended up to 2400°K , leading to the heat of fusion and the common thermodynamic properties well into the liquid range. The infrared matrix spectra of lithium fluoride and an alkali hydroxide (CsOH), with isotopic variations, have been obtained and interpreted, yielding the vibrational frequencies. Lithium fluoride is found as a previously unreported linear dimer (Li_2F_2), and the results for CsOH are consistent with and complement the earlier NBS microwave results for this molecule. Some preliminary mass-spectrometric data on beryllium dichloride are given. These data yield thermodynamic values for the reactions involving $\text{BeCl}_2(\text{c})$, $\text{BeCl}_2(\text{g})$, and $(\text{BeCl}_2)_2(\text{g})$. Thermodynamic values for the reactions involving $\text{AlF}_3(\text{c})$, $\text{AlF}_3(\text{g})$, and $(\text{AlF}_3)_2(\text{g})$, derived earlier using precise NBS entrainment data, are revised in the light of new published information. The volatility of AlF_3 is found to be markedly

enhanced by the presence of AlCl_3 . After reasonable accounting for dimer formation, the data indicate the hitherto unobserved species AlF_2Cl and AlFCl_2 to be formed in the gas phase and each with a very small heat effect ($+1.0 \pm 0.5$ kcal per mol). Studies on the automation of temperature measurements complement previous studies on the automation of electrical-energy measurements--all designed to make low-temperature heat-capacity calorimetry fully automatic. The development of two refinements in oscilloscopic recording improve by at least tenfold the previous high-speed-measurement accuracy for determining specific heats and other properties at very high temperatures.



Thomas B. Douglas
Project Leader



Charles W. Beckett
Assistant Division Chief for Thermodynamics
Heat Division, Institute for Basic Standards

TABLE OF CONTENTS

	<u>Page</u>
Abstract	i
Chap. 1. <u>STUDIES ON THE AUTOMATION OF LOW-TEMPERATURE</u> <u>HEAT CAPACITY CALORIMETRY. II. AUTOMATION</u> <u>OF TEMPERATURE MEASUREMENTS</u>	
(by George T. Furukawa and Martin L. Reilly)	1
I. Introduction	1
II. General Specifications of the Automatic Bridge	1
II.1. Symbols, Abbreviations, and Definitions	2
II.2. Bridge Rate	8
Table 1. Bridge Rates	8
Fig. 1. Critical Rates of the Thermometer Resistance for Upshift and Downshift as Set by the Repeat and Reversal Counts for Shift	10
II.3. Bridge Logic	11
Fig. 2. Bridge Point Patterns when Tracking Thermometer Resistance.	12
II.4. Bridge Circuitry and Switch Arrangement	13
Fig. 3. Bridge Circuitry and Switch Arrangement of the Automatic Mueller Bridge	14
Fig. 4. Equations Associated with the Mueller Bridge for Determining the Thermometer Resistance	15
Table 2. Definitions of Symbols Used in Figure 4	16

TABLE OF CONTENTS (Continued)

	<u>Page</u>
II.5. Bridge Readout	17
Fig. 5. A listing from punched cards of bridge readouts of a typical experiment to determine the "final" and "initial" temperatures associated with electrical energies introduced into a calorimeter	18
III. Temperatures from Bridge Readout	19
Figs. 6a-6i. Bridge Points after Completion of Every Bridge Cycle in a Typical Heat-Capacity Experiment. (Cont'd.)	20
Fig. 7. Calculation of Point Pairs from the Data Listed in Figure 5. Computer Output of the Calculations	29
Fig. 8. Computer Plot of Point Pairs Calculated from Data Listed in Figures 5 and 6. The Results of Calculation of the Initial and Final Temperatures from the Point Pairs	30
IV. Conclusion	31
V. References	31
Chap. 2. <u>IMPROVEMENTS IN OSCILLOSCOPIC MEASUREMENTS</u> <u>OF VARIABLES IN DYNAMIC EXPERIMENTS</u> (by A. Cezairliyan, H. A. Berman, and M. S. Morse).	
Abstract	32
1. Introduction	32
2. Description of the System	33
a. Differential Suppression	33
b. Time Synchronization	34
Fig. 1 Circuit Diagram of Differential Suppression Unit	35

TABLE OF CONTENTS (Continued)

	<u>Page</u>
3. Experimental Arrangement and Operation . . .	36
Fig. 2. Functional Diagram of Improved Oscilloscopic Measurement System . . .	37
Fig. 3. Oscillogram Reproductions of Typical Rectangular and Trapezoidal Pulses . . .	39
Fig. 4. Time Sequence of Major Events in Oscilloscopic Measurement	40
Fig. 5. Schematic Drawing of Trapezoidal Pulse and Baseline	42
4. Oscillogram Measurements and Calculations . .	44
5. Results and Discussion	47
Table 1. Results of Dynamic Resistance Measurements . .	49
Fig. 6. Variation of Resistance Difference and Standard Deviation of an Individual Determination of Resistance as a Function of Percentage of Signal Recorded on Oscilloscope . .	50
6. Conclusions	52
Table 2. List of Major Sources of Error in Oscilloscopic Measurement of a Variable Using Suppression	53
Acknowledgement	54
Chap. 3.. <u>THE ENTHALPY OF SOLID AND LIQUID $\text{BeO} \cdot \text{Al}_2\text{O}_3$</u> <u>FROM 1200 TO 2400°K</u>	
(by S. Ishihara and E. D. West)	55
Introduction	55
Apparatus	55
Experimental Procedure	56
Samples and Containers	57
Results	59
Discussion	61
References	62
Table 1. Enthalpy Measurements of Solid, Premelting, and Liquid $\text{BeO} \cdot \text{Al}_2\text{O}_3$	64

TABLE OF CONTENTS (Continued)

	<u>Page</u>
Chap. 4. <u>THE INFRARED SPECTRUM OF MATRIX ISOLATED</u> <u>CsOH AND CsOD</u> (by N. Acquista, S. Abramowitz, and D. R. Lide) .	66
Abstract	66
Introduction	66
Experimental	67
Experimental Results and Discussion	67
Conclusions	69
References	69
Table 1. Identification and Classification of the CsOH and CsOD fundamental frequencies	70
Fig. 1. The spectrum of matrix isolated CsOH observed from samples effusing at two temperatures .	71
Fig. 2. The spectrum of matrix isolated CsOH and CsOD	72
Fig. 3. The spectrum of matrix isolated CsOD	73
Chap. 5. <u>INFRARED MATRIX SPECTRA OF LITHIUM FLUORIDE</u> (by Stanley Abramowitz, Nicolo Acquista, and Ira W. Levin)	74
Abstract	74
Introduction	74
Experimental	75
Experimental Results and Discussion	75
400-150 cm^{-1} Region	75
900-400 cm^{-1} Region	77
Normal Coordinate Analysis	78
References	81
Table I. Internal coordinates and force constant matrix for the linear Li_2F_2 dimer	82
Table II. Summary of force constants for the linear dimer models of Li_2F_2	83

TABLE OF CONTENTS (Continued)

Page

Table III.	Comparison between the observed and calculated frequencies, in cm^{-1} , for the Σ^+ symmetry species of the linear Li_2F_2 dimer	84
Table IV.	Comparison between the observed and calculated frequencies, in cm^{-1} , for the Π symmetry species of three models for the Li_2F_2 linear dimer	85
Table V.	Comparison between the observed and calculated frequencies, in cm^{-1} , for the bifluoride structure of the Li_2F_2 linear dimer	86
Figs. 1a-1e.	Infrared spectra of matrix isolated ^7LiF , ^6LiF , and a 1:1 mixture of $^6\text{LiF}/^7\text{LiF}$ in various wavenumber regions.	87
Fig. 1a.	240-300 cm^{-1} region	87
Fig. 1b.	150 cm^{-1} region	88
Fig. 1c.	767 cm^{-1} region	89
Fig. 1d.	720 cm^{-1} region	90
Fig. 1e.	490-525 cm^{-1} region	91
Fig. 2.	Monomeric ^7LiF in Ar at various temperatures	92
Chap. 6.	<u>MASS SPECTROMETRIC STUDY OF BeCl_2 VAPORIZATION</u> (by J. Efimenko)	93
Introduction	93
Experimental	93
Data and Results	94
Discussion	95
Table 1.	Data: Ion Intensities of BeCl_2 , Be_2Cl_3 , $(\text{BeCl}_2)_2$	98
Table 2.	BeCl_2 Isotope Intensities, BeCl_2 , Be_2Cl_3 , $(\text{BeCl}_2)_2$	99

TABLE OF CONTENTS (Continued)

	<u>Page</u>
Table 3. Second Law Sublimation Enthalpies for $\text{BeCl}_2(\text{g})$	100
Fig. 1. $\log I_{79}^+T$ vs $1/T$ plot for the data of $\text{BeCl}_2(\text{s}) = \text{BeCl}_2(\text{g})$, $\Delta H_{513}^{\circ} = 37.8$ kcal/mol .	101
Fig. 2. $\log I_{158}^+T$ vs $1/T$ plot for the data of $2\text{BeCl}_2(\text{s}) = (\text{BeCl}_2)_2(\text{g})$, $\Delta H_{513}^{\circ} = 44.5$ kcal/mol .	102
Fig. 3. $\log A_+$ vs $1/T$ plot for the data of $2\text{BeCl}_2(\text{g}) = (\text{BeCl}_2)_2(\text{g})$, $\Delta H_{513}^{\circ} = -30.7$ kcal/mol .	103
References	104
Chap. 7. <u>REVISION OF CHAPTER 4 OF NBS REPORT 9500, "THE VAPOR PRESSURE, VAPOR DIMERIZATION, AND HEAT OF SUBLIMATION OF ALUMINUM FLUORIDE, USING THE ENTRAINMENT METHOD"</u>	
(by Ralph F. Krause Jr. and Thomas B. Douglas) .	105
Table I. Thermodynamic Values for Reactions 1 and 2.	108
Fig. 1. Hypothetical values of (a) $\Delta H^{\circ}(1)$ and (b) $\Delta G^{\circ}(2)$ calculated from P and dP/dT of this work and selected values of $\Delta S^{\circ}(1)$ and $2\Delta H^{\circ}(1) + \Delta H^{\circ}(2)$	109
Chap. 8. <u>HEATS OF FORMATION OF GASEOUS MIXED-HALIDE MONOMERS BY THE CONCURRENT ENTRAINMENT OF AlCl_3 AND AlF_3</u>	
(by Ralph F. Krause Jr. and Thomas B. Douglas) .	110
Abstract	110
Introduction	111
Concurrent Entrainment	113

TABLE OF CONTENTS (Continued)

	<u>Page</u>
Table 1. Concurrent entrainment of $AlCl_3$ and AlF_3 . . .	116
Preliminary Assumption	117
Table 2. Preliminary least square determination of $\Delta H^0(n)$ of eq 1 at 1225°K by assuming eqs 7 and 8 without correction for dimerization and $\Delta H^0(2) = \Delta H^0(1)$ of eq 1	119
Dimerization Correction	120
Table 3. Possible dimers in the $AlCl_3$ - AlF_3 system . . .	122
Derived Values	124
Table 4. Effect of various assumptions on a least square determination of $\Delta H^0(n)$ of eq 1 at 1225°K by assuming eqs 15 and 16 and the published values for the dimerization of $AlCl_3$ and AlF_3 . . .	125
Acknowledgements	127
Table 5. Least square determination of $\Delta H^0(n)$ of eq 1 at 1225°K by assuming eqs 15 and 16, the published values for the dimerization of $AlCl_3$ and AlF_3 , $b=1/2$, and $\Delta H^0(2) = \Delta H^0(1)$ of eq 1	128

Chapter 1

STUDIES ON THE AUTOMATION OF LOW-TEMPERATURE HEAT-CAPACITY CALORIMETRY. II. AUTOMATION OF TEMPERATURE MEASUREMENTS

George T. Furukawa and Martin L. Reilly

I. Introduction

In the National Bureau of Standards Report No. 9500 [1]^{*} under the same chapter title as above, studies on automatic electrical-energy measurements in high-precision heat-capacity calorimetry were discussed. A proposed method for the measurements and for automatic control of the complete calorimetric process was outlined. Only a reference was made to the existing automatic temperature measurement and recording system that had been developed prior to the studies on the electrical energy measurements. In this report, the principles of operation and the results that can be obtained with our automatic temperature measurement system will be described.

The complete automatic temperature measurement system that is used includes the platinum-resistance thermometer [2], automatic bridge for measuring the resistance of the thermometer, and card-punch equipment for recording the switch positions of the bridge and other pertinent data. The data on punched cards are analyzed by means of high speed computer techniques. Since platinum resistance thermometers and card-punch machines are standard commercial equipment and the information on them are readily available, no further description will be made of them. The discussion to follow will center largely on the automatic bridge and the results of computer reduction of the data that can be recorded with the bridge.

II. General Specifications of the Automatic Bridge

The automatic bridge was developed and constructed for us according to the performance specifications needed to meet the requirements of an automatic temperature measurement system. The precision and accuracy were to be comparable to the best manual equipment used for temperature measurements in calorimetry. The development of the automatic bridge was a part of our program to automate low-temperature heat-capacity measurements.

* Numbers in brackets indicate the references given at the end of this chapter.

The development of the bridge was considered the most important "link" in our automation program. This is well exemplified in the previous report [1] by the discussion on the application of time-temperature measurements to calorimetry. The bridge has now been tested and used for about two years. Some relatively minor modifications have been incorporated during this interval in the mechanical features and the bridge logic. The results obtained with the automatic bridge have been found to be as reliable as those with the best manual bridge. The ability of the bridge to make continuous and prolonged measurements has been useful in re-examining the design of the calorimetric equipment now in use. The heat capacity measurements that have previously been reported on Al_4C_3 , $BeO \cdot Al_2O_3$, $BeO \cdot 3Al_2O_3$, and Be_3N_2 were made using the automatic bridge.

The bridge description to follow is in part a condensation of the reports submitted to us by the contractor that developed the bridge. The arrangement of their reports has been changed to blend with the description of the results obtained by us.

II.1 Symbols, Abbreviations, and Definitions

The symbols, terminology, and abbreviations used in this report are defined in this section. The descriptions of some of the operating logic of the bridge are also given here. Some of the definitions of symbols or terms used in equations or in figures are given immediately following the equation or the reference to the figure, or incorporated in the figure.

rate = the change in resistance with respect to time of the thermometer or of the bridge. The resistance changes made with the automatic bridge are incremental.

BR = the bridge rate, $\Delta R_i / \tau_i$, where ΔR_i is the resistance increment (step size) corresponding to the BR_i . Similarly, τ_i is the period of a bridge cycle, the time interval between each resistance step, corresponding to the BR_i . The automatic bridge has at present 11 different BR's identified by numbers 1 through 11, BR No. 1 being the highest bridge rate and No. 11 the lowest. The bridge rate may be defined also by: $BR_i = \Delta R_i \times BC_i$, where BC_i = the number of bridge cycles per second or the number of resistance steps per second, corresponding to the BR_i . A multiple contact stepping switch controls the automatic selection of the bridge rate and the corresponding bridge logic and periods of the bridge cycles.

step = the change by a resistance increment effected by changing switch positions. (See Figure 3.) A down step (decrease in bridge resistance) is made when the detector output is minus (-) and up step (increase in resistance) is made when the output is plus (+). The step size in certain bridge rates can be 1x, 2x, or 5x the "decade" being stepped. When a particular switch position is "zero" and when the detector output is minus, a "carry" circuitry causes the down step resistance increment to occur in the prevailing decade (i.e., $0-1 = 9$, $0-2 = 8$, or $0-5 = 5$) and a down step by one unit in the next higher decade. Similar carry action occurs whenever the switch for the decade is down stepped through zero; e.g., $1-2 = 9$, $4-5 = 9$, etc. In an up step decision, the corresponding carry action occurs whenever the switch for the decade is up stepped to or through zero (i.e., $9+1 = 0$, $9+2 = 1$, $8+5 = 3$, etc.).

bridge cycle = the time interval between the completion of the resistance steps. A bridge cycle includes the following logical operations:

1. Apply voltage to the bridge and allow the detector enough time to sense the unbalance. The detector time is increased with the decrease in the bridge rate in order to make accurate decisions on the decreasing unbalance signals that are associated with the decreasing bridge rates. (See section II.2.)
2. Sample and store the sense of the detector output and remove the voltage from the bridge.
3. Apply the sense of the detector unbalance to the various logic elements to make a decision on the bridge rate, readout or clear buffer, and thermometer connection.
4. Make resistance step in accordance with the sense of the detector unbalance.

repeat = the unbalance detector output in the same sense as that of the preceding bridge cycle. The count of successive repeats is stored for logic operations. Any subsequent reversal resets the repeat count to zero. The count of repeats is also reset to zero after a reverse thermometer connection or a shift in the bridge rate is made.

reversal = the unbalance detector output in the opposite sense from that of the preceding bridge cycle. The count of successive reversals are stored for logic operations. A single subsequent repeat resets the reversal count to zero only if even numbers of successive reversals occurred just previous following the last repeat. (The reason for this is discussed in section II.3 on bridge logic.) If the first repeat does not reset the reversal count to zero, the next repeat (consecutive) will reset the count to zero. The count of reversals is also reset to zero after a shift of the bridge rate.

upshift = the change from a given bridge rate to the next higher bridge rate. The upshift logic is controlled by the count of successive repeats of the detector decisions and the repeat count for upshift preset on the bridge controls. Whenever the upshift logic condition is met by the count of repeats, the resistance step for the bridge cycle is made in accordance with the sense of the detector output after the upshift.

downshift = the change from a given bridge rate to the next lower bridge rate. The downshift logic is controlled by the count of successive reversals of the detector decisions and the reversal count for downshift preset on the bridge controls. (See the definition of reversals for the special case of counting the number of successive reversals. See also the definition for reverse connection of the thermometer for the effect of the downshift logic condition when the thermometer is in the normal and in the reverse connections.) Whenever the downshift logic condition is met by the count of reversals, the resistance step for the bridge cycle is made in accordance with the sense of the detector output after the downshift.

repeat count for upshift:

preset count placed on the bridge controls. When the count of successive repeats reaches this count, the bridge rate is upshifted to the next higher bridge rate.

reversal count for downshift:

preset count placed on the bridge controls. The downshift logic condition is met when the count of successive reversals reaches this number.

balancing resistors =

the resistors switched to achieve an effective bridge resistance equal to the thermometer resistance. The resistance values that can be switched are:

0 to 9×10^{-5} , 0 to 9×10^{-4} , 0 to 9×10^{-3} , 0 to 9×10^{-2} ,
0 to 9×10^{-1} , 0 to 9×10^0 , 0 to 9×10^1 , and 0 to 4×10^2
ohms. In the lower decades step sizes of 2x and 5x the decade units are also made.

compensating resistors =

the resistors switched to equalize the thermometer lead resistances. These resistors are switched only during the reverse thermometer connection. (See the section on bridge circuitry and switch arrangement for the discussion on how the thermometer lead resistances are made equal.) By equalizing the thermometer lead resistances, the readings obtained with the normal and reverse connections of the resistance thermometer are made the same. The resistance values that can be switched are:

0 to 9×10^{-5} , 0 to 9×10^{-4} , 0 to 9×10^{-3} and 0 to 9×10^{-2} .

These resistors are of equal high quality as those of the corresponding balancing resistors.

normal connection =

the resistance thermometer, one of its leads, and the compensating resistance elements are connected in series in the so-called unknown arm of the bridge. The other lead is in series with the balancing resistance elements. The compensating resistors are not switched in this connection. (See Figure 3.) Normal connection is designated by the subscript N.

reverse connection =

the compensating resistance elements and the thermometer lead that was connected to the unknown arm of the bridge while in the normal connection are now connected in series with the balancing resistance elements. The lead that was connected in series with the balancing resistance elements while in the normal connection is now connected in series with the resistance thermometer in the unknown arm of the bridge. (See Figure 3.) The compensating resistors are now stepped in the same sense and bridge rate as the balancing resistors. In the reverse connection, the bridge rate is, therefore, effectively twice that of the corresponding normal connection. The process of switching

from the normal to reverse thermometer connection is referred to as thermometer reversal. This is to be distinguished from the reversal of the sense of the detector output or that of the resistance step. The reverse connection is made only when the bridge balance has progressed to the 0.01 ohm steps and smaller. When the bridge is in normal connection and the bridge rate corresponding to 0.01 ohms and smaller are being stepped, the downshift logic condition causes the bridge to be first switched to the reverse connection in the same bridge rate number. When the downshift logic condition is met in the reverse connection, downshift is made to the next lower bridge rate and the normal bridge connection is made. When the bridge is in the lowest rate (rate No. 11) with the thermometer in reverse connection, the downshift logic condition will cause the normal connection in rate No. 11 to be made. Reverse connection is designated by the subscript R.

bridge quantities =

those quantities associated with the bridge that are necessary to record to make an intelligent analysis of the bridge actions and of the magnitude of the thermometer resistances. The quantities that may vary from one bridge cycle to the next are:

- a. balancing resistors
- b. compensating resistors
- c. thermometer connection (normal or reverse)
- d. counts of repeats and reversals
- e. bridge rate
- f. upshift or downshift
- g. detector output (+ or -)
- h. running clock time

Those quantities that are settable for the control of the bridge or for identification are:

- a. repeat count for upshift
- b. reverse count for downshift
- c. readout criteria
- d. thermometer current
- e. bridge zero
- f. date
- g. experiment number

bridge readout criteria =

bridge conditions or quantities that are variable from one bridge cycle to the next that are used to control the time of readout of the various bridge quantities. The criteria that can be selected are:

- a. whenever the repeat count for upshift is met.
- b. whenever the reversal count for downshift is met.
- c. whenever the "downshift" condition for thermometer reversal is met. (See reverse connection.)
- d. whenever the count of reversals of 2,3,5,7, or 9 is reached.

The logic test for the above readout criteria is made immediately after the detector decision. (See bridge cycle.) Except for the sense of the detector output and the bridge rate number, the quantities that are transferred to the buffer are, therefore, the prevailing quantities. Any combination of the above readout criteria can be set on the bridge controls.

bridge point =

bridge resistance expressed by the relative switch location corresponding to a bridge rate. A series of bridge points are required to determine the resistance of a thermometer.

point pair= average of the best values of thermometer resistances at a particular time in the reverse connection and in the following normal connection in the next lower bridge rate. The values of the compensating resistors are the same for this pair. Five or more bridge points are deduced from the bridge readings to establish the best value of the thermometer resistance in the reverse and in the normal connections. The point pair is the average of these two values at the mid-time of the values. (See section II.3 on bridge logic.)

When the reversal count for downshift is met in the reverse connection in the lowest bridge rate (rate No. 11), the normal connection in rate No. 11 follows. (See definition for reverse connection.) The most significant and useful bridge readings are obtained when the reversal counts for thermometer reversal and downshift are met. Readout criteria for these logic conditions have, therefore, been used in our heat-capacity measurements. The value of five for the reversal count for downshift has also been found most suitable from experience.

II.2. Bridge Rate

As discussed in the introduction of the previous report [1], the heat capacity is determined from the observations of a series of temperatures and known electrical-energy input. Perfect thermal isolation is not achieved even in the best calorimeter design. The heat leak is determined from the observed temperature drifts (temperature observations as a function of time) of the calorimeter. The temperature change corresponding to the electrical energy introduced is determined by extrapolating the steady-state temperature drift observations obtained during the periods before and after heating to the mid-time of the heating interval. The temperature change determined by this process contains the corrections for the heat leak.

The bridge must be designed to track the thermometer resistance as closely as possible within the ability of the detector to sense the unbalance between the bridge and the thermometer resistances and within the electro-mechanical limitations of the various components used. With every thermometer-resistance rate there is an optimum bridge tracking rate. It is not possible to track all rates of the resistance thermometer to within the smallest step size of the bridge. Also a continuous range of bridge rates to fit the possible resistance-thermometer rates that may be encountered is not practical. The following eleven sizes of resistance steps and the corresponding periods of the bridge cycles associated with the steps have been selected for the present. (See definition of bridge cycle.)

Table 1. Bridge Rates

Bridge Rate No.	Size of Resistance Steps ohms	Period of Bridge Cycle secs.
1	100	0.333
2	10	0.333
3	1.0	0.333
4	0.1	0.333
5	0.01	0.333
6	0.002	0.733
7	0.0005	1.133
8	0.0001	1.133
9	0.00005	2.033
10	0.00002	2.833
11	0.00001	3.633

Each bridge rate can track, within the resistance step, the thermometer resistance changing between certain limits. These limits (critical rates) are defined by the repeat count for upshift and the reversal count for downshift preset in the bridge controls.

In Figure 1 are shown for illustration the thermometer resistances by the thin lines and the maximum bridge rate (successive repeats) by the bold lines. The bridge resistance points are indicated by the various symbols shown. The critical rate for upshift of a drifting thermometer resistance may be analyzed by reference to Figure 1 as follows. Consider the portions of Figure 1 labeled upshift limits. Two critical rates are shown corresponding to repeat counts of 4 and 8 for upshift. The thermometer resistances are drawn from one bridge resistance point to another (point A to B). The thermometer resistance is increasing at such a rate that at the first bridge resistance point A (shown to intersect) the thermometer resistance is less than the bridge point so that in the prevailing bridge cycle the detector makes a down step decision and at the other end B of the bridge resistance curve (shown to intersect the bridge resistance point) after $U-1$ repeats, the the thermometer resistance is higher than the bridge point so that in the prevailing bridge cycle the detector makes an up step decision. The critical rate for upshift for the drifting thermometer resistance is given by the slope: $BR_i \times (U_i-1)/(U_i+1)$, where U_i is the repeat count for upshift preset in the bridge control logic for the i^{th} bridge rate BR_i .

The critical rate for downshift for a drifting thermometer resistance is also given by the slope: BR_i/D_i , where D_i is the reversal count for downshift preset in the bridge control logic for the i^{th} bridge rate BR_i . (See thermometer resistance lines labeled downshift limits.) The upward drift of the thermometer resistance is low enough that at the beginning (shown to intersect with the first bridge point x) the thermometer resistance is larger than the first bridge resistance point and after $D-1$ reversals the resistance is smaller than the bridge resistance point y.

The corresponding analysis applies for downward drifting thermometer resistance. (See lines associated with primed letters.) The counts U and D will be referred to as the critical counts for upshift and downshift, respectively. To avoid unnecessary shifting of the bridge rates, the counts U and D are adjusted so that the critical rate for upshift of one bridge rate overlaps the critical rate for downshift of the next higher bridge rate; i.e.,

$$BR_{i+1} \times (U_{i+1}-1)/(U_{i+1}+1) \geq BR_i/D_i$$

or

$$\frac{BR_{i+1}}{BR_i} \times \frac{D_i(U_{i+1}-1)}{(U_{i+1}+1)} \geq 1$$

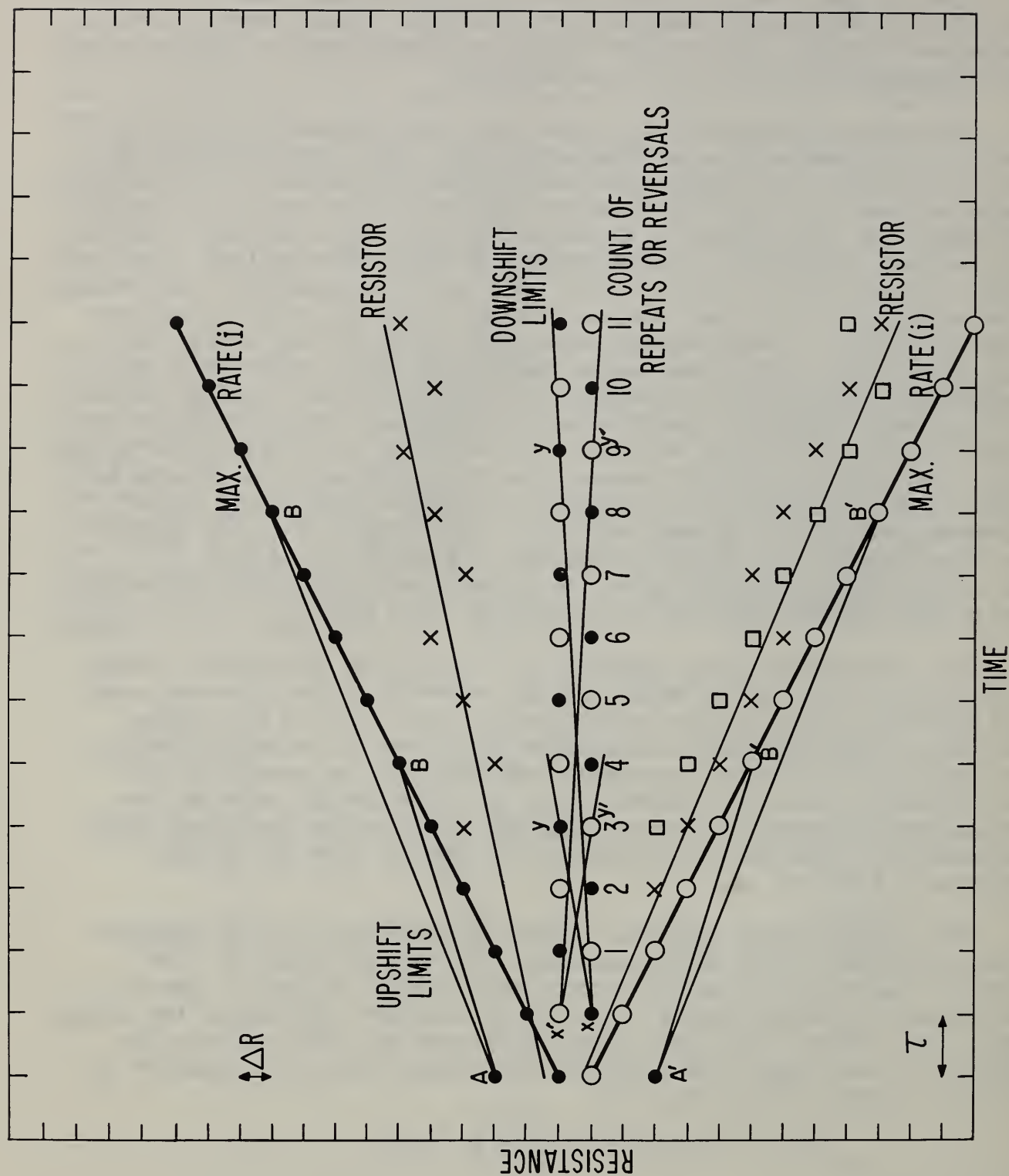


Figure 1. Critical Rates of the Thermometer Resistance for Upshift and Downshift as Set by the Repeat and Reversal Counts for Shift

II.3. Bridge Logic

The bridge logic is built around the sense of the detector unbalance; the magnitude of the unbalance is not applied in the design. The count of the prior bridge decisions is used to change the bridge rate or the thermometer lead connections to the bridge. Each detector decision is either a repeat or a reversal of the previous decision. A continuous series of repeats indicates that a higher bridge rate is needed for tracking. A continuous series of reversals indicates that the thermometer resistance is bracketed and that better tracking can be done at a lower bridge rate.

When the thermometer resistance is the same or very close to that of the bridge, the sense of the detector output becomes random. The likelihood of attaining the downshift logic under these conditions becomes small. To allow for this case the reversal counter is not always reset with the first repeat. (See section II.1 on the definition and counting of reversals.)

Referring to Figure 2, the straight lines indicate the thermometer resistances and the circles are the successive bridge points with increasing time. The relative levels of resistances are designated by letters for case 1 where the thermometer resistance is constant or very slowly drifting. In case 1, for points at level c, the bridge and thermometer resistances are about the same so that random detector decisions can be expected and the sense of the detector output could equally be plus or minus. For points at levels b and d, however, the sense of the detector output will cause the bridge to step in the right direction. Under such conditions the bridge points obey the following two rules: (a) every repeat is preceded and followed by two equivalent reversals (i.e., there are no successive repeats) and (b) every reversal made to bridge points b and d is followed by another reversal to point c. There are two possible types of reversals: cbcdbc... and cdcdcdc..., and two types of repeats: dcb and bcd. For the two types of repeats, the bridge point patterns cdcdbc and cbcdbc must exist (rule a). From point c, the detector output will initiate a step to point b or d. If it is a repeat condition, then the two repeats are separated by a single reversal. If it is a reversal condition, then another reversal to point c must occur (rule b). Any two repeats can, therefore, be separated by only odd number of reversals for case 1. In order to accumulate enough counts of reversals for downshift, the reversal counter is, therefore, not reset for the first repeat unless the number of reversal since the just previous repeat is even.

In cases 2, 3 and 4 where the thermometer resistance is drifting slowly enough that there are no consecutive repeats and every repeat is preceded and followed by at least one reversal, bridge point patterns containing even number of reversals between repeats must exist in order

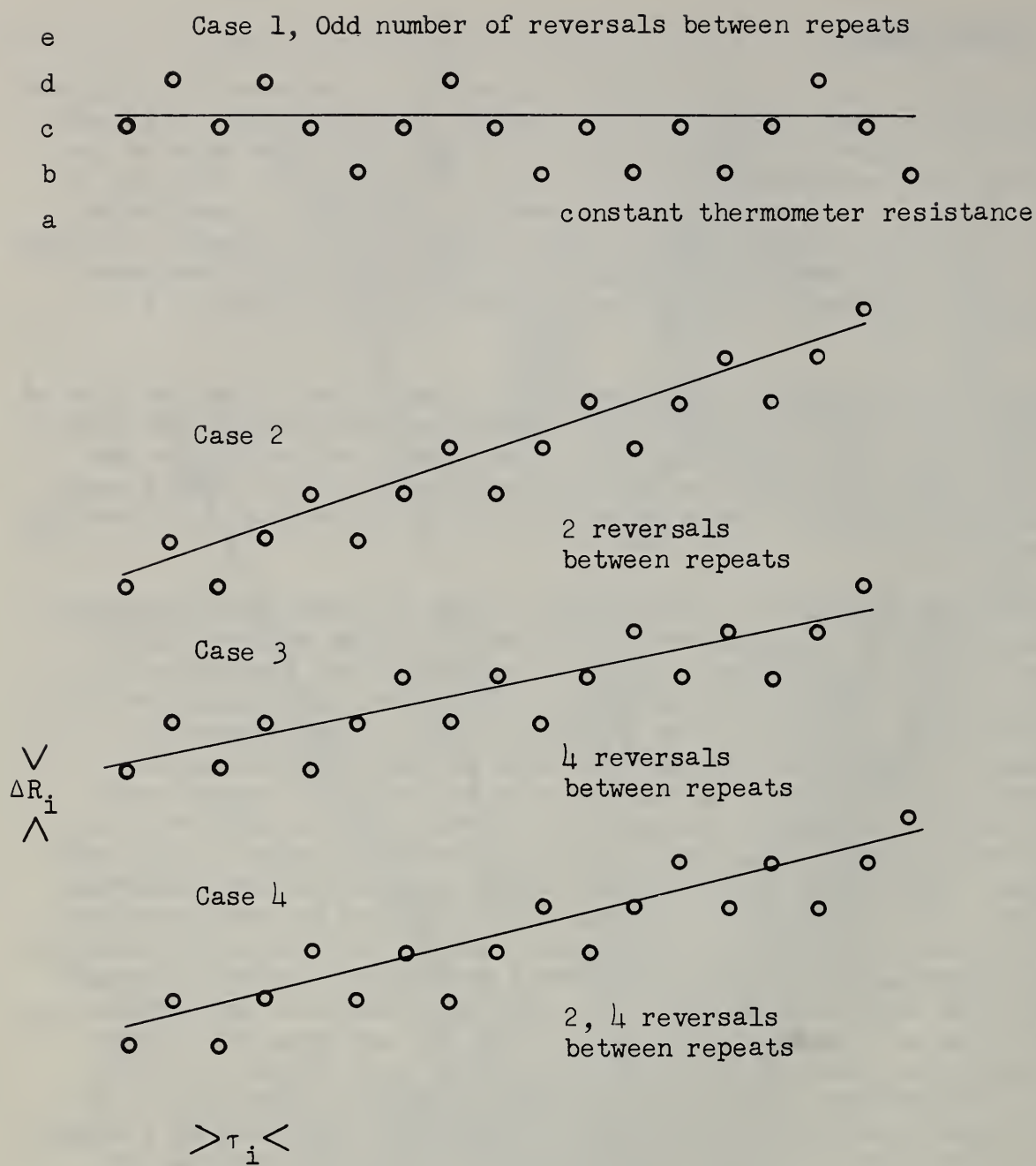


Figure 2

Bridge Point Patterns When Tracking Thermometer Resistance.
Line = Thermometer Resistance

for the bridge to track the thermometer resistance. If all single repeats are separated only by odd number of reversals, the bridge resistance does not change as demonstrated above for the case 1 of the constant thermometer resistance. With even number of reversals between single repeats the senses of the detector output that initiated these repeats are the same, and a slowly drifting thermometer resistance is indicated. The reversal counter is reset on repeats preceded by an even count of reversals since the last repeat. Since only by downshift can the meaningful data be recorded, reversal count for downshift may be reduced to a smaller value for a slowly drifting thermometer resistance even though this can cause the bridge rate to oscillate between two levels. In actual practice the drift of the thermometer resistance during the equilibration period has been found small enough and the bridge fast enough that the value of five for the reversal count for downshift yields satisfactory measurement of thermometer resistances to 0.00001 ohm. (See section IV.)

II.4. Bridge Circuitry and Switch Arrangement

The arrangement of resistors and switches of the automatic bridge corresponds to that of the Mueller bridge. The circuitry is shown in Figure 3. Mercury wetted switches are used for switching the normal-reverse thermometer connections and the resistance steps corresponding to 100, 10, 1, and 0.1 ohms. The 0.01, 0.001, 0.0001, and 0.00001 ohm decades use the shunted Waidner-Wolff arrangement. These switches have enclosed coin-silver contacts. The 2x and 5x resistance steps that were mentioned earlier are made as illustrated in Figure 3.

In the Mueller bridge circuitry and switch arrangement the "multiplier arms" have unit ratio, consequently at balance the resistances in the other two arms are equal. Since the Waidner-Wolff elements can not be set to zero resistance, the 0.1 ohm decade is placed in the opposite arm to balance some of the residual resistance. The balancing resistance is, therefore, increased when the resistance in this decade is decreased. Additional resistance is introduced in the unknown arm so that when all of the bridge dials are set to zero and the connections to the unknown arm is shorted, balancing resistor and the unknown arms have as nearly equal resistances as possible. The deviation from equality is the bridge zero.

Figure 4 illustrates the bridge equations applicable to processes associated with the measurement of a thermometer resistance. The normal and reverse connections are shown with the thermometer leads and the compensating resistors commuted. The ratio arms are also shown commuted. The symbols used in the equations are defined in the following table (2).

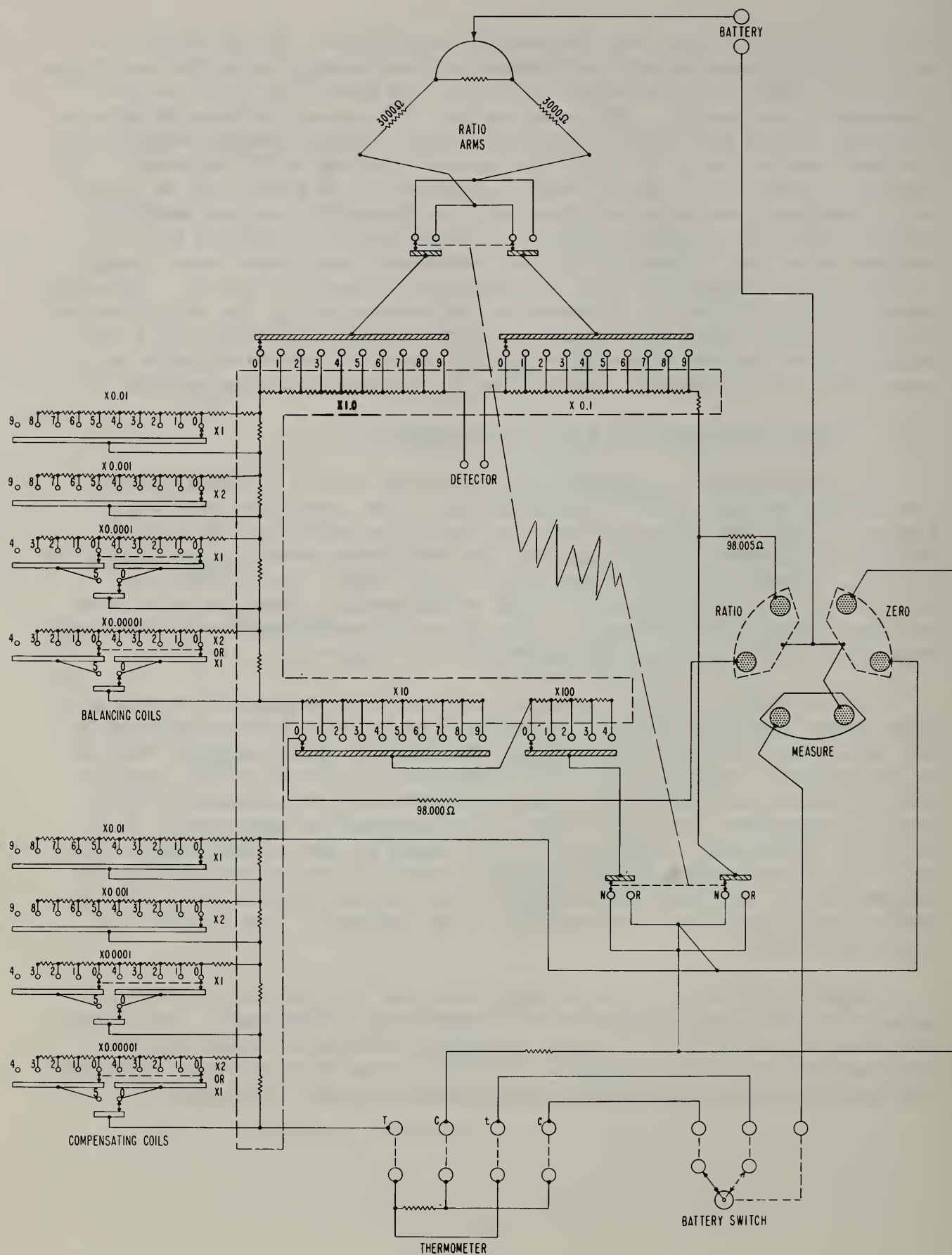
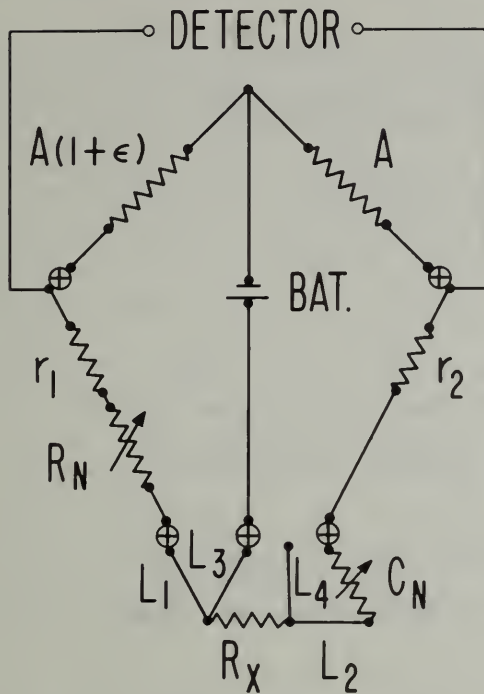
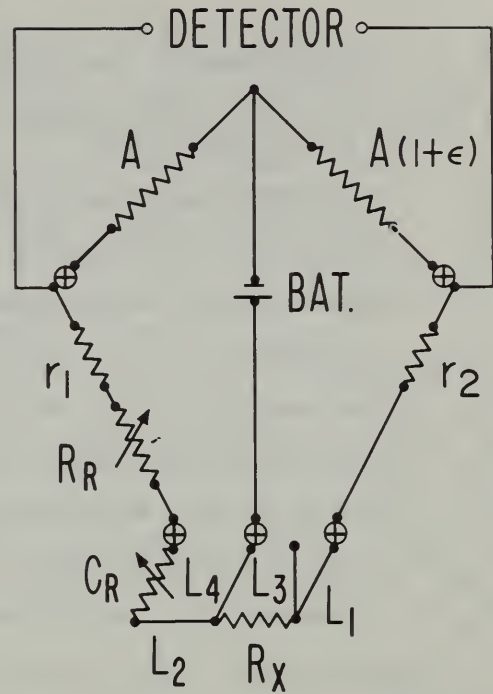


Figure 3. Bridge Circuitry and Switch Arrangement of the Automatic Mueller Bridge.

NORMAL



REVERSE



$$(1.) \quad \frac{A(1+\epsilon)}{A} = \frac{r_1 + R_N + L_1}{R_X + L_2 + C_N + r_2}$$

$$(1') \quad \frac{A}{A(1+\epsilon)} = \frac{r_1 + R_R + C_R + L_2}{R_X + L_1 + r_2}$$

$$(2.) \quad r_1 + R_N + L_1 = (R_X + L_2 + C_N + r_2)(1+\epsilon) \quad | \quad (2') \quad R_X + L_1 + r_2 = (r_1 + R_R + C_R + L_2)(1+\epsilon)$$

$$(2') - (2.): \quad R_X = \frac{(R_R + C_R - C_N)(1+\epsilon) + R_N}{2+\epsilon} - (r_2 - r_1)$$

$$(3.) \quad C_R - C_N = R_R - R_N$$

$$(4.) \quad R_X = \frac{2R_R(1+\epsilon)}{2+\epsilon} - \frac{R_N\epsilon}{2+\epsilon} - (r_2 - r_1)$$

$$(5.) \quad R_X = R_R + \frac{(R_R - R_N)\epsilon}{2+\epsilon} - (r_2 - r_1)$$

BRIDGE ZERO:

$$(6.) \quad r_2 - r_1 = \frac{R_N^I + R_R^I}{2} - \frac{\epsilon^2 r_2}{2(1+\epsilon)}$$

Figure 4. Equations Associated with the Mueller Bridge for Determining the Thermometer Resistance

Table 2. Definitions of Symbols Used in Figure 4.

A	=	resistance of the ratio arms
ϵ	=	deviation from unity of the ratio of the resistances of the ratio arms
r_1	=	residual resistance of Waidner-Wolff elements
r_2	=	resistance to balance r_1
L_1	=	thermometer lead resistance
L_2	=	thermometer lead resistance
R_N	=	balancing resistance at balance in normal connection
R_R	=	balancing resistance at balance in reverse connection
R_X	=	thermometer resistance
C_N	=	compensating resistance at balance in normal connection
C_R	=	compensating resistance at balance in reverse connection

Equation (3) holds since the balancing and compensating resistors are stepped simultaneously in the same sense and bridge rate in the reverse thermometer connection only. Equation (5) shows that when at balance in the lowest bridge rate the thermometer resistance is equal to the reading of the balancing resistors in the reverse connection plus the correction for the deviation from unity (ϵ) of the ratio arms and for the bridge zero $-(r_2-r_1)$. The correction term containing the deviation ϵ is negligible, since the ratio arms can be easily adjusted to a few parts in 10 million [3] and R_R-R_N would at most be 0.00005 ohm when the bridge balancing process is being performed in the lowest bridge rate. The ratio arms can deviate as much as 1 part in 1000, an unlikely situation, without significant errors in the measurements.

The bridge zero (eq (6)) is determined by first shorting the "thermometer connections" and by obtaining automatically normal and reverse readings.. (See Figure 3 for the circuitry during bridge zero determinations.) The correction for the deviation from unity (ϵ) of the ratio arms is negligible

II.5. Bridge Readout

On completion of a bridge cycle, some or all of the following conditions and readings on the bridge are changed: balancing and compensating resistances, thermometer connection, count of repeats and reversals, bridge rate, sense of detector, and the running clock time. All of these quantities are visually displayed on the bridge. For recording purposes the above quantities are first transferred to a buffer storage composed of mercury relay contacts from which card punch records are made. The buffer storage is essential, since precisely timed bridge cycles are used for the different bridge rates. Unless the recording instrument is considerably faster than the shortest bridge cycle, the bridge readings will be altered before the recording is completed when the recording is made directly from the bridge. The buffer storage permits the bridge to proceed to the next bridge cycle while the record is being made. The buffer storage is cleared during the cycle following the completion of the recording process. If the buffer storage is not clear whenever a readout logic condition is reached, the new information is lost and the bridge proceeds into the next bridge cycle.

The recording of the bridge quantities after every bridge cycle is not practical or necessary, since there is a certain amount "memory" in the accumulated count of repeats and reversals. By suitable selection of readout logic conditions that can be set on the bridge, about five or more bridge points before the time of record can be readily deduced from the bridge quantities that are recorded. The combinations of the following readout criteria can be selected: upshift, downshift, reversal of thermometer connections, and pre-selected count of reversals (2,3,5,7, or 9), which may initiate transfer of the bridge quantities to the buffer storage when the logic conditions are satisfied.

Other quantities, such as repeat count for upshift, reversal count for downshift, thermometer current, bridge zero, readout criteria, date, etc. which do not change, are recorded directly from switch contacts in which the quantities are preset manually.

Figure 5 shows a "listing" of a series of measurements that have been recorded on punch cards. Three readings are given per line. The bridge quantities recorded are defined in the figure. The temperature drift in a calorimetric experiment is precisely determined from such a relatively condensed record.

- Figure 5. A listing from punched cards of bridge readouts of a typical experiment to determine the "final" and "initial" temperatures associated with electrical energies introduced into a calorimeter. (See reference 1.)

Although unnecessary in a heat-capacity experiment [1], bridge quantities can be recorded to determine every bridge point during the experiment. Figures 6a through 6i show such a continuous series of bridge points obtained starting from the foreperiod to the after period. (For definitions of these terms, see reference 1.) The overlapping regions of the figures are shown as shaded areas. The time is started at the instant of turning on the electrical heater. The vertical lines drawn upward indicate times at which upshifts occurred and the downward vertical lines at which downshifts occurred. The filled-in circles indicate normal thermometer connection and the open circles the reverse connection.

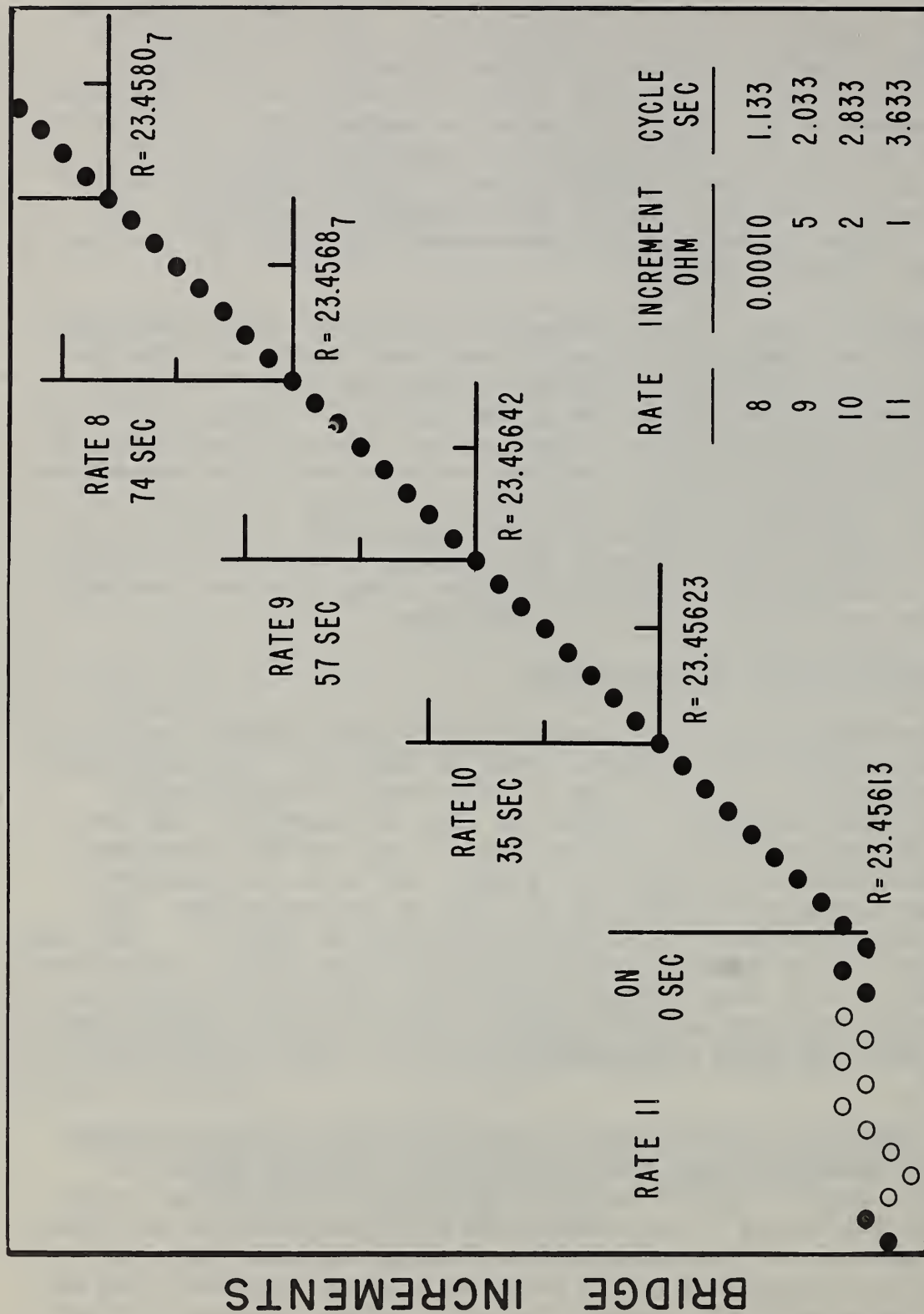
In Figures 6a and 6b, on turning the electrical heater the bridge operating in rate numbers 11 through 5 are shown unable to track the rapidly changing thermometer resistance. When the repeat count for upshift is reached for each of the bridge rates, the bridge is shown to upshift progressively to higher bridge rates. Starting from Figure 6b and on to Figures 6c and 6d the bridge is able to track the thermometer within 0.002 ohm (rate No. 6). The heater was turned off at 600 sec (Figure 6d). As the calorimeter gradually approached thermal equilibrium, the bridge is shown to track the drifting thermometer resistance (Figures 6d through 6i). In Figure 6i, the bridge is shown tracking the thermometer resistance within 0.00001 ohm.

III. Temperatures from Bridge Readout

The resistances are calculated on a high-speed digital computer from bridge readout data as shown listed in Figure 5. The best resistance corresponding to a given time is calculated from each readout. (There are three successive records per line in Figure 5.) The best resistances obtained for the reverse connections and the subsequent normal connections are paired and averaged, the time corresponding to the average (point pair) being the mid-time of the two values. The computer output from such a calculation is shown in Figure 7. The values in the first set of columns are the readouts in the reverse connection and are paired with those of the second set in the normal connection. The values are the same as those listed in Figure 5. The resistances of point pairs and their corresponding times are listed under "true readings".

The point pairs are analyzed to calculate the initial and final temperatures associated with the introduction of a known amount of electrical energy. Figure 8 shows a computer plot of the point pairs (zeros) and the values of the initial and final temperatures with their standard deviations. The straight line through the point pairs is determined by successively adding point pairs going backwards from the last four pairs until the standard deviation becomes greater than that for the last four pairs.

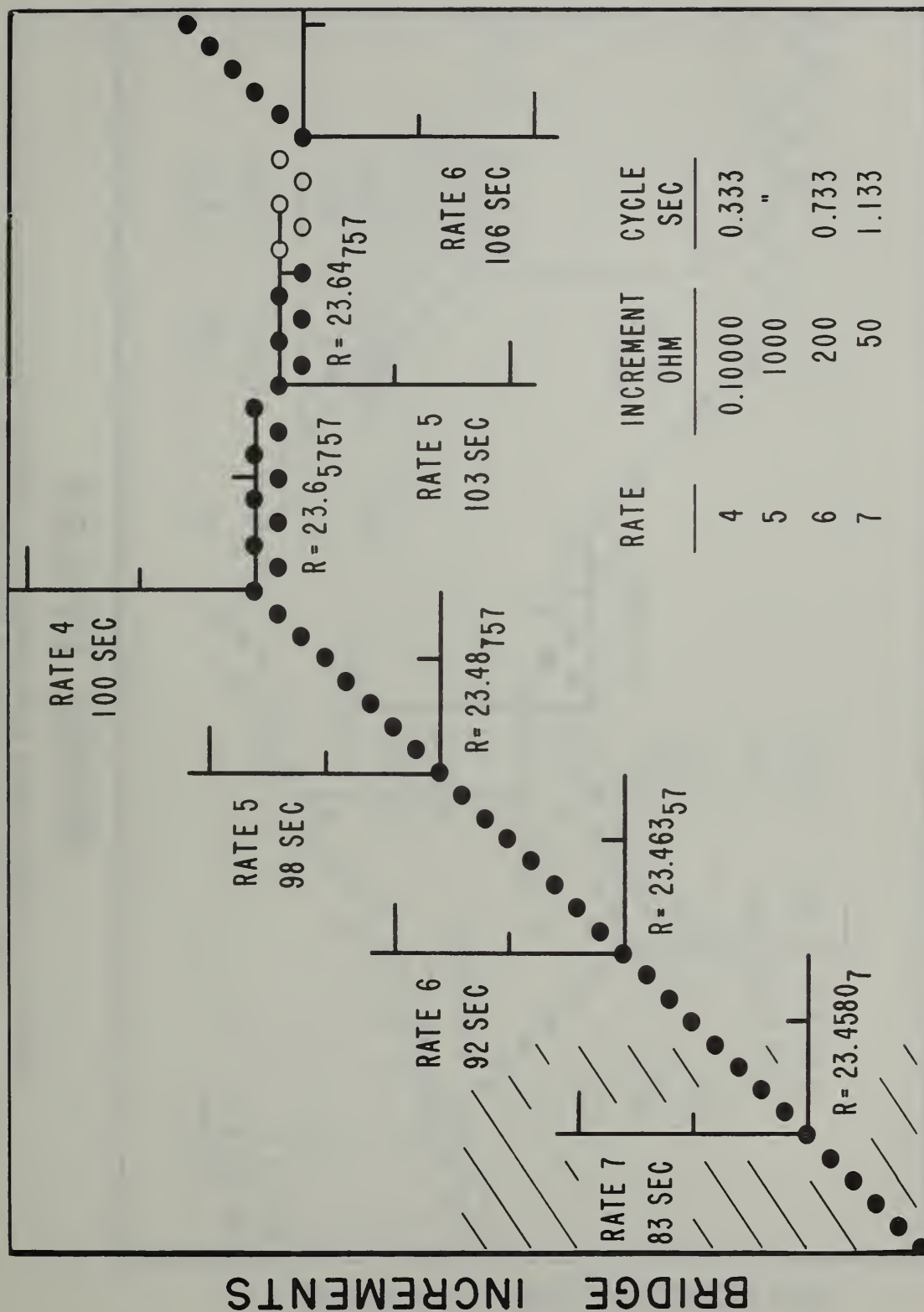
● NORMAL - THERMOMETER CONNECTION - ○ REVERSE



BRIDGE CYCLES

Figure 6a. Bridge Points after Completion of Every Bridge Cycle in a Typical Heat-Capacity Experiment.

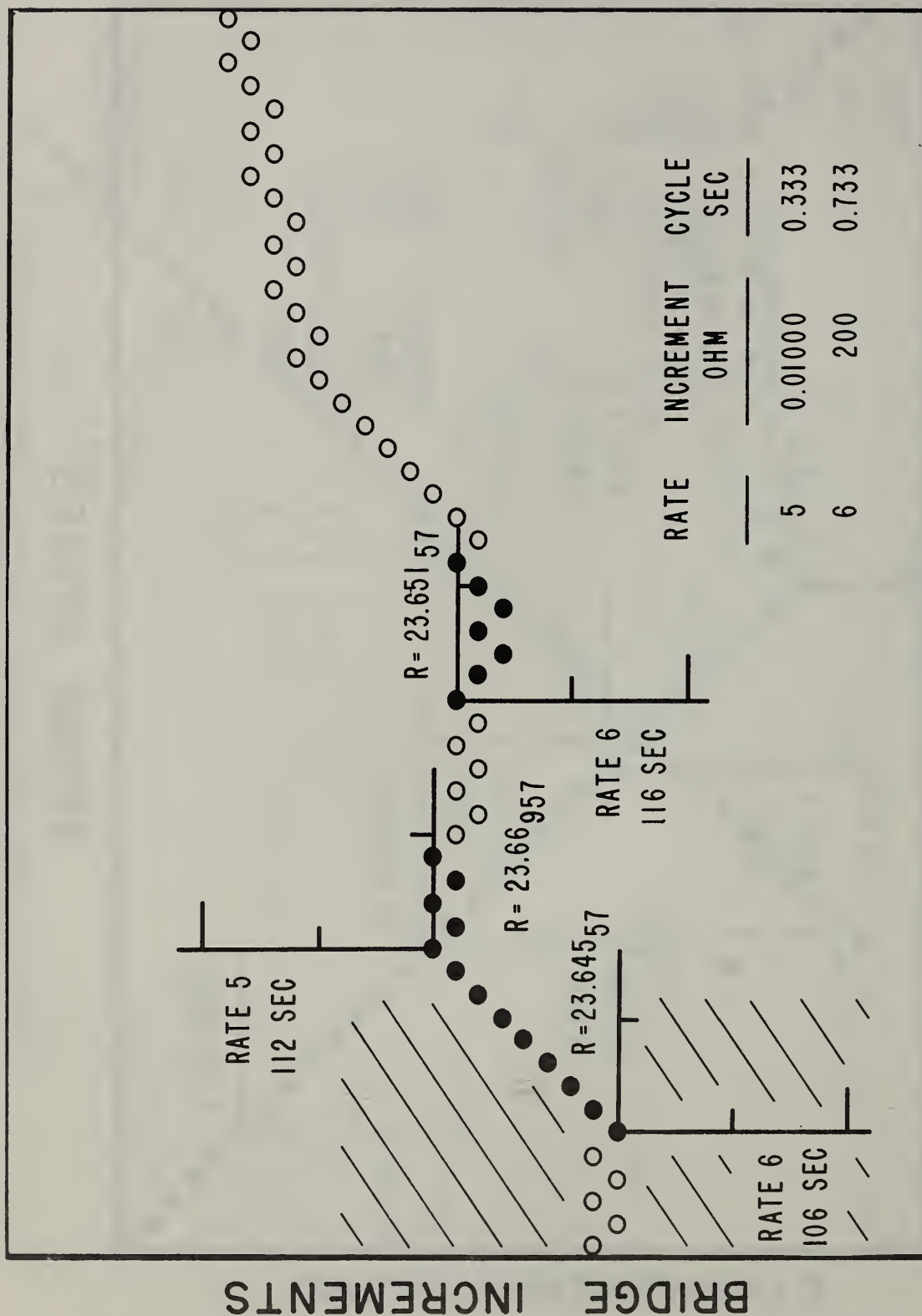
● NORMAL - THERMOMETER CONNECTION - ○ REVERSE



BRIDGE CYCLES

Figure 6b. Bridge Points after Completion of Every Bridge Cycle in a Typical Heat-Capacity Experiment. (Cont'd.)

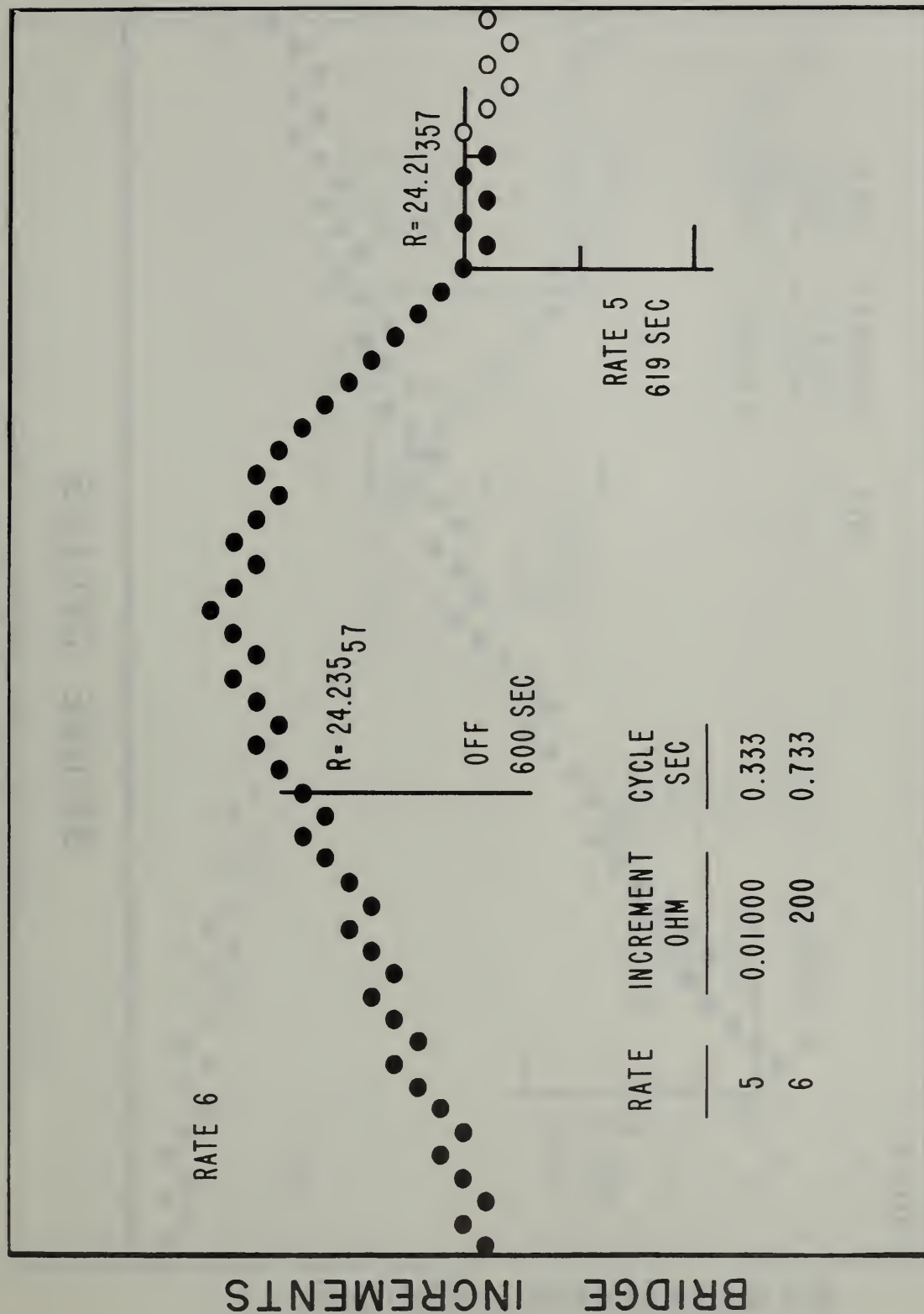
● NORMAL - THERMOMETER CONNECTION - ○ REVERSE



BRIDGE CYCLES

Figure 6c. Bridge Points after Completion of Every Bridge Cycle in a Typical Heat-Capacity Experiment. (Cont'd.)

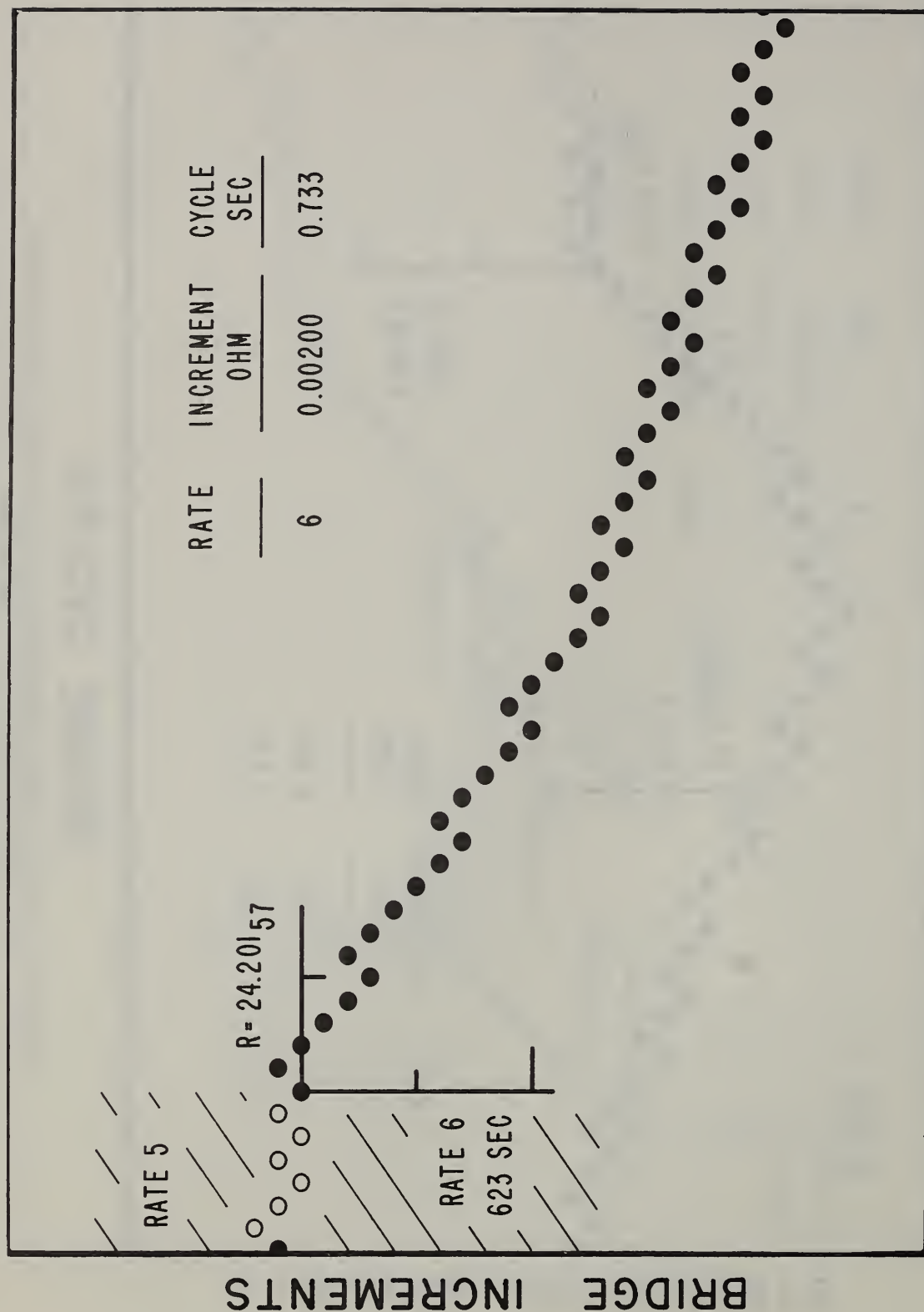
● NORMAL - THERMOMETER CONNECTION - ○ REVERSE



BRIDGE CYCLES

Figure 6d. Bridge Points after Completion of Every Bridge Cycle in a Typical Heat-Capacity Experiment. (Cont'd.)

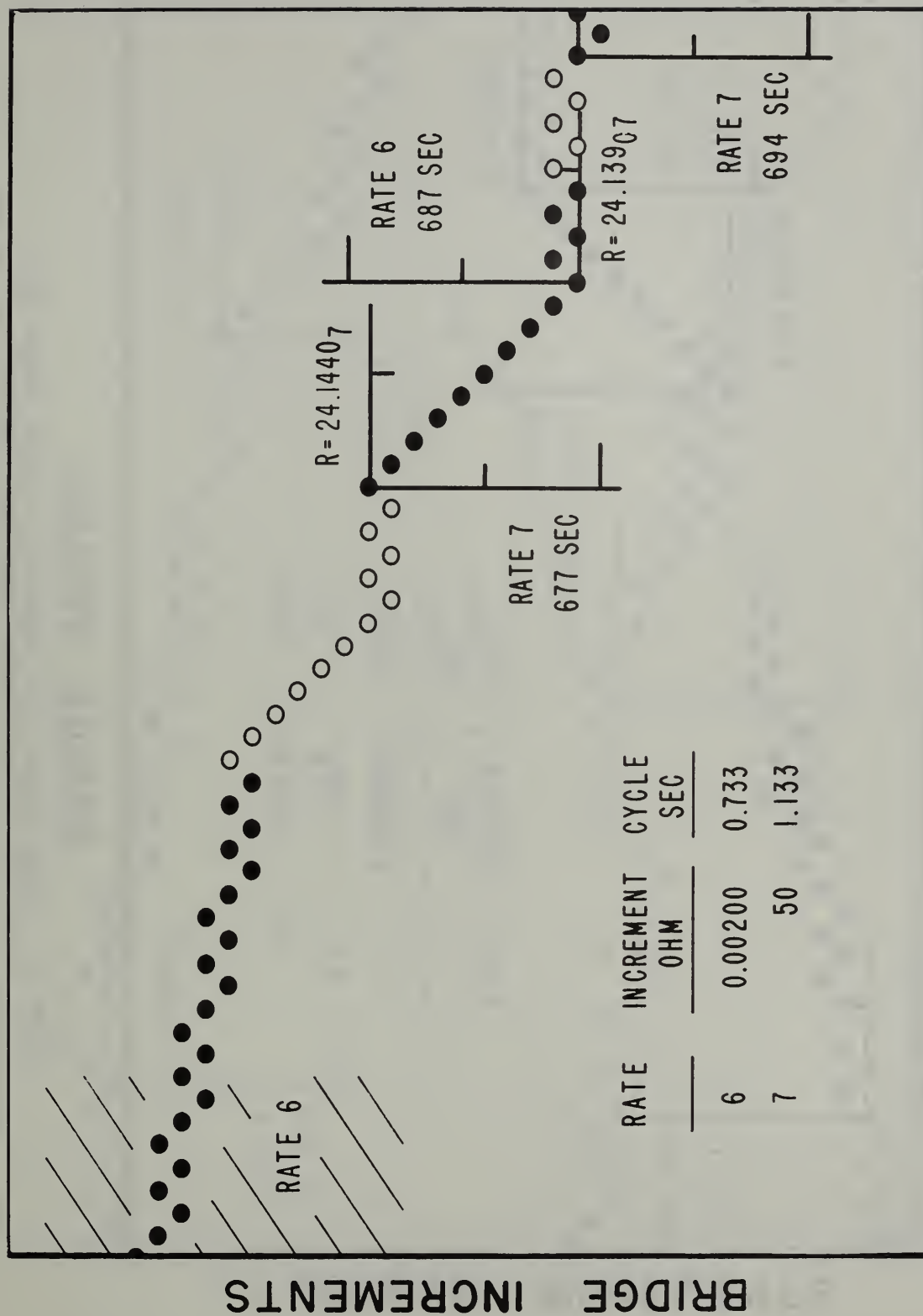
● NORMAL - THERMOMETER CONNECTION - ○ REVERSE



BRIDGE CYCLES

Figure 6e. Bridge Points after Completion of Every Bridge Cycle in a Typical Heat-Capacity Experiment. (Cont'd.)

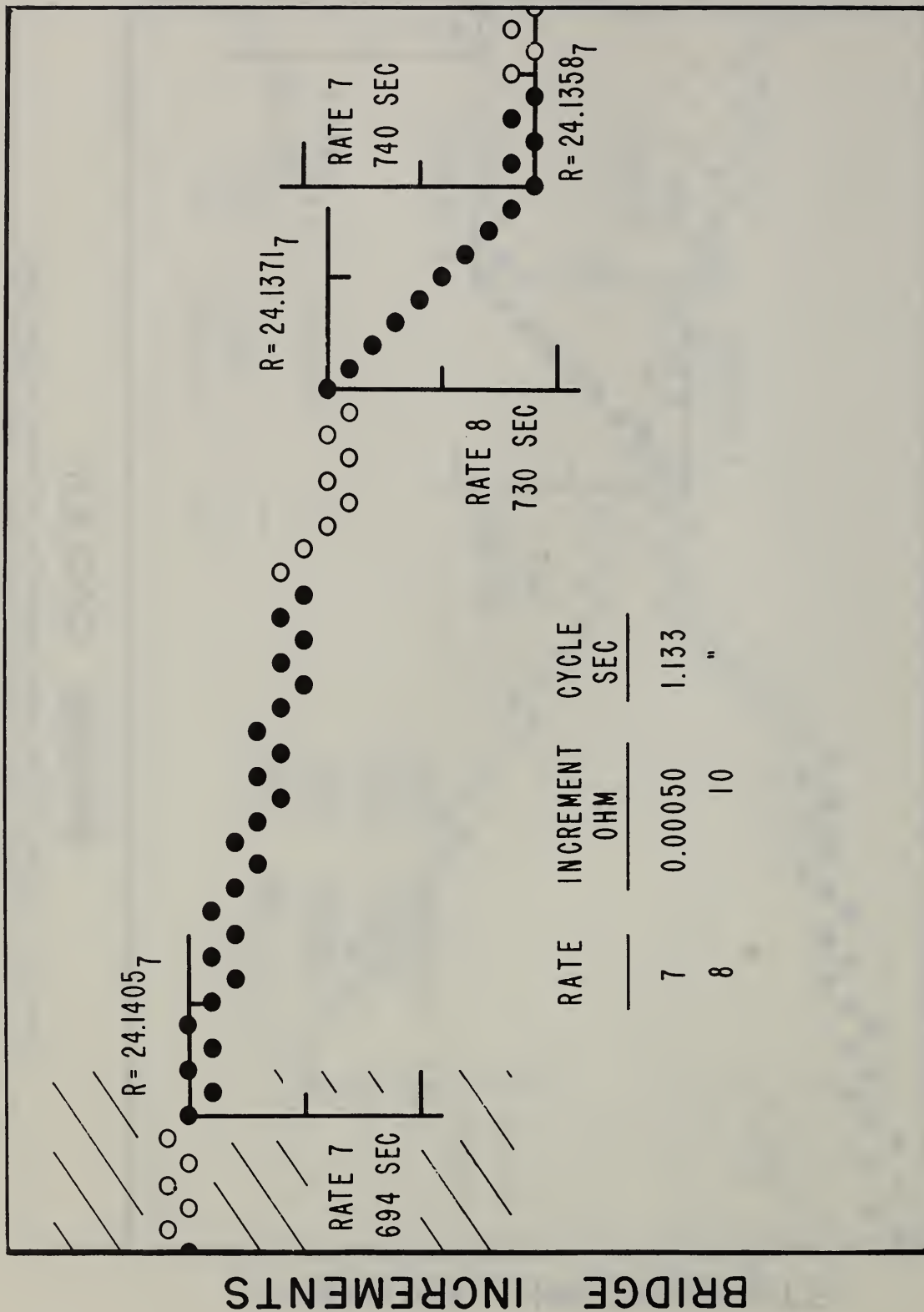
● NORMAL - THERMOMETER CONNECTION - ○ REVERSE



BRIDGE CYCLES

Figure 6f. Bridge Points after Completion of Every Bridge Cycle in a Typical Heat-Capacity Experiment. (Cont'd.)

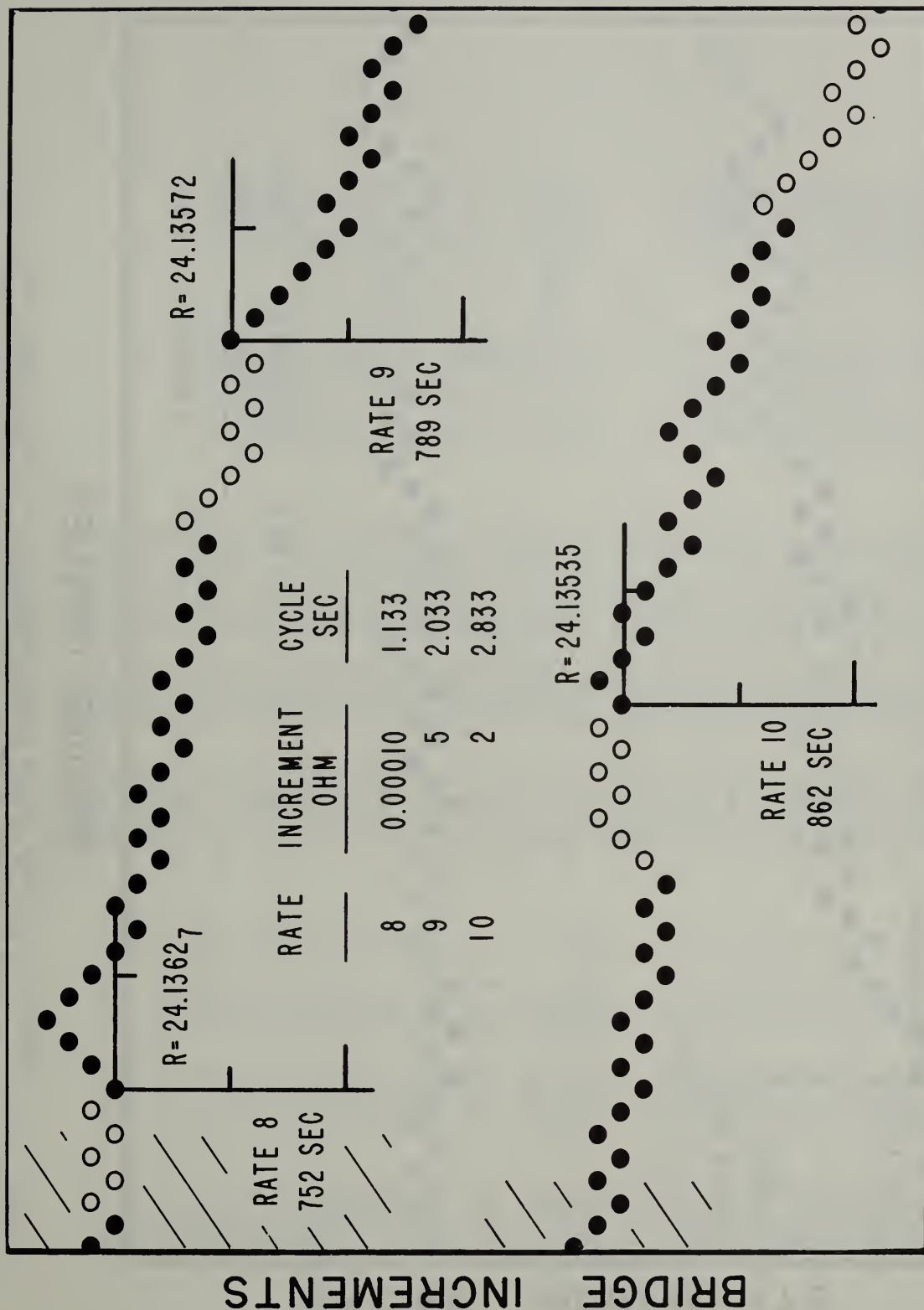
● NORMAL - THERMOMETER CONNECTION - ○ REVERSE



BRIDGE CYCLES

Figure 6g. Bridge Points after Completion of Every Bridge Cycle in a Typical Heat-Capacity Experiment. (Cont'd.)

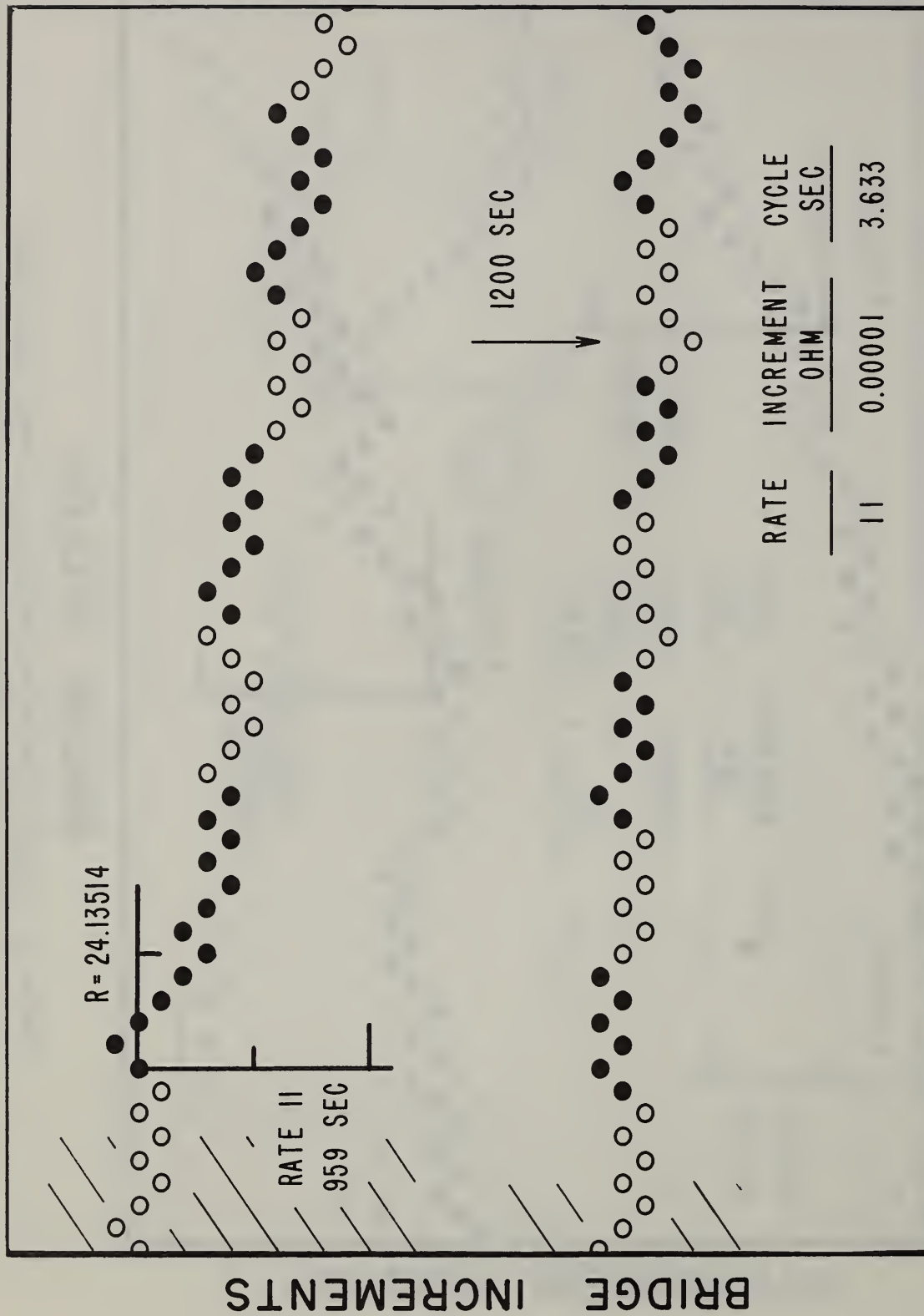
● NORMAL - THERMOMETER CONNECTION - ○ REVERSE



BRIDGE CYCLES

Figure 6h. Bridge Points after Completion of Every Bridge Cycle in a Typical Heat-Capacity Experiment. (Cont'd.)

● NORMAL - THERMOMETER CONNECTION - ○ REVERSE



BRIDGE CYCLES

Figure 6i. Bridge Points after Completion of Every Bridge Cycle in a Typical Heat-Capacity Experiment. (Concluded)

IV. Conclusion

The automatic bridge and the computer code for treating the bridge readout data have been successfully applied to calorimetry. The automation of high precision low-temperature heat-capacity calorimetry is possible as soon as funds become available for obtaining some of the commercially available equipment for electrical energy measurements.

V. References

- [1] Furukawa, G. T., Studies on the Automation of Low-Temperature Heat-Capacity Calorimetry, Chapter 2, 31-49, Preliminary Report on the Thermodynamic Properties of Selected Light-Element and Some Related Compounds, NBS Report No. 9500, January 1, 1967.
- [2] Stimson, H. F., International Practical Temperature Scale of 1948. Text Revision of 1960, J. Res. Natl. Bur. Std. 65A, 139-145 (1961).
- [3] Mueller, E. F., Precision Resistance Thermometry, Temperature, Its Measurement and Control in Science and Industry, 162-179, Reinhold Publishing Corp. 1941.

Chapter 2

IMPROVEMENTS IN OSCILLOSCOPIC MEASUREMENTS OF VARIABLES IN DYNAMIC EXPERIMENTS

A. Cezairliyan, H. A. Berman, and M. S. Morse

Abstract

Two refinements in oscilloscopic recording have been made which improve the measurement accuracy of transient events (where the signals do not vary considerably with time) by at least one order of magnitude. The first is a unit for the differential suppression of the incoming signal by an adjustable amount, and the second is a system by which time markers are sent to every oscilloscope at adjustable time intervals simultaneous with the actual incoming signal. Experiments were conducted to assess the operational characteristics of the system. The value of a test resistance determined under transient conditions (millisecond time resolution) was compared with its resistance under steady-state conditions. The agreement was in the range 0.01 to 0.1 percent depending upon the level of suppression.

1. Introduction

Oscilloscopes are used for the recording of high-speed events; such as transient voltages, etc., resulting from capacitor discharge, pulse, or similar dynamic experiments. However, oscilloscopes in themselves are not accurate recording instruments. Under the most favorable conditions, that is, with adjustments for linearity and calibrations made prior to the experiment, the accuracy of the recorded variable can at best be one percent. Additional difficulties result when more than one

oscilloscope is required to record several variables simultaneously. For example, although the same pulse may be used for triggering all oscilloscopes, internal electronic components may cause differences in the actual triggering of the beam, thereby altering the one-to-one correspondence of the beginning of the trace on the time scale of each oscilloscope. Also, non-linearities of the time scale of different oscilloscopes can contribute an error in locating corresponding points on different oscillograms.

In connection with the high-speed thermodynamic measurements system being developed at the National Bureau of Standards, two refinements in oscilloscopic recording have been made which have improved the accuracy of measurement of transient events by approximately two orders of magnitude. The first is a unit for the differential suppression of the incoming signal by an adjustable amount, and the second is a system by which time markers are sent to every oscilloscope simultaneously with the actual incoming signals.

2. Description of the System

a. Differential Suppression

For the high-speed recording of transient variables, the voltage leads are fed differentially to the oscilloscope input to compensate for the induced voltages in the signal carrying lines and to avoid grounding difficulties. The commercially available suppression preamplifiers are for single inputs only. Therefore, a special suppression unit was constructed, which is placed between the signal line and the preamplifier.

The maximum level of the suppressed voltage may vary depending on the recorded variable. The circuit diagram of such a differential suppression unit designed for a maximum suppression of approximately 9 volts is given in Figure 1.

It must be noted that a voltage suppression is effective only in cases where the portion of the transient voltage to be examined does not vary considerably with time; in other words, when the waveform is of rectangular or flat trapezoidal shape. Such voltage suppression units are being used in connection with dynamic experiments where heavy batteries are used as a pulse power source in order to heat conductors to temperatures close to their melting points within less than one second. In this case, a nearly flat topped current pulse flows through the specimen. In such experiments it has been possible to suppress 90 to 99 percent of the incoming voltage signals. Since the suppression voltage is constant, it can be measured very accurately under steady-state conditions by a potentiometer. Therefore, the oscilloscope inaccuracies are applicable only to the unsuppressed portion of the signal.

b. Time Synchronization

In order to synchronize the operation of all the oscilloscopes, it is not sufficient to use a single trigger signal. The most effective way of insuring a one-to-one correspondence between the simultaneous points on the traces of every oscillogram is to provide a means of making the same time signals on every oscillogram during the transient experiment. A modified time-mark generator is used to achieve this. Its output is fed into the oscilloscope vertical amplifiers and provides small, sharp dots

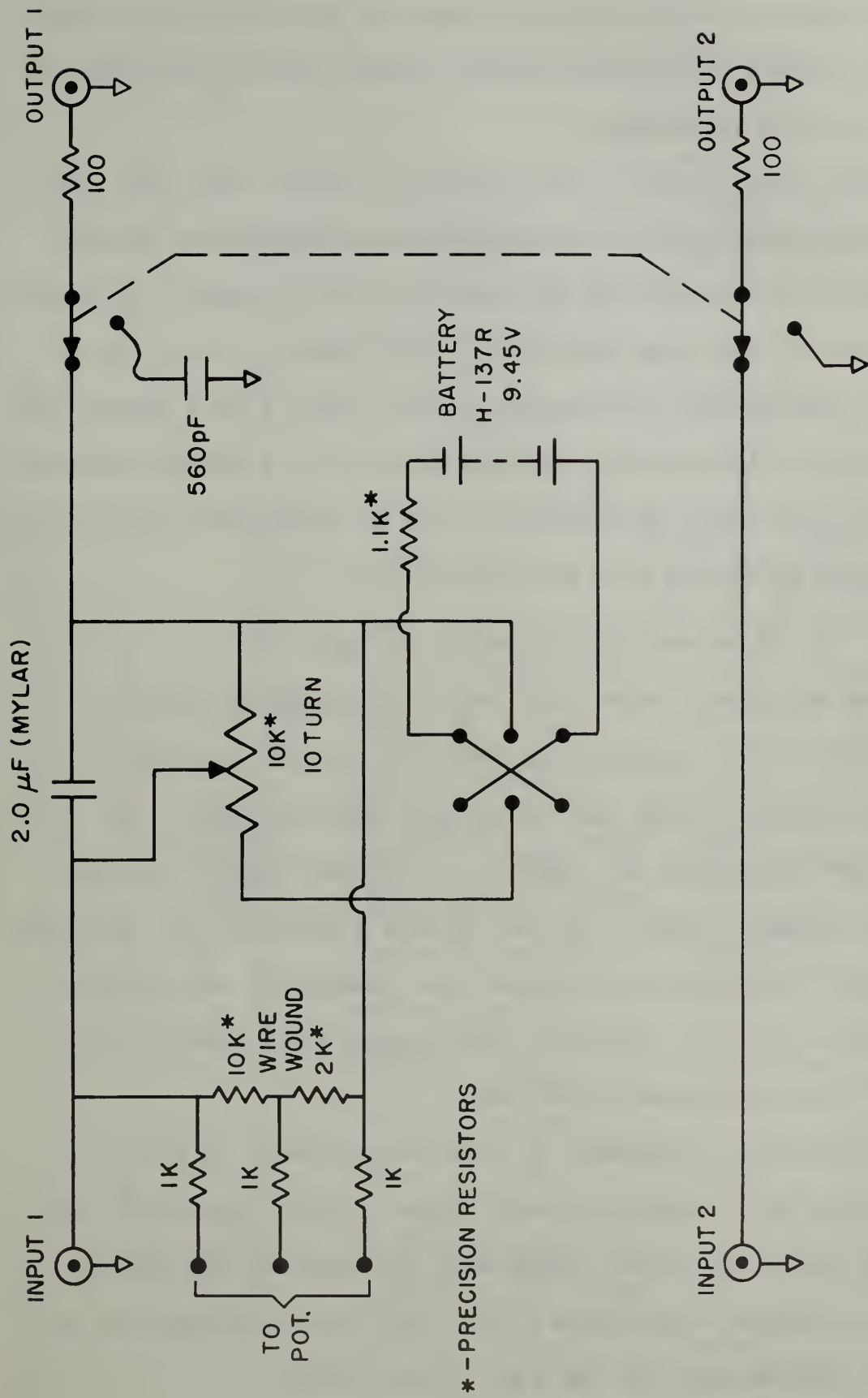


Figure 1. Circuit Diagram of Differential Suppression Unit.

or vertical spikes at regular time intervals, on the oscilloscope signal traces. The frequency of the time markers can be selected according to the duration of the experiment.

Two major modifications in the time-mark generator were made. The first was the installation of an amplifier and a pulse-length control unit to adjust the amplitude and the duration of the markers. The second was a gate unit to start the markers at a given time.

By thus establishing the compatibility of events with a common time base on different oscillograms, uncertainties arising from the triggering of the beams of different oscilloscopes and from non-linearities of the time scales can be reduced to a negligible level.

3. Experimental Arrangement and Operation

Selected experiments were conducted to assess the operational characteristics of the oscilloscopic measurement system containing differential suppression and time synchronization provisions. The objective was to determine the value of a test resistance by measuring the current flowing through it and the voltage drop across its terminals under transient conditions (millisecond time resolution) and comparing this measurement with its resistance under steady-state conditions as determined by the potentiometric method.

The experimental arrangement is shown schematically in Figure 2. The main circuit was designed for heavy pulse currents (up to 5000 A). The value of the pulse current was obtained by measuring the voltage drop across a reference resistance (1 m Ω). The test resistance was an Inconel tube (230 mm long, 25 mm O.D., 3.1 mm thick).

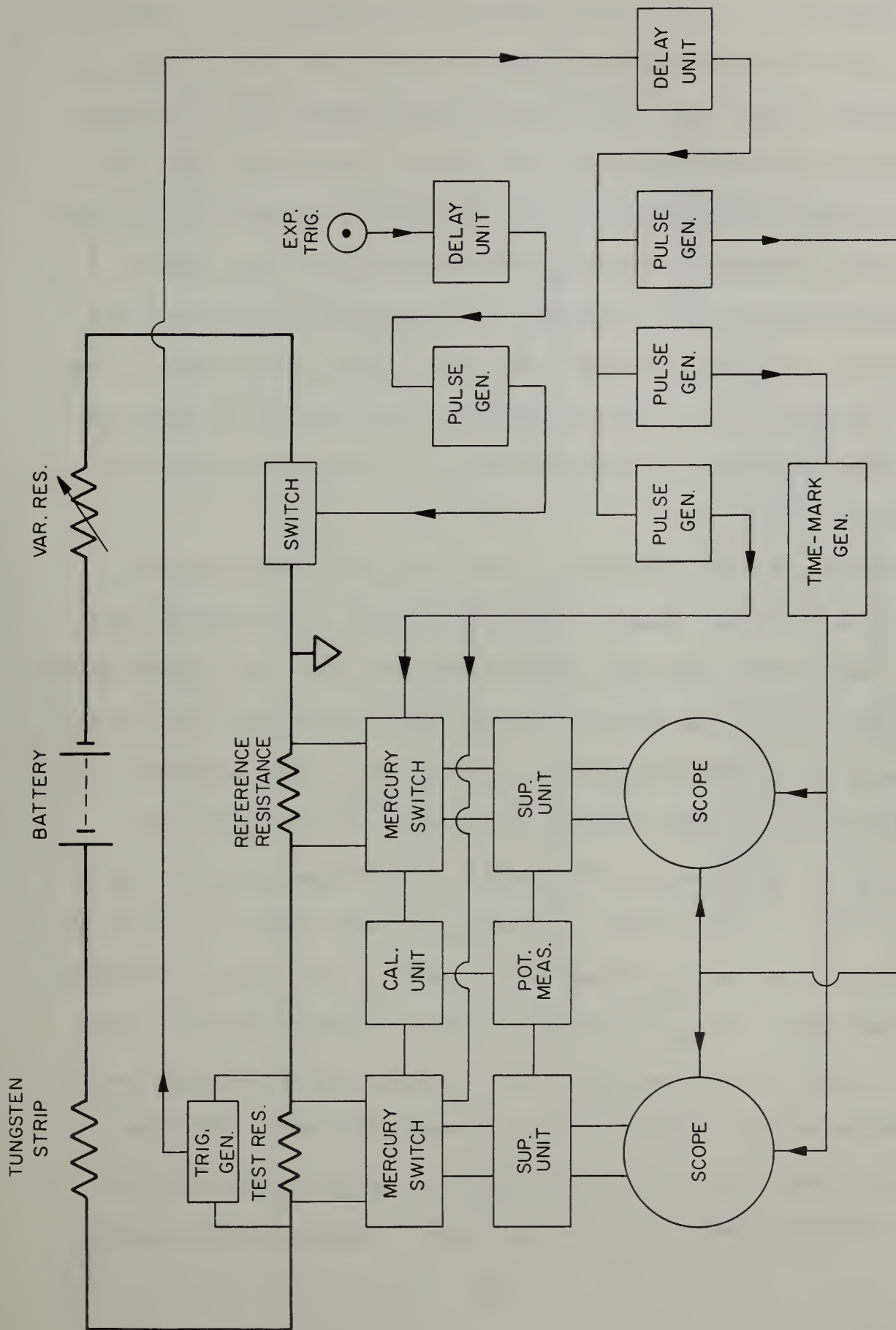


Figure 2. Functional Diagram of Improved Oscilloscopic Measurement System.

Because of the very low resistance, the great mass of the electrical system, and the relatively stable power source (a 28 V battery bank of 1200 ampere - hours capacity), current flowing through the circuit does not change appreciably during the short pulse. This implies that the current pulse is of rectangular form. In order to simulate actual heating conditions, in which the current decreases with time as the specimen resistance increases with temperature, a trapezoidal current pulse was obtained by inserting a tungsten strip (100 mm long, 6.2 mm wide, 0.5 mm thick) in series with the test resistance. The slope of the top of the trapezoidal pulse is then determined mainly by the characteristics of the tungsten strip.

Experiments were conducted both with and without the tungsten strip in the circuit. Figure 3 shows oscillograms of two typical cases of rectangular and trapezoidal pulses. For each case, the complete pulse is shown as well as the partial recording after suppression of the major portion of the pulse. The partial recording is on a more sensitive scale.

Because of the short duration of the heavy current pulses, all operations are synchronized with the aid of time-delay units. As may be seen in Figure 2, after manual triggering, the main switch is closed and the current pulse is sent through the system. At this point, the voltage developed across the test resistance triggers a voltage detector, which sends a signal to the time-delay unit to trigger the oscilloscopes and operate the mercury switches and the time-mark generator. The time sequence of major events in an experiment is shown in Figure 4. The mercury switches play a very important role in the successful operation

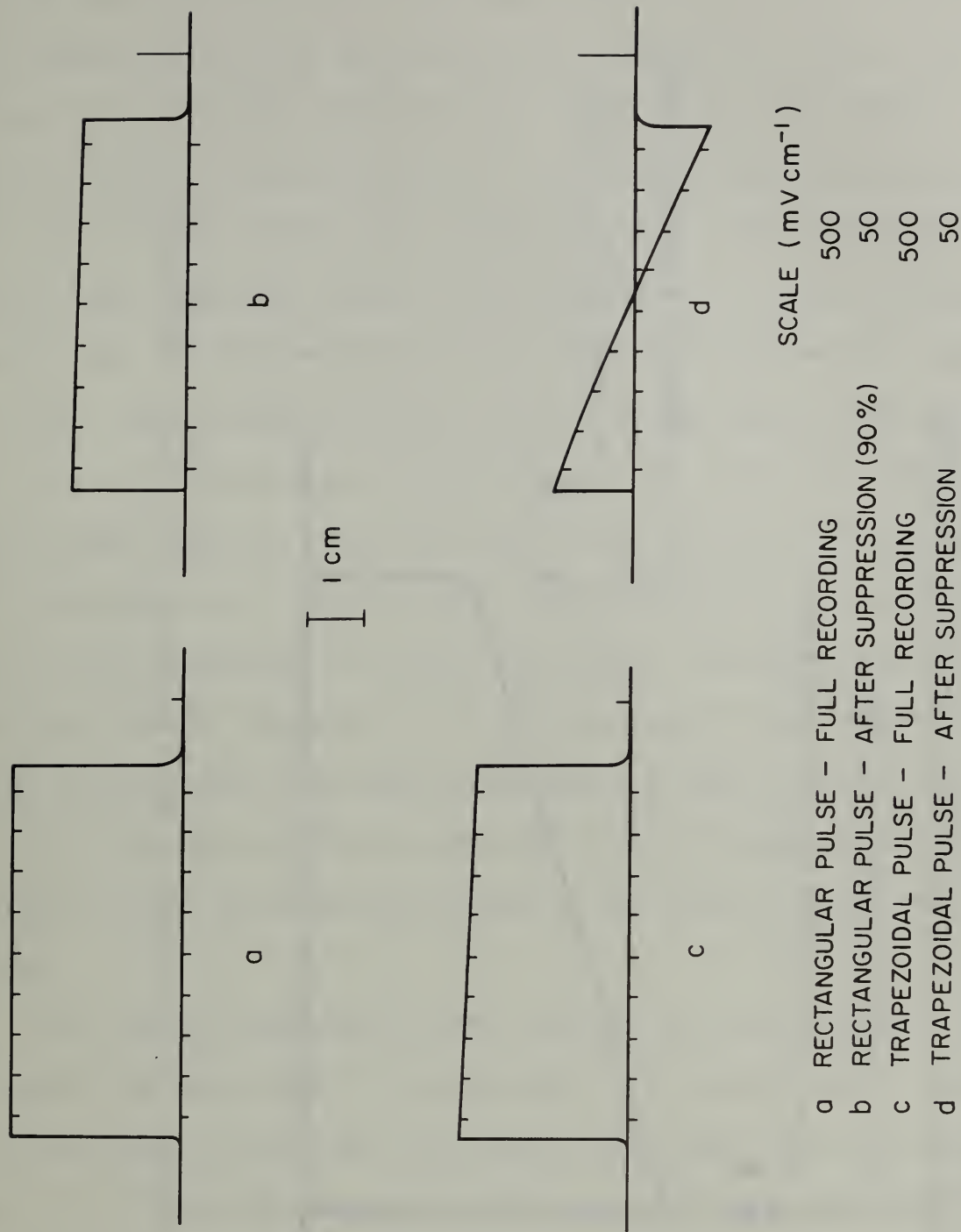
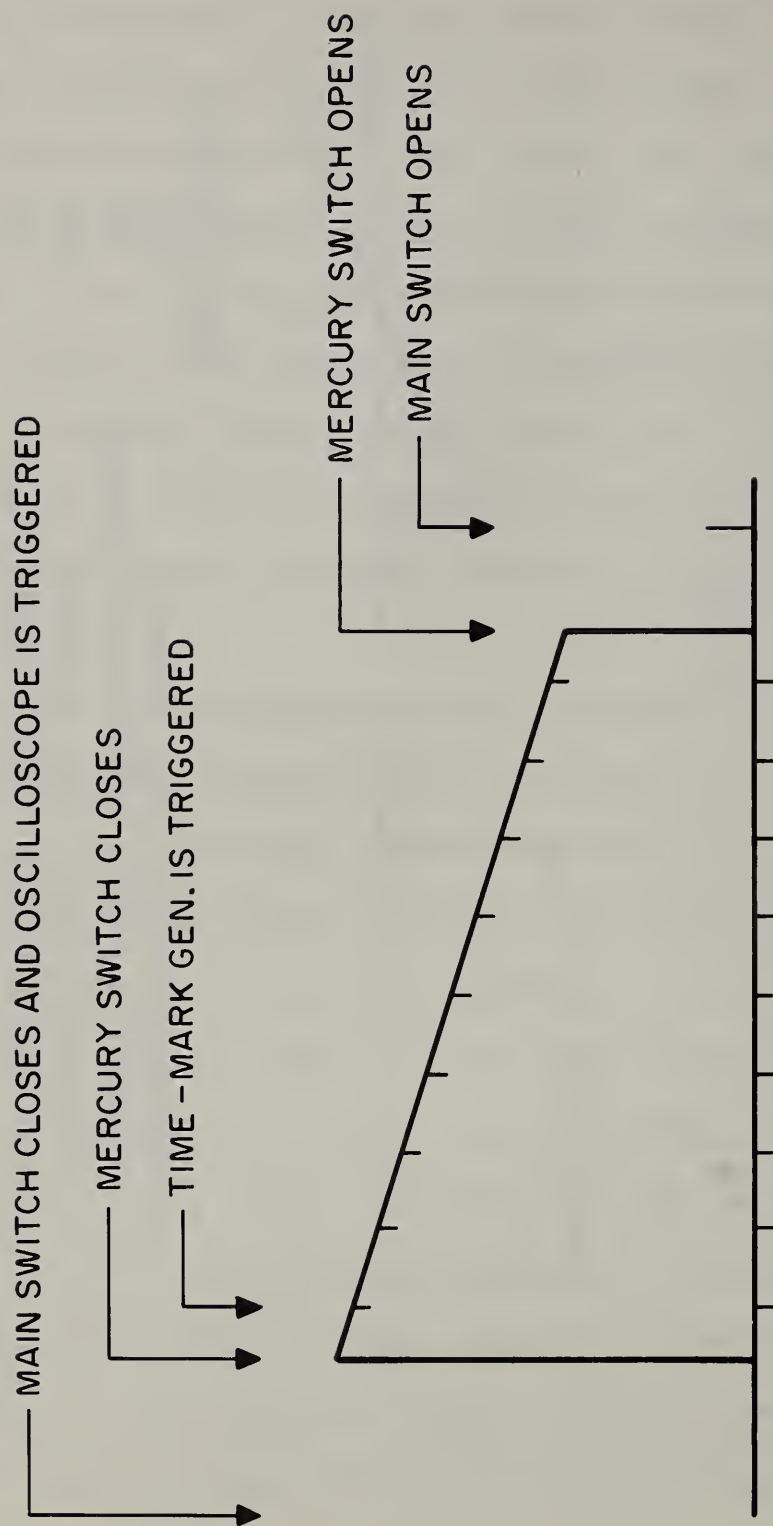


Figure 3. Oscilloscope Reproductions of Typical Rectangular and Trapezoidal Pulses.



40

Figure 4. Time Sequence of Major Events in Oscilloscopic Measurement.

of the measurement system. Normally, each mercury switch is open, placing the suppression unit on open circuit and isolating it from the main circuit. Thus, even though the suppression voltage is at the predetermined level, it is not sensed by the oscilloscope. The mercury switch closes only after the flow of heavy current has started and opens a short time before the pulse ends. Therefore, while the mercury switch is closed, the oscilloscope senses only the difference between the source voltage and the suppression voltage. This arrangement keeps the oscilloscope beam on the screen at all times, eliminating overload conditions that result when the beam goes off screen. Overload conditions tend to alter the base line position of the beam and cause a high degree of irreproducibility and inaccuracy in the results (amounting to several millivolts). In addition, mercury switches provide superposition of the base line of the actual pulse with that obtained under zero signal conditions, as may be seen in Figure 5. The two base lines obtained at slightly different times are thereby compared and a correction can be made in the event of a difference between them.

For dynamic measurement of the value of the test resistance, which requires the measurement of two variables, two oscilloscopes instead of one dual-beam oscilloscope were intentionally used. The time scales of the two oscilloscopes were set on arbitrary "uncalibrated" positions so that the experimenter could rely completely on the time markers in correlating the corresponding current and voltage signals. Since the same time markers appear on both signal traces, non-linearities in the time scales do not cause any errors; in fact, it is not even necessary to calibrate the oscilloscope time scales.

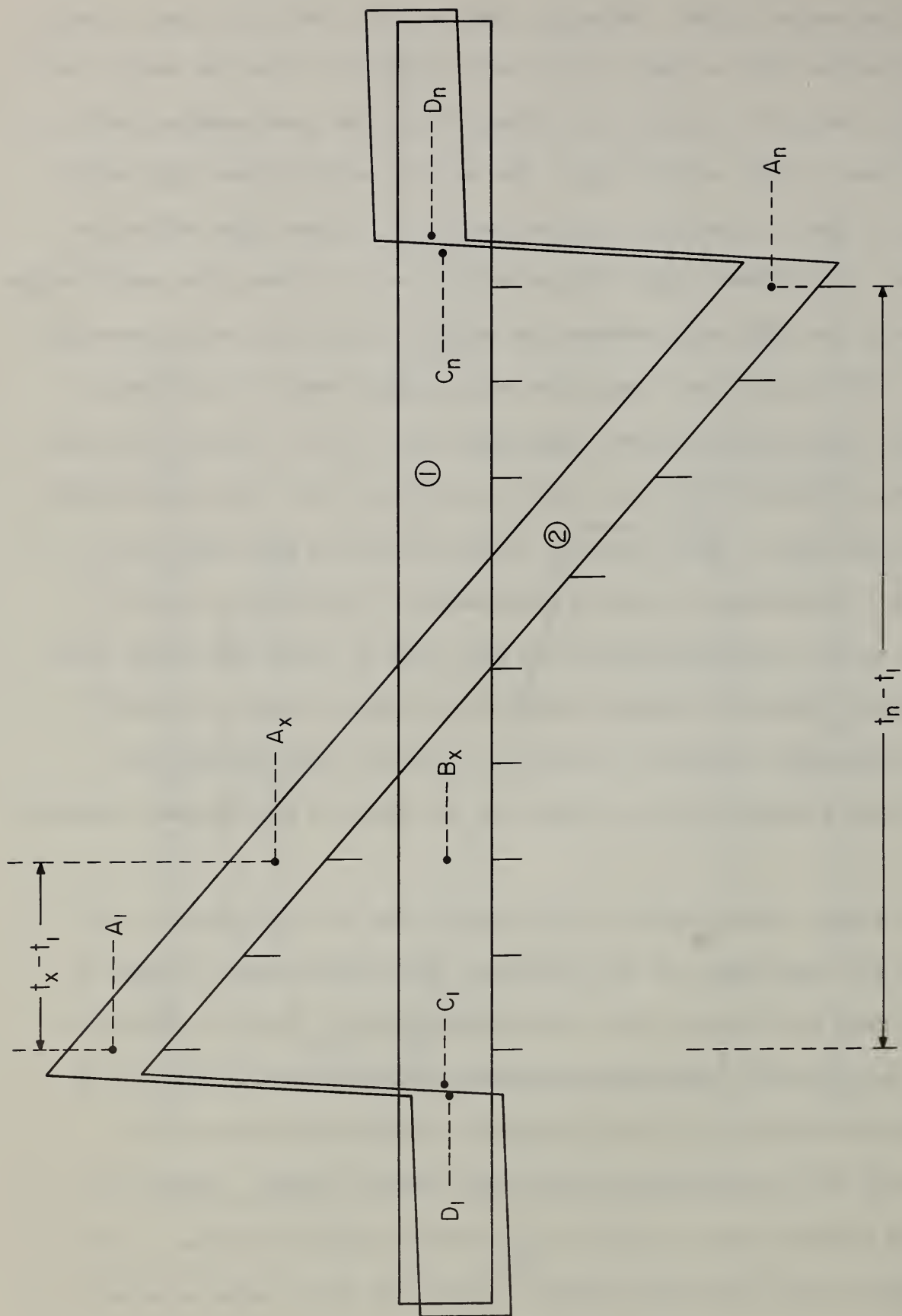


Figure 5. Schematic Drawing of Trapezoidal Pulse and Baseline. Line Thickness and End Imperfections Are Exaggerated.

The two oscilloscopes used in the experiment were electrically isolated from each other by means of isolation transformers at the power-line connections. Isolation transformers were also used ahead of all other inputs, such as trigger signals and time-marker signals. It was found that neglect of such precautions introduced stray currents and erroneous signals. Each oscilloscope was completely floating electrically and its relative ground (reference) point was at the negative potential of either the reference or the test resistance.

A permanent record of the signal traces was made by photographing the oscilloscope screen. The traces on the oscillograms thus obtained were measured with the use of a micrometer microscope.

The foregoing paragraphs have presented the experimental arrangement for measuring the value of a test resistance under pulse conditions, and comparing it with its value under steady-state conditions. However, to measure certain thermodynamic quantities under dynamic conditions, it is necessary to know the power imparted to the specimen as a function of time. Although both resistance and power are obtained through the measurement of the same two variables, the errors associated with them may be different from each other inasmuch as one is represented by a quotient, the other by a product. If the systematic errors in voltage and current are in the same direction, the resulting relative error in resistance will be the difference between these relative errors, whereas the corresponding power error will be their sum; conversely, if these errors are of opposite sign, the resistance error will be their sum and the power error their difference.

An additional experiment was performed to assess the errors involved with the dynamic measurement of one variable, such as current or voltage.

In this experiment the same basic circuit as that given in Figure 2 was used. The original $1\text{ m}\Omega$ reference resistance was replaced by one of $100\text{ m}\Omega$. A direct current of approximately 12 A was allowed to flow under steady-state conditions through the main circuit. The potential across the reference resistance was measured by a potentiometer, and, at the same time, recorded with the improved oscillographic technique following the procedure developed for the pulse experiments. The comparison of the two results obtained by the two different methods gives the accuracy of the dynamic recording of one variable under quasi-dynamic conditions. This procedure was used separately to check each of the two oscilloscopes. The only difference between this quasi-dynamic method and that of a pulse experiment is the absence of possible fields and skin effects. It is shown in Section 5 that errors of this origin are negligibly small.

Thus, the results of two separate experiments, (1) pulse experiments yielding a comparison of steady-state resistance with that under pulse conditions, and (2) quasi-dynamic experiments yielding a comparison of one variable under steady-state and quasi-dynamic conditions, determine the accuracy of measurement of the variables of dynamic experiments by the improved oscilloscopic technique.

4. Oscillogram Measurements and Calculations

The signal traces on the oscillogram are converted into the corresponding voltages by performing a calibration experiment in which a known constant voltage (measured potentiometrically) is applied to the oscilloscope and the ratio of this voltage to the deflection in the oscilloscope is determined.

Because of oscilloscope imperfections, this ratio, or "calibration factor," is a function of three semi-independent parameters: the horizontal position of the trace on the oscillogram, its vertical level, and the magnitude of the deflection.

Ideally, for every point measured, the known applied voltage should be chosen to produce a deflection equal to that accompanying the unknown pulse signal and at the same horizontal and vertical positions. In the case of rapidly changing pulses, one calibration would then be required for each point of measurement, or a study of the variation of deflection with the three parameters would be needed for each oscilloscope used. However, to avoid an excessive number of calibrations, two calibration measurements were made for each pair of pulses, one equal in deflection to that of the extreme left end of the pulse range to be measured, and similarly positioned (usually a positive deflection at the start), and a corresponding one for the extreme right end (usually a negative deflection at the finish in a trapezoidal pulse). The calibration factor k_x for any intermediate point x was then interpolated as follows:

$$k_x = k_1 + (k_n - k_1)(t_x - t_1)/(t_n - t_1) \quad (1)$$

where k_1 and k_n are, respectively, the initial and final calibration factors and t_x , t_1 , t_n are the corresponding times.

This technique assumes that the calibration factor has a linear variation with each of the two position parameters. It automatically corrects for the effect of these two parameters regardless of drift in the calibration from day to day or with a change in oscilloscope. The correction for pulse deflection magnitude was found to be negligible in

comparison with those for position. The errors due to interpolation and neglect of the deflection magnitude parameter are minimized by the fact that pulse experiments are designed to intersect the baseline approximately at the midpoint of the trace. Thus, the calibration factor is accurately measured at the extreme positions where the contribution of oscilloscope error to the total signal is greatest, and interpolated at intermediate points where the contribution of the more accurate potentiometric measurement is more important.

The deflections themselves in the pulse and calibration oscillograms are measured by reading the difference between the center of the pulse trace and the center of a baseline which represents the position of the beam when only the suppression voltage is present. The pulse trace (Figure 5) shows initial and final traces at the baseline level and an intermediate trace at the pulse level. Because the absent portion of the base level may not be linear, a separate baseline trace, superimposed on the pulse trace 2, is taken before the pulse, and a baseline level is thus obtained for each pulse position measured. A correction must be made, however, for an imperfection which often occurs in superposition of the base level of the pulse trace and the level of the baseline. This correction is obtained by algebraically adding the pulse-baseline difference at the ends to that measured at the intermediate points. The overlap is different at the two ends of the pulse and must therefore be interpolated between them as for the calibration factor. The corrected pulse deflection, Δ , is obtained as follows:

$$\Delta = B_x - A_x + 2 [D_1 - C_1 + (D_n - C_n + C_1 - D_1)(t_x - t_1)/(t_n - t_1)] \quad (2)$$

where,

$B_x - A_x$ is the uncorrected pulse deflection at point x, A representing the pulse trace center and B the corresponding baseline center, C_1 is the level of the baseline just after it diverges from the overlap, D_1 is the level of the overlapping pulse and baselines just before divergence,

Subscript n refers to the corresponding points after the end of the pulse,

C_n before convergence, D_n after convergence,

t_1 , t_n , t_x are the corresponding times.

These points are shown on Figure 5.

5. Results and Discussion

The method was assessed by comparing the resistance of an Inconel tube measured as described in Section 3 under steady-state and under pulse conditions at 25°C. The following measurements were made:

1. A steady-state potentiometric measurement of the resistance of the Inconel tube before the series of pulse measurements and, three months later, after the series. The mean of six measurements in each case was 3.07755 mΩ before and 3.07778 mΩ after (at 25°C). The average of the two means, 3.07767 mΩ was used as a standard for the pulse measurements.
2. A group of 14 rectangular 100-ms pulses of about 600 A, in which an average of 12.6 percent of the pulse amplitude was recorded on the oscilloscope, the remainder measured before and after the pulse by potentiometer. Five measurements on the current and voltage oscilloscope traces were made at equally spaced time intervals for a total of 70 measurements.

3. A group of three rectangular pulses similar to the last, but with an average of 0.5 percent of the pulse amplitude recorded.
4. A group of eight trapezoidal 90-ms pulses of about 500 A, in which an average of 6 percent of the pulse was recorded at the start, 1.5 percent at the midpoint, and -6 percent at the end, that is, the suppression voltage measured potentiometrically was greater than the amplitude of the last half of the pulse resulting in a negative deflection on the oscilloscope. These pulses are representative of the pulse shape to be expected in a calorimetric experiment in which the specimen temperature is changing rapidly over a range of several hundred or thousand degrees. For each pulse, a total of five measurements at equally spaced time intervals were made.
5. A group of 11 trapezoidal 50-ms pulses of about 1300 A., in which an average of 4 percent of the pulse was recorded at the start, 0.2 percent at the midpoint, and -4 percent at the end.

Table 1 lists the difference between steady-state and pulse resistance values and the standard deviation of each group of measurements described in items 2 to 5. Figure 6 shows the dependence of the above on the fraction recorded on the oscilloscope for both rectangular and trapezoidal pulses. In general, if the fraction recorded is kept as low as 6 percent of the total, an accuracy of 0.1 percent or better and a reproducibility of ± 0.07 percent or better are possible, and for fractions of 1 percent or less, errors of the order of 0.01 percent in resistance can be achieved.

The average systematic error of all the determinations reported in this paper was positive. This positive systematic error decreased almost

Table 1

RESULTS OF DYNAMIC RESISTANCE MEASUREMENTS

Pulse Shape	Fraction Recorded On Oscilloscope, Per Cent	Number of Measurements	Resistance Difference Per Cent	Standard Deviation Per Cent
Rectangular, 600 A	12.6	70	+0.08	0.09
Rectangular, 600 A	0.5	15	+0.003	0.01
Trapezoidal, 500 A	6	16	+0.08	0.06
	3	16	+0.03	0.04
	1.5	8	+0.009	0.02
Trapezoidal, 1300 A	4	22	+0.07	0.06
	2	22	+0.04	0.03
	0.2	11	+0.005	0.03

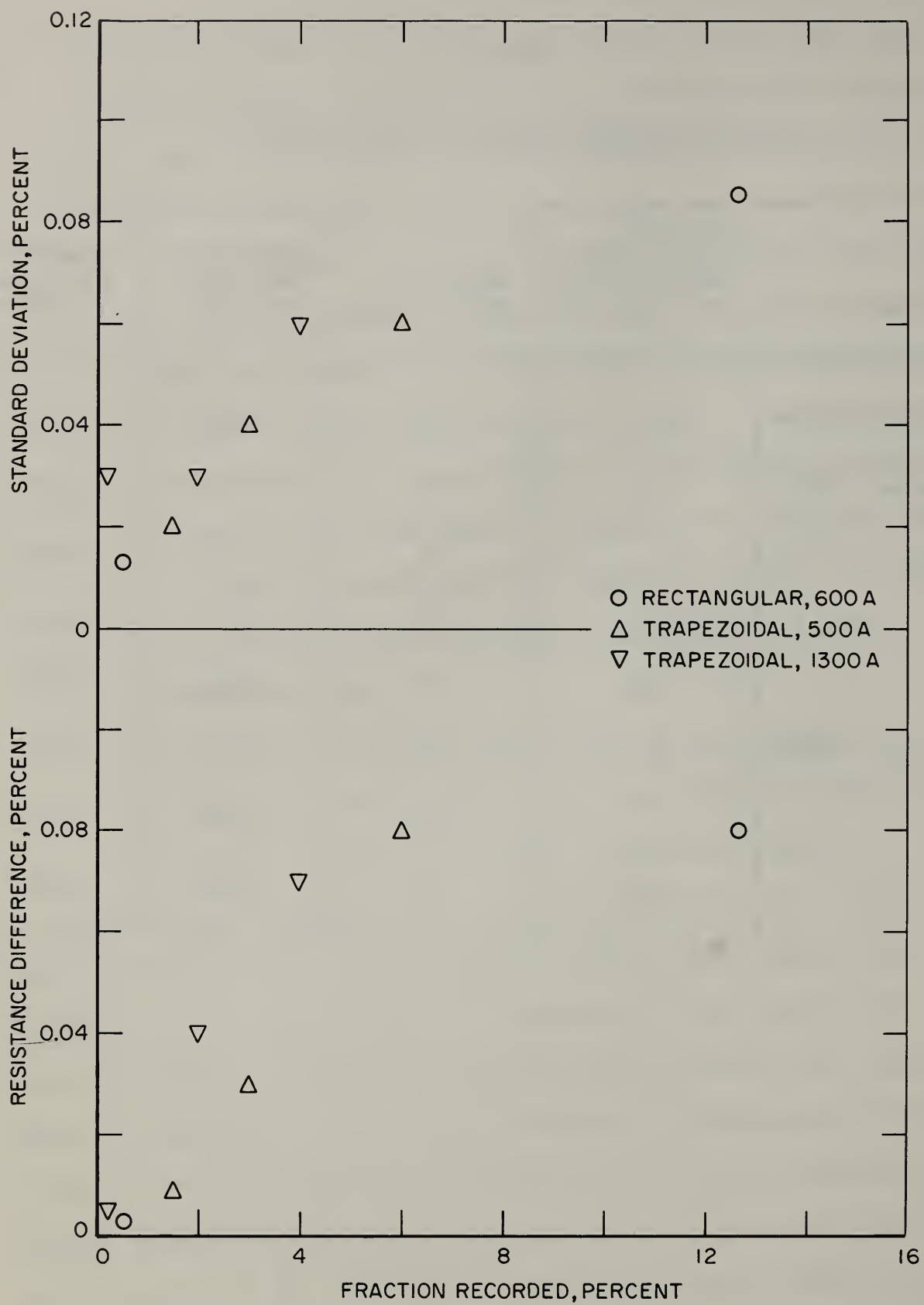


Figure 6. Variation of Resistance Difference and Standard Deviation of an Individual Determination of Resistance as a Function of Percentage of Signal Recorded on Oscilloscope.

to zero as the fraction recorded approached zero, whereas the resistance corresponding to the negative limit of the standard deviation remained almost constant. There is apparently a bias of unknown origin in the oscilloscope recordings.

The possibility of decreasing the number of calibration measurements is indicated by the fact that calibration factors at a given oscilloscope position are reproducible from one experiment to another on a given day to about 1 percent. The results reported in these experiments were obtained with one calibration between each two pulses.

The quasi-dynamic experiments described in Section 3 (with steady-state current of approximately 12 A and effective measurement duration of 50 ms) produced the following results: for 20 measurements at each suppression level recorded, the voltage oscilloscope showed a mean systematic error of -0.027 percent at 90 percent suppression and -0.003 percent at 98.9 percent suppression; the current oscilloscope +0.024 percent at 92 percent suppression and -0.004 percent at 99.2 percent suppression. At the higher fractions recorded, the systematic errors for voltage and current were each about one-third the systematic error of a resistance measurement and were opposite in sign. This limited group of data would favor the idea that the power measurements would be no less accurate than the resistance measurements.

There are several sources of error that contribute to the measured difference between steady-state and pulse resistance values. Steady-state resistance measurements are one or two orders of magnitude more accurate than pulse measurements. Therefore, most of the difference can be attributed to errors in pulse measurements. A list of major sources of error and their estimated magnitudes in oscilloscopic measurement of a variable in dynamic experiments is given in Table 2. It may be noted that the table includes also errors due to phenomena affecting the components of the overall system in addition to the suppression unit-oscilloscope combination.

6. Conclusions

The results of the present investigation have shown that it is possible to measure variables in dynamic experiments with an accuracy of 0.1 to 0.01 percent using an improved oscilloscopic technique. This method is applicable primarily to dynamic experiments where the pulse shape is rectangular or flat trapezoidal.

The method was checked by conducting pulse experiments of millisecond time resolution, in which the resistance of an Inconel tube measured under dynamic conditions was compared with its direct-current value. An increase of one or two orders of magnitude in the measurement accuracy was achieved by (1) suppressing the major portion of the signals by known constant voltages, and (2) providing time synchronization between traces on different oscilloscope screens. It was observed that the increase in accuracy was approximately proportional to the suppression level.

Table 2

LIST OF MAJOR SOURCES OF ERROR IN OSCILLOSCOPIC
MEASUREMENT OF A VARIABLE USING SUPPRESSION

Source of Error	Error (percent)		
	On Overall Signal	On Recorded Portion	On Suppressed Portion
Skin effect	< 0.01		
Self-inductance [*]	0.0002-0.02		
Mutual-inductance	< 0.01		
Temperature variations	< 0.01		
Frequency response ^{**}	< 0.01		
Time synchronization		0.05	
Oscillogram reading		0.1	
Calibration		1	
Suppression voltage			0.001
Potentiometer, etc. ^{***}			0.005

* The exact value depends upon the nature of the pulse and geometry of resistance across which potential measurements are made.

** The frequency response of the suppression units was checked for frequencies up to 10 kHz.

*** The potentiometer error does not enter into a comparison of pulse and steady-state resistances, voltages, or currents, but does affect power measurements in a calorimetric experiment.

The improved oscilloscopic recording system has potential applications in various high-speed (millisecond time resolution) measurements of thermodynamic, transport, and other related properties at high temperatures with an unprecedented accuracy. The basic concept of this method, after some modifications, may also be applied to other experiments of even higher time resolution (microsecond), such as, capacitor discharge, exploding wire, etc.

Acknowledgment

The authors wish to extend their appreciation to Dr. C. W. Beckett without whose encouragement this study could not have been made.

Chapter 3

THE ENTHALPY OF SOLID AND LIQUID $\text{BeO} \cdot \text{Al}_2\text{O}_3$ FROM 1200 TO 2400°K.

S. Ishihara and E. D. West

Introduction

Measurements of the heat capacity and relative enthalpy of $\text{BeO} \cdot \text{Al}_2\text{O}_3$ from 15°K to 1200°K and derived thermodynamic properties have been reported previously [1,2,3]. These measurements have now been extended to 2400°K, to include the heat of fusion and part of the liquid range. The new measurements will permit revision of the present tables of thermodynamic quantities, which are based on extrapolations from 1200°K.

Apparatus

The apparatus used in this work has been described in an earlier report in this series [4]. A number of changes have been made since that report.

The apparatus was moved to a laboratory in which the temperature is regulated to $\pm 1^\circ\text{C}$. This environment eliminates much of the problems of the effect of room temperature on the pyrometer. The effect was further reduced by replacing some temperature-sensitive germanium transistors with silicon transistors.

A solid-state reference voltage supply for furnace control has replaced the mercury cell. The constancy of the furnace temperature depends directly on the constancy of this supply and corrections are made for variations in the furnace temperature. These changes are now so small that they have a virtually negligible effect on the measured heat ($< 0.02\%$).

A copper thermometer wound non-inductively and cemented with an epoxy resin in a groove in the copper block has replaced the platinum resistance thermometer. Comparisons made between the two over a period of years indicated that the copper thermometer was stable within the precision of measurement. Its resistance is about 80 ohms, so that the change in resistance per degree is about three times as large as the resistance change in the platinum thermometer. It also has the advantage of excellent thermal contact with the calorimeter so that its excess temperature due to heat generated by the thermometer current is $6 \times 10^{-5} \text{ }^{\circ}\text{C}$ at 2 mA, compared to $2 \times 10^{-3} \text{ }^{\circ}\text{C}$ for the platinum thermometer. The change in the excess temperature for ordinary variations in thermometer current is now negligible. Electrical calibrations with the copper thermometer in the new laboratory have a standard deviation of 0.005% compared to 0.006% with the platinum thermometer in the old location.

The insulating powders in the furnace have been replaced several times since the earlier report. These powders sinter at 2700-2800°K and become much less efficient insulators. Replacement then becomes necessary.

Routine reduction of experimental data to relative enthalpies is now done by digital computer. The probability of small errors in computation is much smaller than for hand-operated machines.

Experimental Procedure

The experimental procedure is designed to account for gains in weight of the outer container. Three or four individual experiments are made in a day and are ordered so that the first and last experiments

are duplicates. When the weight of the outer container changes between the first and last experiments, any difference in the total heat for these experiments, after appropriate corrections, is assumed to be proportional to the weight gain and intermediate experiments are to be corrected according to the weight gain in each. In practice, the correction factor in joules per milligram is determined by plotting determinations for all experiments and drawing a smooth curve through them. Above 2000°K, the correction factor is virtually constant. The magnitude of the correction ranges from negligible at 1600°K to 5% of the enthalpy of the liquid $\text{BeO} \cdot \text{Al}_2\text{O}_3$. (The liquid sample is about one-half the weight of the solid sample.)

The weight gain was formerly assumed to be due to carbon from the furnace atmosphere, but data corrected on this assumption showed systematic trends. Weights are now determined after each individual experiment, which considerably slows the work but permits the empirical correction for each experiment. The advantage of the empirical correction is that it does not assume any particular chemical process for the weight gain.

Samples and Containers

The preparation and analysis of the $\text{BeO} \cdot \text{Al}_2\text{O}_3$ are described by Furukawa and Saba [3]. Our samples were made up from a portion of this material from which the fine material had been removed with a 16-mesh screen. A few particularly dark particles were discarded. The water content was found to be 0.16% as determined in a carbon-hydrogen-nitrogen analyzer, separated by gas chromatography, and determined by thermal

conductivity. A new spectrochemical analysis of the dried sample shows small differences from the earlier one [3]: 0.01-0.1% Fe instead of 0.001-0.01, but no Ni instead of 0.01-0.1; 0.01-0.1 Mg instead of 0.001-0.01; 0.01-0.1 Si instead of <0.01.

In high-temperature work it is necessary to use a variety of samples in order to check on the possibility that a single sample is not representative in the way it loses weight or reacts with the container, for example. We have therefore used a variety of samples, as well as containers, in order to randomize these effects. To some extent, these effects are included in statistical variations in the data and not left as undetected systematic errors.

Two types of containers are used. The first type, which we call an outer container, is used at lower temperatures where weight losses from the sample are negligible. It is not sealed, so that the sample can be loaded into the container as small lumps and removed to obtain a sample and container weight for each individual experiment. The second type, used at higher temperatures and throughout the liquid range, consists of the unsealed outer container and an inner container electron-beam welded after adding a weighed amount of sample. This technique has the advantage that the weight of the inner container is virtually constant and the significant changes in weight of the outer container can be accounted for experimentally. It has the disadvantage that the experiment gives the combined enthalpy of sample plus inner container.

The samples are lettered as in Table 1:

- A. Unsealed Mo container. No prior treatment. Total weight loss in two experiments at 1700°K, 0.38%. Spectrochemical analysis showed a decrease in Cu from 0.001-0.01% to <0.001 and an increase in Mo from nil to 0.01-0.1%.
- B. Unsealed Mo container. Weight loss on first exposure to 1700°K, 0.4%; additional weight loss in first exposure to 2000°K, 0.07%; no further significant changes in weight.
- C. Unsealed Mo container. Weight loss in first exposure to 1175°K, 0.25%; additional loss at 1700°K, 0.1%.
- D. Unsealed Mo container. Weight loss on first exposure at 1175°K, 0.24%.
- G. Welded Mo inner container. Heated 6 hr in platinum crucible in flame of Meker burner before loading (approx. 1200°K). The container lost 3.06 mg during the welding process. Because of the extremely localized heating in this process the weight loss was taken to be Mo. No further significant weight changes were observed (variations less than 0.1 mg).
- H. Welded W inner container. Pretreated as E. Container lost 2.70 mg in welding. This compares with the 4.7 mg lost in earlier work on Al_2O_3 [4]. No further significant weight changes.

Results

Results of individual experiments are presented in Table 1. Corrections to the temperature have been made as described earlier [4]. The quantity of heat includes corrections for the enthalpy of the container

and contents between the final calorimeter temperature and 298.15. Data for these corrections are taken from references [5,6,7].

The number of moles of $\text{BeO} \cdot \text{Al}_2\text{O}_3$ were calculated from weight in vacuo, using a molecular weight of 126.9728 (density 3.71 g/cm³).

The enthalpy of the solid can be represented by the equation

$$\begin{aligned} H_T - H_{298.15} = & (.303002)T - (5.43721)10^{-5} T^2 + (1.25980)10^{-8} T^3 \\ & (56.1960) \ln(T) + 234.342 \text{ kilojoules/mole} \end{aligned} \quad (1)$$

$$1175^\circ < T < 2025^\circ, \quad T = ^\circ\text{C} + 273.15$$

Experimental points from the work of Ditmars and Douglas [1] for the range 973 to 1173°K were included in obtaining eq (1) so that it would join smoothly with their data. The root-mean-square deviation of a single enthalpy determination (1 empty and 1 full) from this equation is 0.18%. The enthalpy of the liquid can be represented by the equation

$$\begin{aligned} H_T - H_{298.15} = & -(0.950768)T + (.267103)10^{-3} T^2 \\ & + (1.31156)10^3 \text{ kilojoules/mole} \end{aligned} \quad (2)$$

$$2168^\circ < T < 2350^\circ, \quad T = ^\circ\text{C} + 273.15$$

The root-mean-square deviation of a single enthalpy determination (3 individual experiments) is .03%.

Some results have been obtained for the enthalpy of molybdenum. When sealed inner containers are used, the enthalpy of the container material must be subtracted from the experimental result to obtain the enthalpy of the sample. Results are therefore sensitive to the value used for the enthalpy of the container material. Because differences between laboratories are rather large for high temperature enthalpies, the uncertainty in the enthalpy of the sample can be reduced if the enthalpy

of the container material is measured in the same apparatus. We had not determined the enthalpy of molybdenum in our apparatus, so the enthalpy of a sample of molybdenum (76.1002 mM) used for the inner container was determined simultaneously with the beryllium aluminate. The experimental data are included in Table 1. On a molar basis these enthalpy data are 51.60 kJ/mole at 2027.3°K; 55.11 at 2121.0; 57.94 at 2191.9; 59.91 at 2244.7. These data are lower than those reported by Kirillin, et al [8] by 0.48, 0.42, 0.16 and 0.08% respectively. These differences are well within their estimated maximum error of $\pm 1.2\%$.

Discussion

At 1200°K, eq (1) gives a value for the enthalpy of $\text{BeO} \cdot \text{Al}_2\text{O}_3$, 0.17% greater than the corresponding equation of Ditmars and Douglas [1]. This difference is well within the accuracy of 0.3% of our pyrometer calibration. At 2100°, the enthalpy calculated from eq (1) is 2.5% greater than the value from their extrapolation. This agreement is rather good for such a long extrapolation, but the difference is large enough to warrant the preparation of new tables of thermodynamic properties.

The heat of fusion at 2143°K, which we take to be the melting point, is 173.8 kJ/mole. The heat of fusion is the difference between eqs (1) and (2). Since the difference varies slightly with temperature, the choice of melting point has some influence on the heat of fusion. Lang, et al. [9], give the melting point of $\text{BeO} \cdot \text{Al}_2\text{O}_3$ as $2143 \pm 10^\circ\text{K}$. Our enthalpy data bracket the melting point. In the experiments at 2132°, the sample is about one-half melted. In the experiments at 2168°, the sample is entirely melted, because this point fits the equation for the

liquid. These data are consistent with a melting point of $2143 \pm 10^\circ\text{K}$. The change in the heat of fusion calculated from eqs (1) and (2) for a 10°K uncertainty is about 0.25 kJ/mole, which is probably less than some other uncertainties.

A larger uncertainty is associated with the amount of impurity present in the liquid — principally from the containers. This amount appears to depend on the container material, since the experiments in tungsten in the premelting range indicate a higher melting point than those in molybdenum. Analytical data are not yet available for use in estimating this uncertainty.

Another uncertainty is associated with the uncertainty in eqs (1) and (2). The standard deviation of the difference is 0.18% or 0.31 kJ/mole; the uncertainty in the heat of fusion would be slightly larger because the curves are extrapolated.

References

- [1] D.A. Ditmars and T.B. Douglas, NBS Report 9028 to AFOSR, 1 Jan. 1966, p. 80; J. Res. Natl. Bur. Stds. 71A, 89 (1967).
- [2] T.B. Douglas and W.H. Payne, NBS Report 8186 to ARPA, 1 Jan. 1964, p. 62.
- [3] G.T. Furukawa and W.G. Saba, NBS Report 8186 to ARPA, 1 Jan. 1964, p. 50; J. Res. Natl. Bur. Stds. 69A, 13 (1965).
- [4] E.D. West and S. Ishihara, NBS Report 9028 to AFOSR, 1 Jan. 1966, p. 71.
- [5] G. T. Furukawa, private communication.
- [6] K. F. Starrett and W.E. Wallace, J. Am. Chem. Soc. 80, 3176 (1958).

- [7] M. L. Reilly and W. G. Saba, "Analysis of Specific Heat Capacity Data from Literature on Cr, Mo, and W". To be published.
- [8] V. A. Kirillin, A. E. Sheindlin, and V. Ya. Chekhovskoi, Int. J. Heat Mass Transfer 5, 1 (1962).
- [9] S. M. Lang, C. L. Fillmore, and L. H. Maxwell, J. Res. Nat. Bur. Std. 48, 298 (1952).

*

Table 1. Enthalpy Measurements of Solid, Premelting, and Liquid $\text{BeO} \cdot \text{Al}_2\text{O}_3$.

Furnace Temperature °K, Date, and Container material	Heat to Calorimeter at 298.15°K	Millimoles $\text{BeO} \cdot \text{Al}_2\text{O}_3$, and Sample Designation	Enthalpy $H_L - H_{298.15}$	% Deviation from Smoothed Curve
	Joules		Kilojoules/mole	
1181.1 2-6-67 Molybdenum	4549.9	15.456 D	139.62	.028
	2391.9			
	2391.1	16.370 B	139.69	.078
	4677.8			
1181.1 2-3-67 Mo	4674.4	16.370 B	139.52	-.044
	2390.5			
	2390.5	16.370 B	139.60	.011
	4675.8			
1306.2 2-21-67 Mo	2760.7	16.370 B	162.29	.038
	5417.4			
	5418.7	16.370 B	162.38	.093
	2760.6			
1408.9 2-13-67 Mo	6039.0	16.369 B	181.21	.063
	3072.7			
	3072.7	16.369 B	181.91	.052
	6038.5			
1409.0 1-30-67 Mo	6154.3	17.025 C	181.07	-.023
	3071.6			
	3071.3	17.022 C	181.20	.048
	6155.7			
1509.3 2-16-67 Mo	3376.7	16.369 B	200.01	.108
	6650.6			
	6651.5	16.369 B	199.93	.069
	3378.9			
1608.2 2-27-67 Mo	7272.5	16.368 B	218.18	-.155
	3701.3			
	3703.0	16.368 B	218.31	-.094
	7276.5			
1713.6 1-18-67 Mo	7935.1	16.477 B	239.33	.209
	3991.6			
	3989.9	16.476 B	239.77	.390
	7940.3			
1716.0 1-11-67 Mo	3973.0	16.603 A	239.23	-.034
	7945.0			
	7945.4	16.603 A	239.21	-.041
	3973.7			
1813.9 2-23-67 Mo	8601.2	16.369 B	258.28	-.123
	4373.4			
	4374.8	16.369 B	258.08	-.202
	8599.4			
1917.4 3-1-67 Mo	4771.9	16.368 B	278.74	-.256
	9334.1			
	9336.0	16.367 B	278.95	-.189
	4770.4			
2021.8 1-20-67 Mo	10048.7	16.387 B	300.62	-.148
	5122.4			
	5120.2	16.371 B	300.98	-.027
	10047.6			
2027.3 5-24-67 Tungsten, Sample in sealed Mo	4330.3	10.8297 G	303.72	.496
	9419.7			
	(8258.5)**			
	4332.6			

* M.W. 126.9728
Density 3.71 gm/cc.

** Molybdenum experiment.

Table 1. (Cont'd.)

Enthalpy Measurements of Solid, Premelting, and Liquid $\text{BeO} \cdot \text{Al}_2\text{O}_3$. *

Furnace Temperature °K, Date, and Outer and Inner Container material	Heat to Calorimeter at 298.15°K	Millimoles $\text{BeO} \cdot \text{Al}_2\text{O}_3$, and Sample Designation	Enthalpy $H_T - H_{298.15}$	% Deviation from Smoothed Curve
	Joules		Kilojoules/mole	
2091.7 6-5-67 Tungsten, Molybdenum	4620.5	10.8297 G	321.37	
	9983.4			
	4626.8			
2121.0 5-29-67 W, Mo	4611.1	10.8297 G	380.29	
	10649.0			
	(8804.1)** 4609.8			
2132.8 7-17-67 W, W	5600.0	7.5154 H 7.5154 H	397.56 398.63	
	12210.6			
	12229.2 5610.6			
2168.1 7-26-67 W, W	5737.5	7.5154 H 7.5154 H	505.81 506.03	.01
	13243.0			
	13244.6			
2191.9 6-7-67 W, Mo	12494.9	10.8297 G 10.8297 G	510.30	-.11
	(9359.4)** 4951.5			
	12497.3			
2244.7 6-9-67 W, Mo	5243.6	10.8297 G	523.73	.10
	(9802.6)** 130028			
2244.8 6-23-67 W, W	5365.6	7.5154 H	522.91	-.06
	13174.9			
	5357.6			
2297.6 7-7-67 W, W	13899.3	7.5154 H 7.5154 H	537.15	.01
	5858.5			
	13909.5			
2344.4 7-11-67 W, W	6203.7	7.5154 H	550.58	-.01
	14456.6			
	6190.6			

* M.W. 126.9728
Density 3.71 gm/cc

** Molybdenum experiment.

THE INFRARED SPECTRUM OF MATRIX ISOLATED CsOH and CsOD

N. Acquista, S. Abramowitz, and D. R. Lide

ABSTRACT

The infrared spectra of matrix isolated CsOH and CsOD have been observed. Both the CsO stretching modes and the bending modes have been assigned for both isotopic species. The isotopic shift observed for the bending mode, ν_2 , satisfies the relationship expected for a linear molecule using the bond distances recently derived from the microwave spectra of these species. ν_1 of CsOH is at 335.6 cm^{-1} , while a value of 330.5 cm^{-1} is found for CsOD. ν_2 is found at 309.8 and 302.4 cm^{-1} for CsOH and at 230 and 225.6 cm^{-1} for CsOD.

INTRODUCTION

Recently successful efforts to study the molecular structure of gaseous metal hydroxides were reported by Lide and co-workers.^{1,2} They observed the microwave spectrum of monomeric KOH and CsOH in the saturated vapor above the liquid in the temperature range of 500 to 600°C . Previous attempts to observe the infrared and microwave spectra of metal hydroxides have been largely unsuccessful except for the work of Spinar and Margrave,³ who observed weak bands in the infrared spectra of NaOH, KOH, and RbOH vapors. Other spectral observations on the metal hydroxides have been confined to the near infrared mainly in solutions and crystals.⁴ Little structural information about the gaseous species was obtained from these studies. With significant amounts of monomeric CsOH present in the vapor, as determined both by mass spectrometric^{5,6} and microwave studies^{1,2} it appeared possible that the CsOH monomeric species could be isolated in an argon matrix at liquid hydrogen temperatures and its infrared spectrum observed. The results of such a study of CsOH and CsOD are reported here.

EXPERIMENTAL

Since the experimental techniques used have been described in detail by Mann *et al.*⁷ only a short account will be given here. The spectra were obtained with a Perkin-Elmer 301 grating spectrophotometer with a wavenumber range of 4000 to 50 cm^{-1} .⁸ Refrigeration was provided by an Air Products Cryotip operated in the range of 20 to 33°K. An electron bombardment furnace contained in a vertical housing was used to vaporize the samples from silver double-boiler Knudsen cells.

The CsOH, which was obtained from commercial sources, was heated gradually to a temperature of 700°C to remove water and other volatile impurities. It was necessary to outgas the sample for periods greater than 24 hours in order to remove the impurities which masked the spectrum of monomeric CsOH. The CsOD, which was prepared from CsOH,¹ was treated similarly. The difficulties in estimating the temperature of the effusing gas and the ratio of the matrix diluent to the sample (M/S) have been discussed.^{7,9} It is felt that M/S ratios in the range 300:1 to 1000:1 and temperatures to 700°C are representative of the conditions utilized in these experiments.

Diffusion studies, in which the deposited sample was allowed to warm up to 33°K were performed in an effort to differentiate between monomeric and polymeric species. This method proved to be unsuccessful since CsOH does not diffuse readily up to 33°K, probably because of its relatively large molecular weight. More useful information was obtained by studying the spectra of samples produced at several effusing temperatures. As the temperature of the gas effusing from the double boiler of a Knudsen cell is increased the mole ratio of the monomer to polymer is enhanced, thus permitting the monomer bands to be identified.

The spectrum was calibrated by using atmospheric water lines as standards. Spectral slit widths of about 1 cm^{-1} were used and frequencies of the observed bands are accurate to about 0.5 cm^{-1} .

EXPERIMENTAL RESULTS AND DISCUSSION

CsOH and CsOD have three fundamental frequencies; two of these, ν_1 and ν_3 are approximately Cs-O and O-H stretching modes, while ν_2 is the bending mode. The approximate frequencies of two of the fundamental modes have been predicted by Lide and Kuczkowski from

satellite intensity measurements in the microwave spectrum.¹ They estimate $\nu_1 = 400 \pm 80 \text{ cm}^{-1}$, while a frequency of about 300 cm^{-1} is quoted for ν_2 . It is also expected that the Cs-O stretching mode in CsOH would be close in frequency to the CsF diatomic fundamental at 352 cm^{-1} .¹⁰ Three strong bands appear in the infrared spectrum in the region of $600\text{-}200 \text{ cm}^{-1}$. With prolonged deposition, weaker features begin to appear as shown in Fig. 1a. When the temperature of the furnace is raised, thereby increasing the mole ratio of monomer, the features below 300 cm^{-1} lose intensity with respect to the absorption bands above 300 cm^{-1} as can be seen in Fig. 1b. The features at 335.6 and 309.8 and 302.4 cm^{-1} maintained their intensity relative to each other in the two samples. These features are therefore due to the same molecular species. The bands which are modulated with temperature are due to polymeric species of CsOH, leaving the bands at 335.6 , 309.8 , and 302.4 cm^{-1} assigned to monomeric CsOH.

Fig. 2 shows the spectrum of CsOH and CsOD in the region of 350 to 300 cm^{-1} under conditions of higher resolution. The CsOD spectrum shown in this figure contains a residual amount of CsOH. The band position for both isotopic species together with their assignment are given in Table 1. The only other strong feature in the spectrum of CsOD is shown in Fig. 3. This band which is located at 225.6 cm^{-1} , is complex with shoulders on the high frequency side. It is included in the table with estimates for the shoulder frequencies.

Since the 335.6 cm^{-1} band in CsOH is shifted only 5.1 cm^{-1} by deuterium substitution, it may be readily assigned to ν_1 , the Cs-O stretching mode. This frequency is also consistent with the estimate of $400 \pm 80 \text{ cm}^{-1}$ from the microwave spectrum, and it is close to the fundamental of CsF at 352 cm^{-1} . The multiplet at $302\text{-}309 \text{ cm}^{-1}$ in CsOH must then be assigned to ν_2 , the bending mode. In CsOD the corresponding band appears at 225 cm^{-1} as a broad feature with partially resolved structure. The observed isotope shift in ν_2 is in agreement with calculations, as shown in Table 1. Calculations using reasonable force constants show that the isotope shift observed for ν_1 is the right order of magnitude.

The OH stretching mode ν_3 , which is expected in the region of 3600 cm^{-1} in CsOH and 2500 cm^{-1} in CsOD could not be observed because of the heavy water absorption in these regions.

CONCLUSIONS

The spectra of matrix isolated CsOH and CsOD have been observed. Assignments of ν_1 and ν_2 have been made which are supported by isotope shifts and which are consistent with estimates from the microwave spectrum. The infrared and microwave data indicate that the Cs-O bond is highly ionic and that the bending force constant is very low. The force field will be discussed in more detail when data are available on the other alkali hydroxides.

REFERENCES

1. D. R. Lide, R. L. Kuczkowski, J. Chem. Phys. 46, 4768 (1967).
2. R. L. Kuczkowski, D. R. Lide, and L. C. Krisher, J. Chem. Phys. 44, 3131 (1966).
3. L. H. Spinar and J. L. Margrave, Spectrochem. Acta 12, 244 (1958).
4. K. Nakamoto, Infrared Spectra of Inorganic and Coordination Compounds (John Wiley and Sons, Inc., New York, 1963, p. 73).
5. R. C. Schoonmaker and R. F. Porter, J. Chem. Phys. 28, 454 (1958).
6. R. F. Porter and R. C. Schoonmaker, J. Chem. Phys. 62, 237 (1958).
7. D. E. Mann, G. V. Calder, D. White, K. S. Seshadri, and M. J. Linevsky, J. Chem. Phys. 46, 1138 (1967).
8. Certain commercial instruments are identified in this paper to specify completely the experimental procedure. In no case does such identification imply a recommendation or endorsement by the National Bureau of Standards.
9. S. Abramowitz, N. Acquista, and I. W. Levin, To be published.
10. S. E. Veazey and W. Gordy, Phys. Rev. 138, A1303 (1965).
11. G. Herzberg, Molecular Spectra and Molecular Structure II. Infrared and Raman Spectra of Polyatomic Molecules (D. Van Nostrand Co. Inc., Princeton, New Jersey, 1945).

Table 1. Identification and classification of the CsOH and CsOD fundamental frequencies.

	CsOH	CsOD	$\nu_{\text{CsOD}}/\nu_{\text{CsOH}}$
ν_1	335.6	330.5	
ν_2	309.8	230	$0.742 \pm .003$
	304.2 sh		
	302.4	225.6	$0.746 \pm .003$
ν_3	?	?	
		calculated ratio 0.745	

MATRIX ISOLATED CSOH IN ARGON

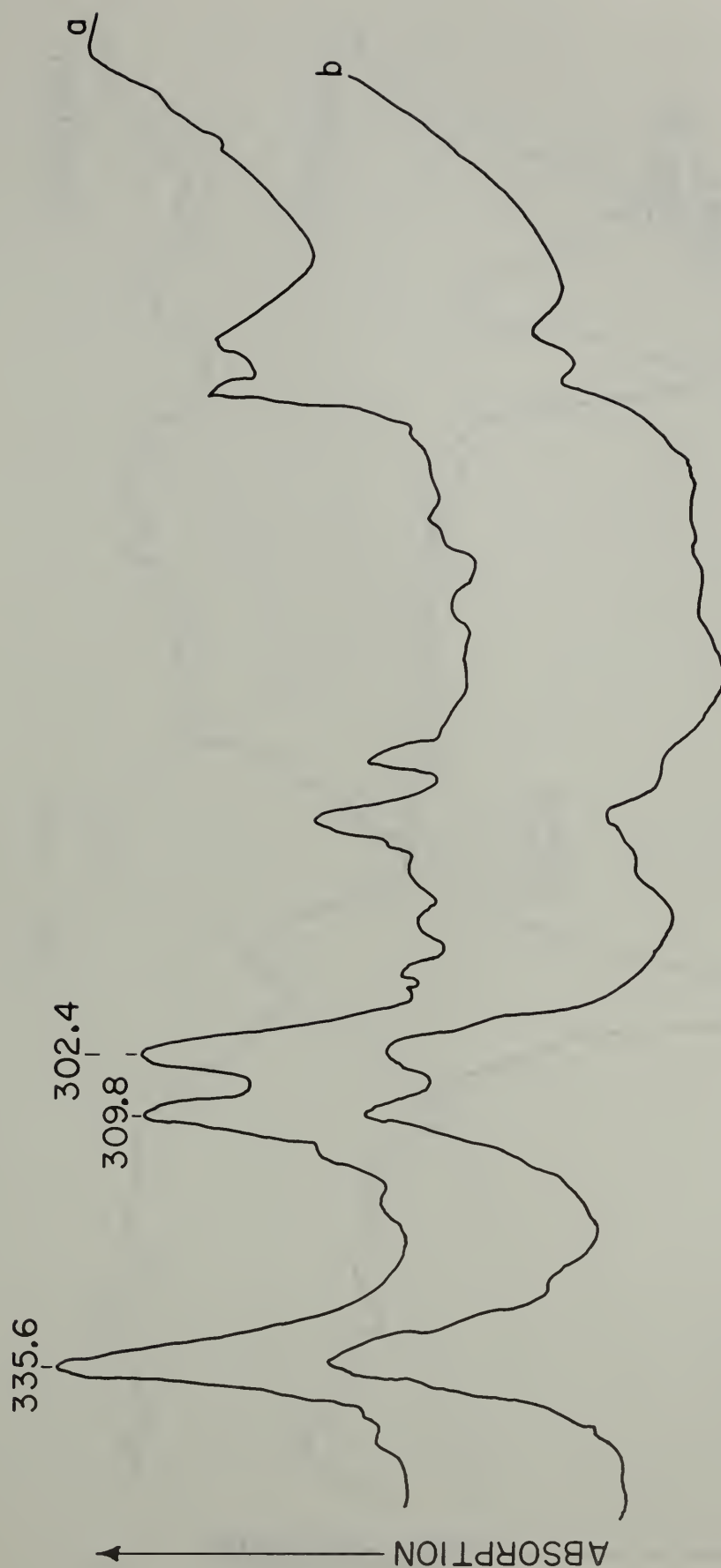


Fig. 1 - The spectrum of matrix isolated CSOH observed from samples effusing at two temperatures (b higher than a).

MATRIX ISOLATED CsOH AND CsOD

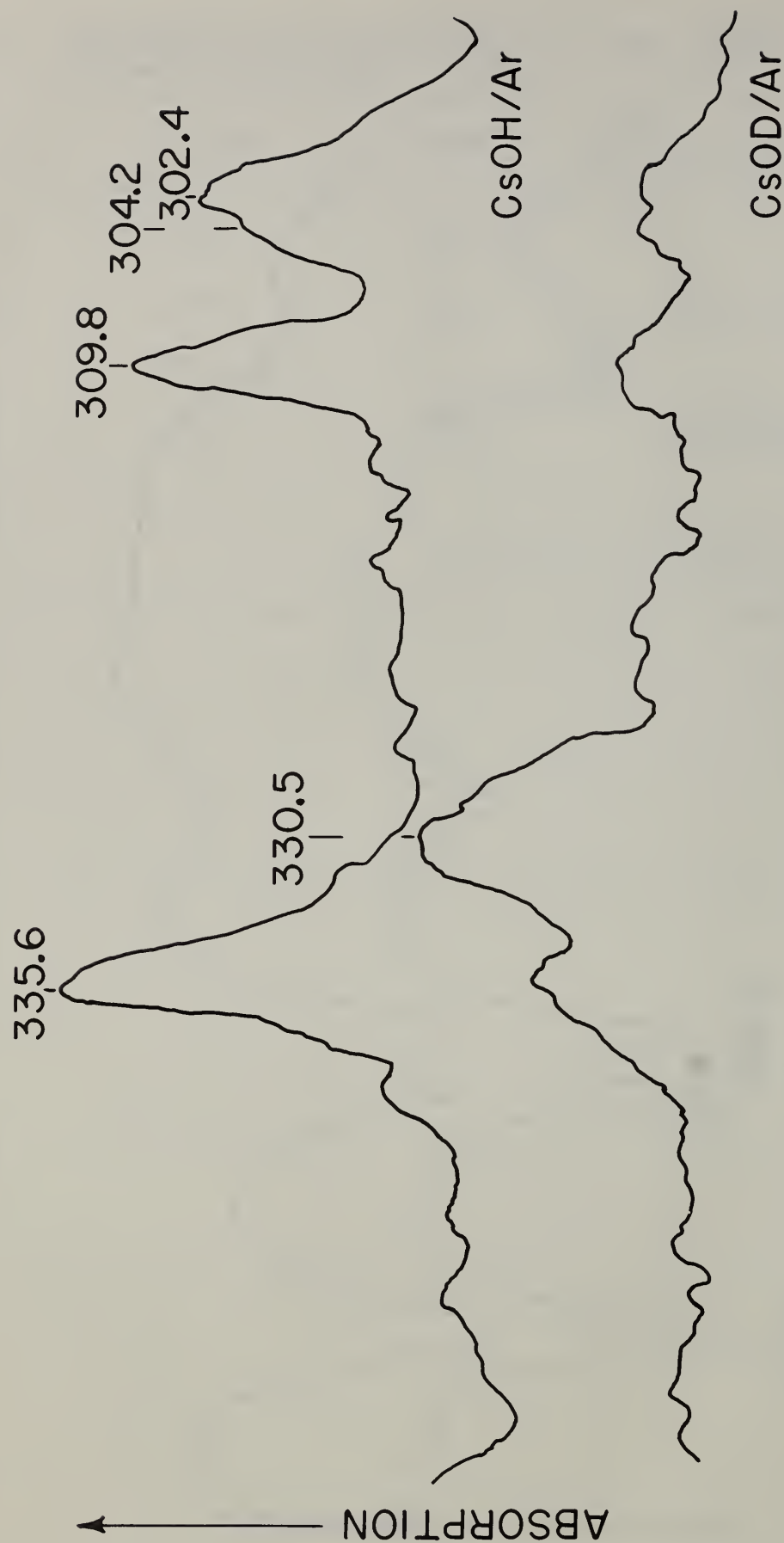


Fig. 2 - The spectrum of matrix isolated CsOH and CsOD.

MATRIX ISOLATED CsOD

230. 225.6

ABSORPTION



Fig. 3 - The spectrum of matrix isolated CsOD.

INFRARED MATRIX SPECTRA OF LITHIUM FLUORIDE

Stanley Abramowitz, Nicolo Acquista, and Ira W. Levin

ABSTRACT

Evidence for a linear dimer Li_2F_2 has been obtained by extending the spectral measurements² for matrix isolated lithium fluoride into the far infrared region. The vapors from solid ^6LiF , ^7LiF , and $^6\text{LiF}/^7\text{LiF}$ were deposited in argon matrices at liquid hydrogen temperatures. Vibrational assignments were made on the basis of the following linear species: $^6\text{Li}_2\text{F}_2$, $^7\text{Li}_2\text{F}_2$, $^6,^7\text{Li}_2\text{F}_2$, and $^7,^6\text{Li}_2\text{F}_2$. Although the specific geometry of the dimer could not be determined, a normal coordinate analysis supported the spectral interpretation of a linear structure ($C_{\infty v}$).

INTRODUCTION

Infrared spectra of matrix isolated lithium fluoride species indicate the formation of, at least, a rhomboid dimer of D_{2h} symmetry in addition to the presence of the monomeric form.¹⁻⁵ Several prominent spectral features, however, are not satisfactorily assigned to a specific LiF system, particularly, the sets of relatively strong bands that occur in argon matrices at 722 and 495 cm^{-1} and at 769 and 522 cm^{-1} for the isolated vapors of ^7LiF and ^6LiF , respectively. Since the matrix absorption bands for the two isotopic forms of the monomer appear at 842 and 888 cm^{-1} , some workers attribute the additional bands to monomeric LiF¹⁻² absorptions arising from supplementary matrix trapping sites. Alternatively, other investigators believe that the origin of the unassigned bands may lie in the formation of either a trimer or higher polymeric species.^{3,6} Reddington, however, suggests that the controversial features possibly reflect the two high frequency stretching modes of a matrix stabilized linear dimer.⁵

In the present study the infrared measurements of matrix isolated LiF are extended into the far infrared region in an effort to characterize the absorptions of a linear dimer. The use of several isotopic species, as well as mixtures of various isotopic compositions, facilitated the vibrational assignment. A normal coordinate analysis provided additional support for the spectral interpretation of a linear Li_2F_2 structure.

EXPERIMENTAL

The methods used to isolate high temperature species in rare gas matrices have been described in detail elsewhere.⁷ Depending upon the spectral region studied, the infrared spectra were obtained either with a Perkin-Elmer model 99G monochromator or a Perkin-Elmer model 301 spectrophotometer.⁸ An Air Products Cryotip supplied the necessary refrigeration at liquid hydrogen temperatures, while an electron bombardment furnace vaporized the LiF samples. ⁶LiF and ⁷LiF samples, supplied by the Stable Isotopes Division, Oak Ridge National Laboratory, were evaporated in double oven crucibles and were deposited in an argon matrix on thin CsI windows. These samples, as well as 1:1 isotopic mixtures, were investigated in the region from 1000 to 150 cm⁻¹. The identification of various molecular species required warm-up procedures in which the rates of appearance or disappearance of bands were measured. Supplementary information for interpreting the data was obtained by trapping in the matrix the LiF effusing at various temperatures from the double oven Knudsen cell. The difficulties in estimating both the temperature of the effusing gas and the ratio of the matrix diluent to the sample (M/S) has been discussed.^{1,2,5,7} It is felt that M/S ratios of 500:1 to 1000:1, and temperatures of 800° to 1200°C are representative of the conditions used in these experiments.

Internal and external absorption standards were used to calibrate the observed spectra. Spectral slit widths of about 0.5 cm⁻¹ and 1.0 cm⁻¹ were obtained in the region from 1000 to 400 cm⁻¹ and from 400 to 150 cm⁻¹, respectively.

EXPERIMENTAL RESULTS AND DISCUSSION

400-150 cm⁻¹ Region

The observed infrared spectrum of matrix isolated ⁷LiF, ⁶LiF, and a 1:1 mixture of ⁷LiF/⁶LiF appears in Fig. 1 for the 240-300 cm⁻¹ region. The strong features at 293.8 and 276.4 cm⁻¹ in ⁶LiF and ⁷LiF are assigned to the lowest infrared active vibration ν_6 of the planar rhomboid dimer of LiF. Confirmation is given by the triad at 293.8, 284.7, and 276.4 cm⁻¹ in the 1:1 mixture of ⁷LiF/⁶LiF with the expected relative intensities of 1:2:1 for a dimer with equivalent lithium atoms. A sample containing equal parts of ⁶LiF and ⁷LiF would be expected to exhibit bands of relative intensity of 1:2:1 and 1:1:1:1 for the cases of a dimer containing equivalent and nonequivalent lithium atoms, respectively. The observed ratio of 1.0630 for $\nu_6(^{6}\text{Li})/\nu_6(^{7}\text{Li})$ agrees quite well with the calculated ratio of 1.0594 from the product rule for this mode. The behavior

of this absorption area upon warming the matrix and allowing diffusion to occur is identical to the bands at 626, 646, and 661 cm^{-1} and 537, 550, and 569 cm^{-1} which were previously assigned to the ν_4 and ν_5 species of the rhomboid dimer of $^7\text{Li}_2\text{F}_2$, $^6\text{Li}^7\text{LiF}_2$, and $^6\text{Li}_2\text{F}_2$, respectively.² The three sets of features also exhibit the same relative intensity diminution relative to the monomeric species when spectra are observed in samples deposited from higher effusing temperatures.

The other set of bands in this region exhibit a different rate of disappearance on warming the matrix than that demonstrated by the features ascribed to the ring shaped dimer. Also, the diminution in intensity of these bands upon deposition from a higher effusing temperature relative to the change in intensity of the monomeric species is distinctly less than that observed for the ring shaped dimer. These features occur at 270.2 and 261.0 cm^{-1} for ^6LiF and at 255.2 and 245.7 cm^{-1} for ^7LiF . The spectrum of the isotopic mixture gives additional bands at 265.5, 260.1, 252.9 and 249.6 cm^{-1} . These absorptions are assigned to the linear dimer species. Since the frequencies for the pure isotopic molecules are less than 10 cm^{-1} apart, the vibrations probably correspond to different symmetry representations; namely, the stretching (Σ) and bending (π) modes of the dimer. Thus, we assign the bands at 255.2, 270.2, 265.5, and 260.1 to the ν_3 vibration, the lowest stretching mode, of $\text{F-}^7\text{Li-F-}^7\text{Li}$, $\text{F-}^6\text{Li-F}^6\text{Li}$, $\text{F-}^7\text{Li-F-}^6\text{Li}$, and $\text{F-}^6\text{Li-F-}^7\text{Li}$, respectively. The bands at 245.7, 261.0, 252.9, and 249.6 cm^{-1} then correspond to the ν_4 bending modes of $\text{F-}^7\text{Li-F-}^7\text{Li}$, $\text{F-}^6\text{Li-F-}^6\text{Li}$, $\text{F-}^7\text{Li-F-}^6\text{Li}$, $\text{F-}^6\text{Li-F-}^7\text{Li}$, respectively. The measurements reported were obtained under high resolution conditions than those shown. In addition to trapping the species from the isotopic mixtures, thick deposits of the nearly pure isotopic samples, as well as 1:1 to 1:3 mixtures were observed. Since the natural and enriched samples of the ^6LiF and ^7LiF , respectively, contained about 5% of the other isotope, the thick deposits of the individual species gave features of the mixed isotope spectra with the appropriate intensity ratios expected.

Absorption bands at 152.8 and 157.1 cm^{-1} for the ^7LiF and ^6LiF samples presented the same behavior upon diffusion in the matrix and the same intensity diminution upon deposition from a higher temperature as the previous features. The spectrum appears in Fig. 1b. The mixed isotopic sample indicates a superposition of the spectra of the two pure samples. These bands are assigned to ν_5 of the $\text{F-}^7\text{Li-F-}^7\text{Li}$ and $\text{F-}^6\text{Li-F-}^6\text{Li}$ species. It was not possible to resolve the spectrum for the mixture into the $\text{F-}^6\text{Li-F-}^7\text{Li}$ and

$F-^7Li-F-^6Li$ components, although it appears clear from the normal coordinate analysis described below that the frequencies for ν_5 of these mixed species are between about 152 and 157 cm^{-1} .

Several other absorption features, both broad and narrow, were observed in the spectra of the pure and mixed isotopes. Their behavior upon diffusion, however, indicates that these bands arose from systems other than either the dimeric or monomeric species.

900-400 cm^{-1} Region

The absorption bands arising from the two stretching modes of a linear Li_2F_2 molecule are expected in this region. The higher frequency stretching mode of Li_2F_2 occurs at 767.8 and 720.5 cm^{-1} in 6Li_2F_2 and 7Li_2F_2 , respectively. Spectra of these regions are given in Figs. 1c and 1d. In addition to these features, one observes the two stretching modes ν_4 and ν_5 (B_{2u} and B_{3u}) of the rhomboid dimer, as well as the bands for the monomer. These species occur at substantially the same frequencies as reported previously.¹⁻⁵

Features also appear which are attributed to species other than the monomer or either dimer. These bands increase in intensity upon diffusion which indicates that they are possibly due to a polymer of three or more LiF aggregates. No further discussion concerning the species responsible for these absorptions will be given here.

High resolution spectra of 1:1 mixtures of $^6LiF/^7LiF$ show the 767.8 cm^{-1} band split into two components of equal intensity. These correspond to ν_1 of $F-^6Li-F-^6Li$ and $F-^6Li-F-^7Li$ at 767.8 and 766.8 cm^{-1} , respectively. The approximate equality of intensities of these two components (in a 1:1 isotopic mixture) is expected and provides further evidence for a dimer with two nonequivalent lithium atoms. The corresponding absorption in 7LiF is found at 720.5 cm^{-1} . This band is complicated by a shoulder to the low frequency side which is more prominent in a 1:1 mixture of $^6LiF/^7LiF$. Two weaker bands also were found in the mixed isotopic sample. These features, as shown by diffusion experiments, are not due to the linear dimeric form. Careful measurements of 7LiF and various mixtures of 6LiF and 7LiF indicate that ν_1 of $F-^7Li-F-^7Li$ is at 720.5 cm^{-1} while ν_1 of $F-^7Li-F-^6Li$ is at 720.8 cm^{-1} . The small isotope shifts for the ν_1 and ν_2 modes, as seen in the normal coordinate calculations, supports the existence of the linear dimer model.

Features attributed to the ν_2 symmetric stretching mode of F-Li-F-Li occur at 497.5 and 518.6 cm^{-1} in ${}^7\text{Li}_2\text{F}_2$ and ${}^6\text{Li}_2\text{F}_2$, respectively. The mixed isotopic spectra, given in Fig. 1e, show features at 493.5 and 514.4 cm^{-1} that are not due to any dimeric or monomeric species. These bands increase markedly in intensity upon diffusion and may be due to the same species responsible for the unassigned absorptions in the 768 and 721 cm^{-1} regions. Measurements of various mixed isotopic samples of ${}^7\text{LiF}$ and ${}^6\text{LiF}$ show ν_2 of F- ${}^6\text{Li}$ -F- ${}^7\text{Li}$ to be at 497.8 cm^{-1} , while the corresponding frequency of F- ${}^7\text{Li}$ -F- ${}^6\text{Li}$ is at 518.3 cm^{-1} . In this region it was again useful to measure the spectrum of ${}^7\text{LiF}$ at 768 and 518 cm^{-1} and ${}^6\text{LiF}$ at 721 and 497 cm^{-1} with thick samples in order to obtain the mixed isotope spectrum in a 5% concentration. The sets of observed frequencies for the final assignment of the linear Li_2F_2 molecule appear in Tables III and IV, along with the calculated frequencies from the normal coordinate analysis.

The absorption spectrum of monomeric ${}^7\text{LiF}$ in the argon matrix is shown in Fig. 2. The doublet ascribed to the fundamental modes of the diatomic species ${}^7\text{LiF}$ and ${}^6\text{LiF}$ are the only absorption bands in the spectrum which exhibit reversible temperature dependent behavior. As the temperature is raised from 20-33°K, the doublet is smeared out with an apparent blue shift of about 1 cm^{-1} for one of the components. No conclusion regarding the cause of this behavior will be given here, except to note that only the absorption bands attributed to monomeric ${}^6\text{LiF}$ and ${}^7\text{LiF}$ at 842 and 888 cm^{-1} , respectively, exhibited such a phenomenon.

NORMAL COORDINATE ANALYSIS

In order to support the interpretation of a linear Li_2F_2 dimeric species, we performed a normal coordinate analysis for the four isotopic systems. Several models for the linear structure were considered; namely, a F-Li-F-Li dimer in which all bonds were equivalent, a F-Li-F-Li dimer with a bifluoride structure, and a species F-Li....F-Li containing an elongated central bond. For the normal LiF bonds of the model structures, a length of 1.51 Å was assumed, while a value of 2.01 Å from crystalline LiF was taken for the long bonds.⁹ The force field for a chosen model was first refined about the ${}^6\text{Li}$ and ${}^7\text{Li}$ isotopic species. Interaction force constants were systematically varied until close fits to the observed frequencies were attained. This force field was then used to calculate the frequencies for the mixed isotopic species, namely, the F- ${}^6\text{Li}$ -F- ${}^7\text{Li}$ and F- ${}^7\text{Li}$ -F- ${}^6\text{Li}$ molecules. In view of the assumptions concerning the bond lengths and interactions in the force constant matrix, the significance of the force field is limited. Consequently, rather than stressing the values of the individual force constants recognizing that the force field is not

unique, we prefer to emphasize the closeness of the frequency fit for the four isotopic molecules as evidence favoring the linear dimeric structure.

For a linear dimer, F-Li-F-Li of $C_{\infty v}$ symmetry, the vibrational representation is $\Gamma = 3\Sigma^+ + 2\Pi$, with the stretching vibrations occurring in the Σ^+ species and the bending modes conforming to Π symmetry. The vibrational problem was cast in terms of the internal coordinates and force constant matrix that appear in Table I. Familiar GF matrix methods were used in solving the vibrational secular equation.

Since the elements of the G matrix for the stretching vibrations are independent of bond length, the frequency fits for the Σ^+ species of the three linear dimers are equivalent. The force constants for the various stretching force constants and the comparison between the observed and calculated frequencies appear in Table II and III, respectively. Again, the force constants were refined about the ${}^6\text{Li}_2\text{F}_2$ and ${}^7\text{Li}_2\text{F}_2$ isotopes only. The frequencies for the mixed isotopes are determined from this potential function. Since a unique potential function probably cannot be determined from the frequency data alone in this manner, it is not worthwhile to refine the force field over all isotopes. The results of the normal coordinate calculation for the Π species appear in Table IV. For these vibrations, the change in geometry affects the calculated frequencies. Table IV indicates, however, that within the framework of this calculation, a distinction in geometry cannot be made decisively since the frequency fits are quite reasonable for the three models.

Approximate descriptions of the stretching Σ^+ modes for the ${}^7\text{LiF}$ and ${}^6\text{LiF}$ species are defined by the calculated normal coordinate vectors. The highest frequency ν_1 appears to be mainly a F-Li-F out-of-phase stretching mode, while the ν_3 vibration is composed primarily of the Li-F-Li out-of-phase motion. The ν_2 vibration is approximately a F-Li, F-Li symmetric stretching motion. Since it is not clear which linear dimer model is preferred, detailed descriptions of the bending modes are not given.

A further problem arises in the assignment of the ν_3 and ν_4 vibrations to the Σ^+ and Π species, respectively, since the assignment may reasonably be reversed. A choice cannot be made on the basis of the product rule. For example, the assignment presented in Table III for ${}^6\text{Li}_2\text{F}$ and ${}^7\text{Li}_2\text{F}$ gives an isotopic

frequency ratio of 1.176 for $\nu_1\nu_2\nu_3/\nu_1'\nu_2'\nu_3'$, which is compared to a calculated value of 1.144 from the product rule. Reversing the assignments for the stretching and bending modes, ν_3 and ν_4 , respectively, gives an isotopic frequency value of 1.180. Table V presents the frequency fit for the bifluoride model, as an example, for an assignment with the two frequencies reversed. As before, the force field that was refined about the $^6\text{Li}_2\text{F}_2$ and $^7\text{Li}_2\text{F}_2$ isotopic frequencies was used to calculate the frequencies for the mixed species. The fit for the reversed frequency assignment is only slightly worse than the fit in Tables III and IV. Although it is difficult to resolve definitely the choice, we prefer the assignment with the stretching motion at the higher frequency.

In summary, we wish to stress that the probable nonuniqueness of the force field precludes a choice of structures on the basis of individual values of the force constants. The close frequency fit determined from the modified potential function, however, strongly indicates the linear nature of the trapped species. Further characterization of the force field will require additional molecular information, as for example, rotational distortion data or mean-square amplitude data for the gas phase species.

REFERENCES

1. M. J. Linevsky, J. Chem. Phys. 34, 587 (1961).
2. M. J. Linevsky, J. Chem. Phys. 38, 658 (1963).
3. A. Snelson and K. S. Pitzer, J. Phys. Chem. 67, 882 (1963).
4. S. Schlick and O. Schnepp, J. Chem. Phys. 41, 463 (1964).
5. R. L. Reddington, J. Chem. Phys. 44, 1238 (1966).
6. A. Snelson, Report No. IITR1-C6013-7, Illinois Institute of Technology Research Institute, Chicago, Illinois.
7. D. E. Mann, G. V. Calder, K. S. Seshadri, D. White, M. J. Linevsky, J. Chem. Phys. 46, 1138 (1967).
8. Certain commercial instruments are identified in this paper to specify completely the experimental procedure. In no case does such identification imply a recommendation or endorsement by the National Bureau of Standards or the National Institutes of Health.
9. "Tables of Interatomic Distances and Configuration in Molecules and Ions," L. E. Sutton, Ed. (The Chemical Society, London, 1958).
10. E. B. Wilson, J. C. Decius, and P. C. Cross, Molecular Vibrations (McGraw-Hill Book Co., Ins., New York, 1955).

Table I. Internal coordinates and force constant matrix for the linear Li_2F_2 dimer.

a) Internal coordinates

F-Li-F-Li

$r \quad s \quad t$

$\alpha = \angle \text{F Li F}$

$\beta = \angle \text{Li F Li}$

b) Force constant matrix

f	r	s	t	α	β
r	f_r	f_{rs}	f_{rt}		
s		f_s	f_{st}		
t			f_t		
α				f_α	$f_{\alpha\beta}$
β					f_β

Table II. Summary of force constants for the linear dimer models of Li_2F_2 . The stretching force constants are in units of millidynes per angstrom, while the bending force constants are in units of millidynes·angstroms.

Model	Species	Force Constant
F-Li-F-Li	Σ^+	$f_r + f_s = 3.71$
		$f_{rs} = 0.96$
		$f_t = 0.59$
		$f_{rt} + f_{st} = 1.41$
	Π	$f_\alpha + f_\beta = 0.26$
		$f_{\alpha\beta} = 0.05$
F-Li-F....Li ^a	Π	$f_\alpha + f_\beta = 0.36$
		$f_{\alpha\beta} = 0.10$
F-Li....F-Li ^a	Π	$f_\alpha + f_\beta = 0.46$
		$f_{\alpha\beta} = 0.18$

^a A dotted line represents a longer bond distance.

Table III. Comparison between the observed and calculated frequencies, in cm^{-1} , for the Σ^+ symmetry species of the linear Li_2F_2 dimer.

	Obs	Calc	$\Delta\nu$	Obs	Calc	$\Delta\nu$
	$\text{F}^6\text{LiF}^6\text{Li}$			$\text{F}^7\text{LiF}^7\text{Li}$		
ν_1	767.8	768.0	+0.2	720.5	720.3	-0.2
ν_2	518.6	518.8	+0.2	497.5	498.2	+0.7
ν_3	270.2	266.5	-3.7	255.2	258.7	+3.5
	$\text{F}^6\text{LiF}^7\text{Li}$			$\text{F}^7\text{LiF}^6\text{Li}$		
ν_1	766.8	767.7	+0.9	720.8	720.8	0
ν_2	497.8	499.5	+1.7	518.3	517.2	-1.1
ν_3	260.1	258.9	-1.2	265.5	266.3	-0.8

Table IV. Comparison between the observed and calculated frequencies, in cm^{-1} , for the π symmetry species of three models for the Li_2F_2 linear dimer.

	Obs	Calc	$\Delta\nu$	Obs	Calc	$\Delta\nu$
a) F-Li-F-Li						
		${}^6\text{Li}_2\text{F}_2$			${}^7\text{Li}_2\text{F}_2$	
ν_4	261.0	261.1	+0.1	245.7	245.5	-0.2
ν_5	157.1	158.5	+0.6	152.8	151.3	-1.5
		${}^{6-7}\text{Li}_2\text{F}_2$			${}^{7-6}\text{Li}_2\text{F}_2$	
ν_4	252.9	260.7	+7.8	249.6	247.6	-2.0
ν_5		152.3			154.6	
b) F-Li-F....Li						
		${}^6\text{Li}_2\text{F}_2$			${}^7\text{Li}_2\text{F}_2$	
ν_4	261.0	261.7	+0.7	245.7	244.9	-0.8
ν_5	157.1	157.8	+0.7	152.8	152.0	-0.8
		${}^{6-7}\text{Li}_2\text{F}_2$			${}^{7-6}\text{Li}_2\text{F}_2$	
ν_4	252.9	261.7	+8.8	249.6	245.0	-4.6
ν_5		152.1			157.8	
c) F-Li....F-Li						
		${}^6\text{Li}_2\text{F}_2$			${}^7\text{Li}_2\text{F}_2$	
ν_4	261.0	261.0	0	245.7	245.7	0
ν_5	157.1	158.8	+1.7	152.8	151.0	-1.8
		${}^{6-7}\text{Li}_2\text{F}_2$			${}^{7-6}\text{Li}_2\text{F}_2$	
ν_4	252.9	252.0	-0.9	249.6	255.4	+5.8
ν_5		153.9			155.3	

Table V. Comparison between the observed and calculated frequencies, in cm^{-1} , for the bifluoride structure of the Li_2F_2 linear dimer. The ν_3 and ν_4 frequencies are reversed from the assignment presented⁴ in Tables III and IV.

	Obs	Calc	2ν	Obs	Calc	$\Delta\nu$
		⁶ Li_2F_2			⁷ Li_2F_2	
ν_1	767.8	768.0	0.2	720.5	720.3	-0.2
ν_2	518.6	518.1	-0.5	497.5	498.5	1.0
ν_3	261.0	257.3	-3.7	245.7	249.3	4.6
ν_4	270.2	271.3	1.1	255.2	254.1	-1.1
ν_5	157.1	157.9	0.8	152.8	151.9	-0.9
		⁶⁻⁷ Li_2F_2			⁷⁻⁶ Li_2F_2	
ν_1	766.8	767.7	0.9	720.8	720.7	-0.1
ν_2	497.8	499.8	2.8	518.3	516.6	-1.7
ν_3	252.9	249.5	-3.4	265.5	257.1	-8.5
ν_4	260.1	271.2	11.1	249.6	254.0	4.4
ν_5		152.1			157.7	

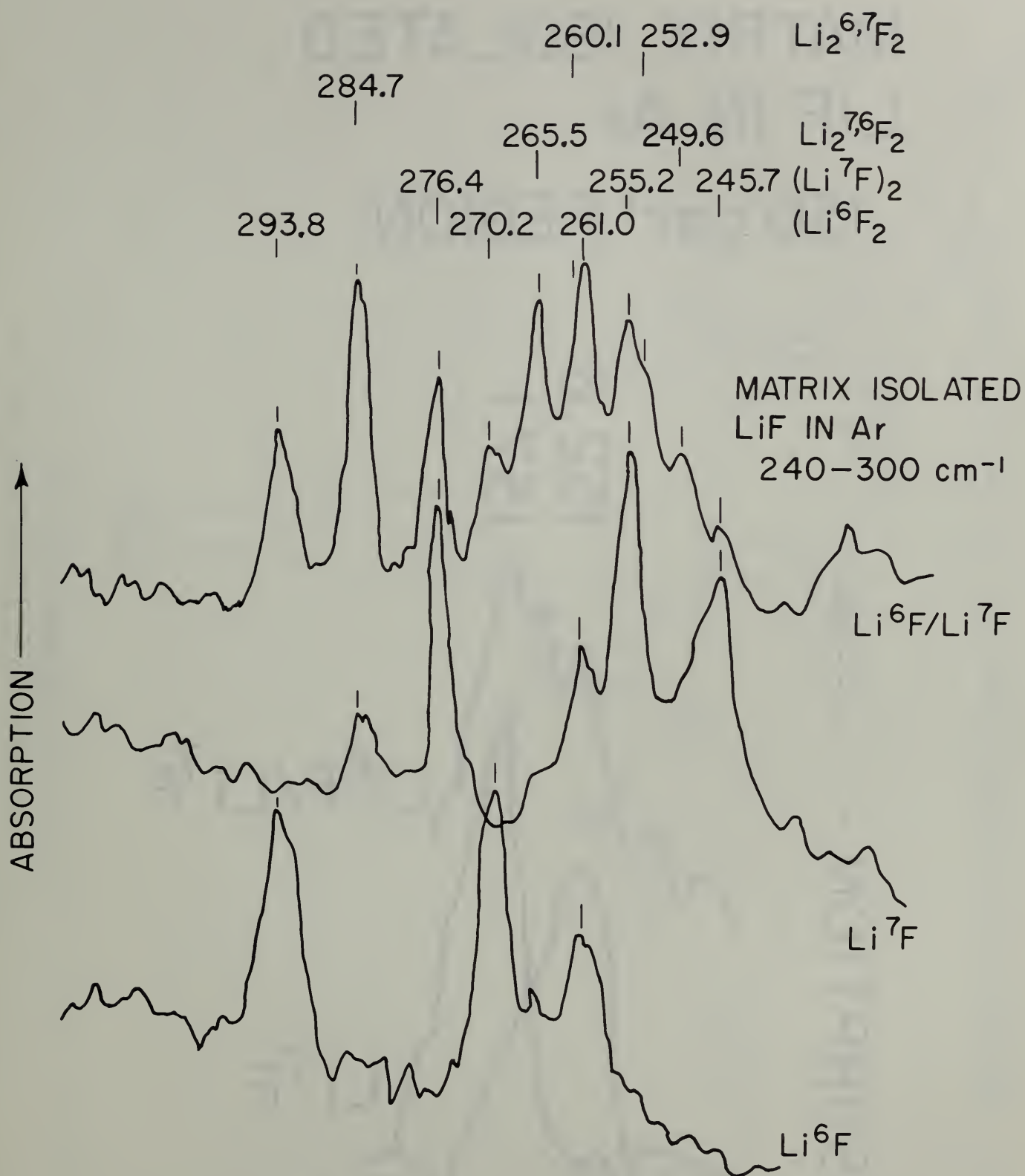


Fig. 1a - Infrared spectra of matrix isolated ^7LiF , ^6LiF , and a 1:1 mixture of $^6\text{LiF}/^7\text{LiF}$ in the 240–300 cm^{-1} region.

MATRIX ISOLATED LiF IN Ar

150 cm^{-1} REGION

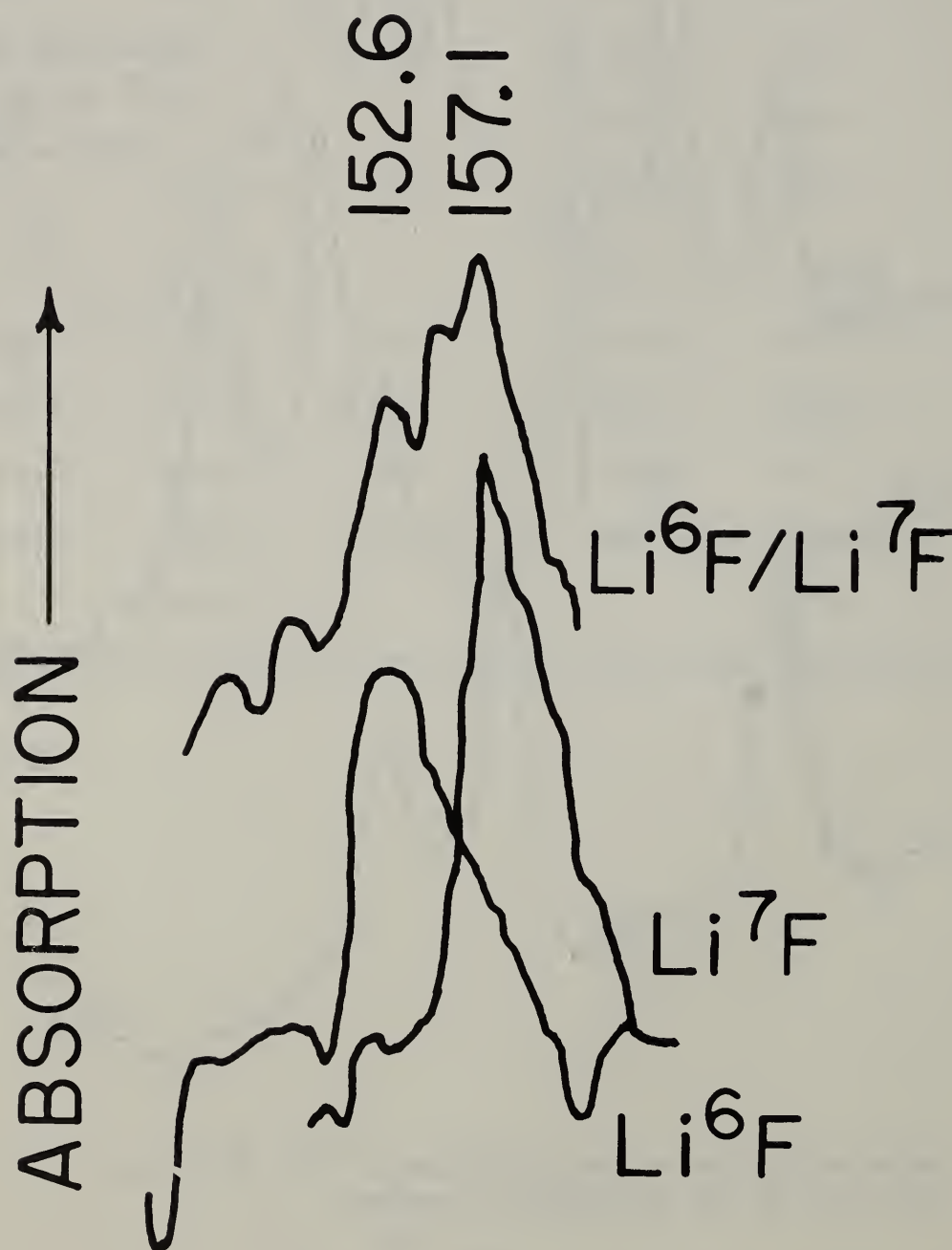


Fig. 1b - Infrared spectra of matrix isolated ^7LiF , ^6LiF , and a 1:1 mixture of $^6\text{LiF}/^7\text{LiF}$ in the 150 cm^{-1} region. 88

MATRIX ISOLATED LiF IN Ar
767 cm⁻¹ REGION

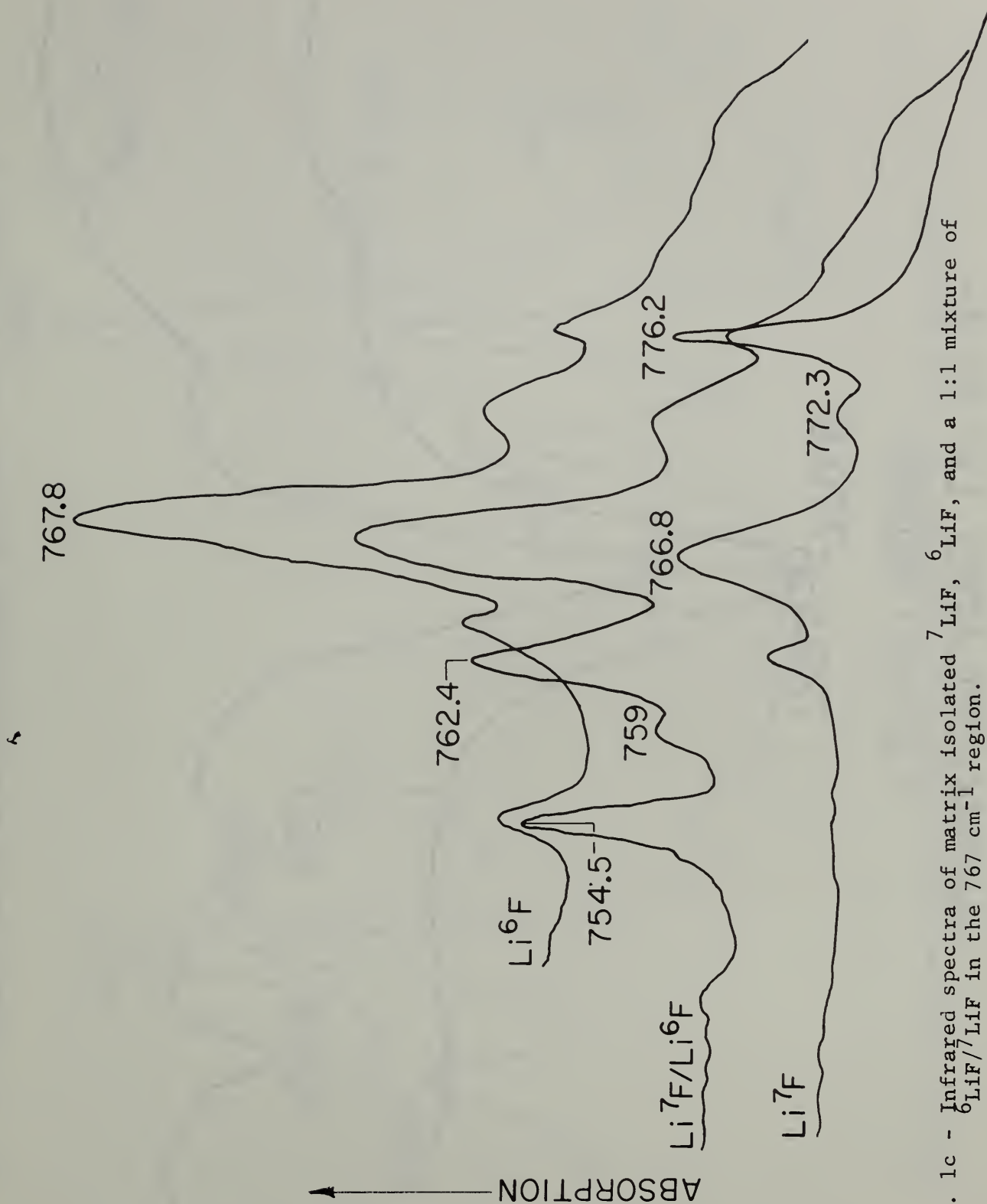


Fig. 1c - Infrared spectra of matrix isolated ⁷LiF, ⁶LiF, and a 1:1 mixture of ⁶LiF/⁷LiF in the 767 cm⁻¹ region.

MATRIX ISOLATED LiF IN Ar 720 cm⁻¹ REGION

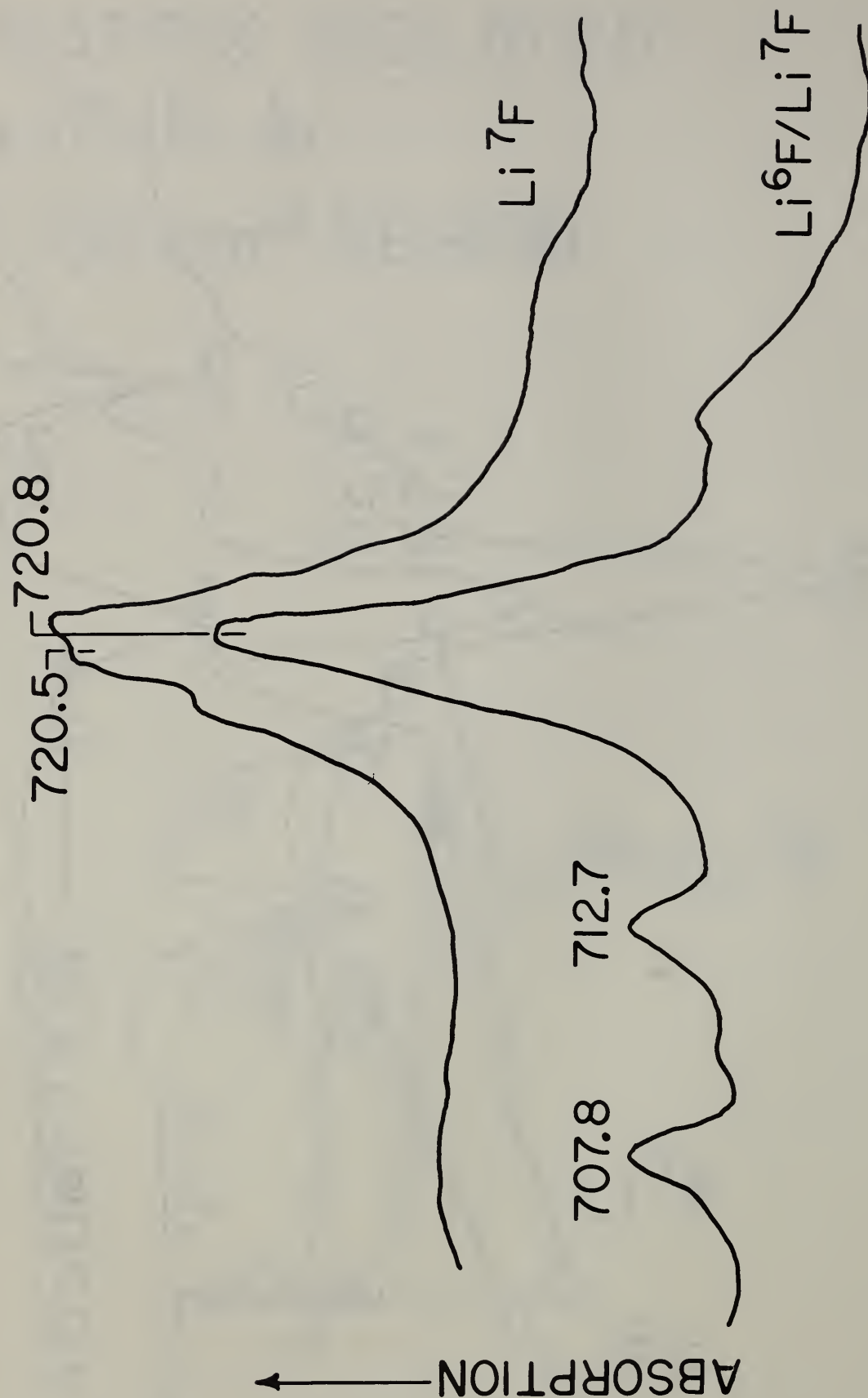


Fig. 1d - Infrared spectra of matrix isolated ⁷LiF, ⁶LiF, and a 1:1 mixture of ⁶LiF/⁷LiF in the 720 cm⁻¹ region.

MATRIX ISOLATED LiF IN Ar

490 - 525 cm^{-1}

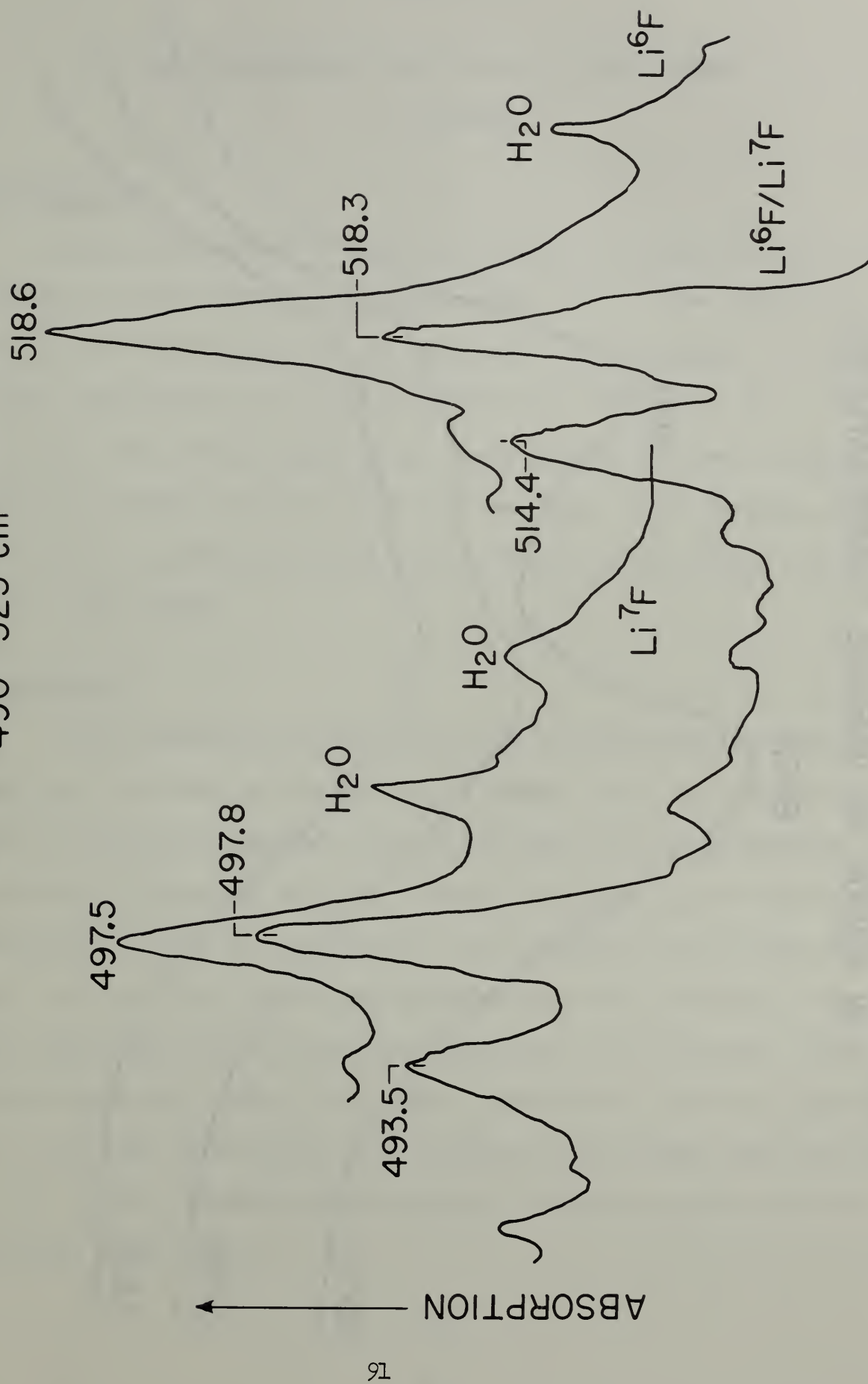


Fig. 1e - Infrared spectra of matrix isolated ^7LiF , ^6LiF , and a 1:1 mixture of $^6\text{LiF}/^7\text{LiF}$ in the 490-525 cm^{-1} region.

MONOMER ABSORPTION OF MATRIX ISOLATED Li^7F
IN ARGON AT VARIOUS TEMPERATURES

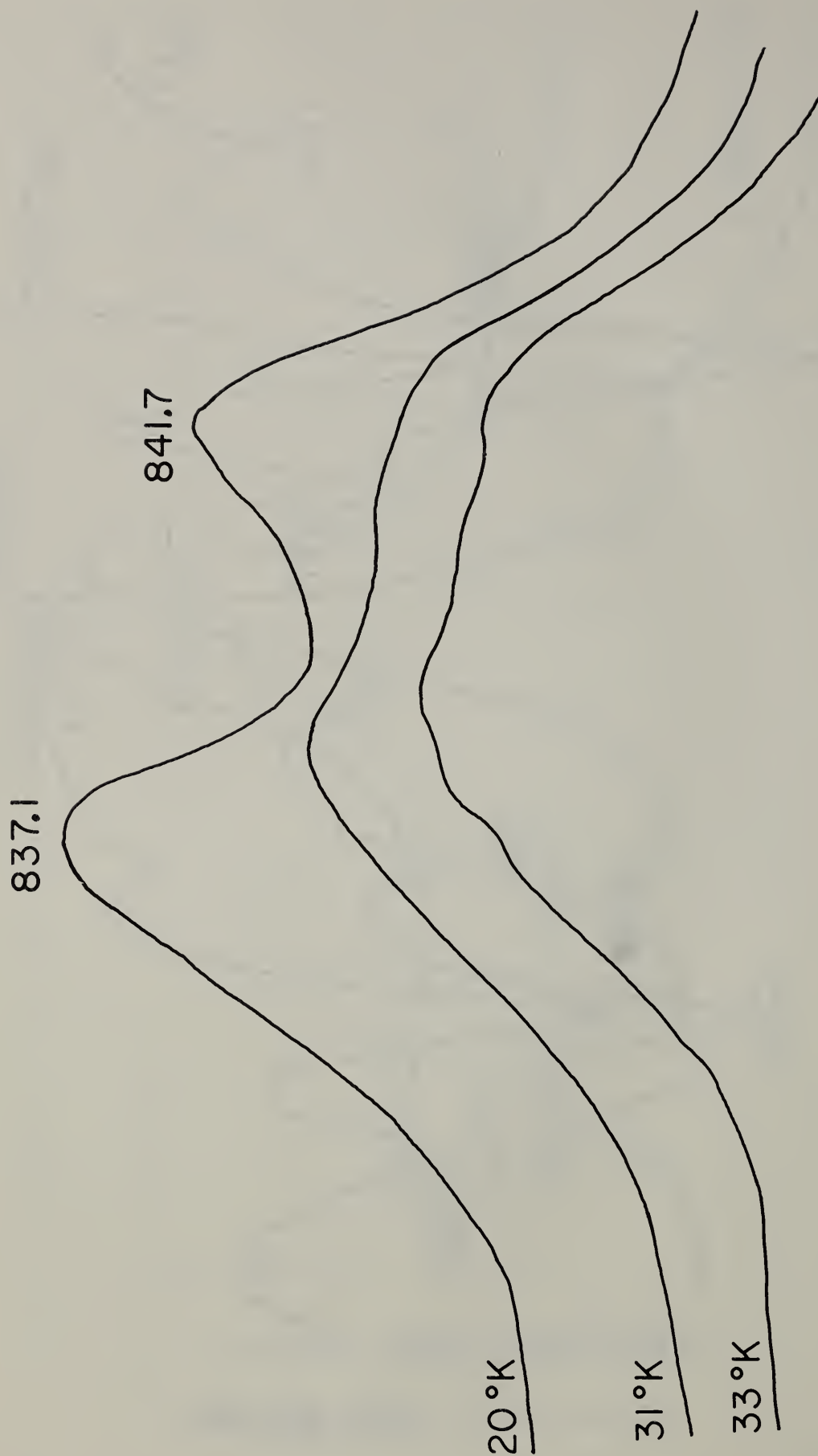


Fig. 2 - Monomeric ^7LiF in Ar at various temperatures.

Chapter 6

MASS SPECTROMETRIC STUDY OF BeCl_2 VAPORIZATION

J. Efimenko

Introduction

A mass spectrometric investigation has been undertaken to detect and study Be-F-Cl species in the BeCl_2 - BeF_2 system. Some preliminary sublimation data are presented for the second reactant, BeCl_2 . A study of BeF_2 vaporization was reported in NBS Report 8033, July 1963. The condensed state phase diagram of the BeCl_2 - BeF_2 system shows a simple eutectic at 300°C and about 73 mol per cent BeF_2 , (O. N. Kuvyrkin, O. N. Breusov, A. V. Novoselova, Nauchn. Dokl. Vyssei Shkoly, Khim. i Khim. Tekhnol. 662 (1958)).

Experimental

Beryllium dichloride was volatilized from two effusion cells, one made from molybdenum and the other from copper. Each cylindrical cell was 12.5 mm outside diameter, 25.4 mm in length with 0.5 mm diameter cylindrical orifice in the cover. Heater for the Mo cell was fabricated from Nichrome wire, 0.75 mm diameter, in continuous hairpin strips 12 mm wide. One strip was placed concentrically about the top half of the cell and another was similarly positioned about the bottom half. Each heater strip was powered by a separate transformer - powerstat supply. A Pt-PtRh(10%) thermocouple (10 mil diameter) was fastened into the bottom of the cell for temperature measurements. The emf was read on Type K-3 Universal potentiometer.

The copper effusion cell was surrounded with a single strip of hairpin design, Nichrome wire 0.60 mm diameter and the hairpin lengths were 27.5 mm. Tantalum radiation shields surrounded the effusion cells completely but allowed unobstructed flow of the effusion beam.

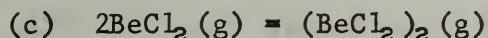
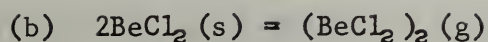
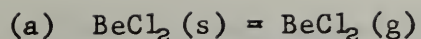
The ion intensities and temperatures were recorded when the effusion cell reached a steady state temperature. The desired ion intensities were differentiated from background by interposing a stainless steel shutter into the molecular beam.

The beryllium dichloride (anhydrous) was obtained from K and K Laboratories, Inc., Plainview, New York. A spectrographic analysis at NBS on a portion of the beryllium dichloride indicated the following foreign elements (in per cent): 0.001-0.01, Al, Fe, Mg, Pt; 0.01-0.1, Ni; less than 0.001, Ba, Ca, Cu, Mn, Si.

Data and Results

The data presented in table 1 were obtained using the copper effusion cell. The ion intensities are expressed in volts as the output from a secondary electron multiplier. Included are the average multiplier efficiencies for $(\text{BeCl}_2)^+(g)$ and $(\text{BeCl}_2)_2^+(g)$, obtained from simultaneous ion measurements on a grid collector ahead of the electron multiplier detector. All the isotopic species of BeCl_2 were observed and their intensities are shown in table 2 for a few select temperatures. For computations only the intensities of the BeCl_2 species formed by the chlorine isotope Cl_{35} were used, table 1.

The following reactions were considered in the vaporization of beryllium dichloride:



The enthalpies of these reactions were computed by application of the second law. In figures 1 and 2 are shown $\log I^+T$ vs $1/T$ plots applicable to reactions (a) and (b). For reaction (c) the quantity A, proportional to the equilibrium constant, was plotted as $\log A_4$ vs $1/T$. The second law results for these reactions are listed in table 3, with collected literature values. The BeCl_2 sublimation enthalpy $\Delta H_{s,13}^0 = 38.2$ kcal/mol was reduced to the reference temperature 298°K, with the aid of JANAF Thermochemical Tables, $\text{BeCl}_2 (\beta)$, June 30, 1965; $\text{BeCl}_2 (g)$, June 30, 1965. A heat of formation for $\text{BeCl}_2 (g)$ of -79.6 ± 2.4 kcal/mol was calculated from the experimental sublimation enthalpy, $\Delta H_{298}^0 = 38.9 \pm 2.4$ kcal/mol and the heat of formation for β -solid BeCl_2 , $\Delta H_{f,298}^0 = -118.5$ kcal/mol (NBS Report No. 9500, pg. 138).

Discussion

The data, table 1, were obtained from successive days of operation and include temperature cycles within a set of measurements. The scatter of points is most probably due to incomplete temperature equilibration with the sample. Although the BeCl_2 was labeled "anhydrous" appreciable hydrolysis was evident during the sublimation and whether the resulting BeO also contributed to the data scattering is not certain. A compromise had to be established in attaining a steady state temperature and the speed of data reading. If the waiting period is made too long, or if the vaporization rate is high, the compound, aside from being depleted

in the Knudsen cell, is deposited in the ionization source creating an increasing background signal which adds to the difficulty of obtaining reproducible data. The low atomic weight species as, H_2O , Cl , HCl , Cl_2 , and BeCl do not condense readily nor are pumped out rapidly, thus, interfere with their intensity measurements.

In figures 1, 2, and 3 are shown the best straight-line fits and in table 3 are the calculated enthalpies based on least squares computations. For the least squares calculations all the data points were given equal weight but the experimental conditions did not warrant such equilization.

In table 2 are presented ion intensities resulting from the use of 70 ev and 28 ev ionizing electrons. The increase in ion intensities with the lower energy electrons and at approximately the same temperature is evident. It appears that temperature equalization with the sample was slower in a Mo cell as the lower ion intensities show for the temperatures, 225-226°C. At the highest temperatures, 250°C Mo cell and 291°C Cu cell, groups of moderate intensity peaks appeared above mass 200. These peaks are not identified completely yet but are likely the chlorides of Mo and Cu.

The ratios of $(\text{BeCl}_2)_2^+ / (\text{BeCl}_2)^+$ are presented in table 1. In the short temperature range studied, this ratio shows a factor of 2 increase. Also, the ratio observed is greater than obtained by previous investigators (references 1, 5, table 1). The ratio $(\text{Be}_2\text{Cl}_3)^+ / (\text{BeCl}_2)_2^+$ does not vary remarkably with temperature, except for a few anomalies, but indicates that all or part of the $(\text{Be}_2\text{Cl}_3)^+$ originates from electron

impact. If it were assumed that it resulted entirely from electron impact, then the dimer/monomer ratio would be increased still more.

Table 1

DATA: Ion Intensities of BeCl_2 , Be_2Cl_3 , $(\text{BeCl}_2)_2$

Index No.	T, °K	I_{79}^+ , Volt	I_{123}^+ , Volt	I_{158}^+ , Volt	$\frac{I_{158}^+ \times 10^2}{I_{79}^+}$	$\frac{I_{123}^+}{I_{158}^+}$
1	541	27.0×10^{-1}	42.0×10^{-2}	23.1×10^{-2}	8.56	1.82
2	525	12.3×10^{-1}	14.1×10^{-2}	85.5×10^{-3}	6.95	1.65
3	510	54.0×10^{-2}	37.0×10^{-3}	31.0×10^{-3}	5.74	1.19
4	495	10.2×10^{-2}	84.0×10^{-4}	55.0×10^{-4}	5.40	1.53
5	472	25.8×10^{-3}	10.0×10^{-4}	6.0×10^{-4}	2.32	1.66
6	447	22.0×10^{-4}	12.0×10^{-5}	6.0×10^{-5}	2.73	2.00
7	517.5	73.0×10^{-2}	54.0×10^{-3}	43.0×10^{-3}	5.90	1.25
8	508	12.3×10^{-2}	15.3×10^{-3}	69.0×10^{-4}	5.60	2.22
9	498	92.0×10^{-3}	45.0×10^{-4}	96.0×10^{-4}	10.4	4.70
10	476	12.3×10^{-3}	12.0×10^{-4}	7.5×10^{-4}	6.10	1.60
11	511	13.6×10^{-2}	15.6×10^{-3}	99.0×10^{-4}	7.28	1.58
12	479	10.2×10^{-3}	10.0×10^{-4}	5.0×10^{-4}	4.90	2.00
13	564	50.0×10^{-1}	82.0×10^{-2}	46.0×10^{-2}	9.20	1.78
14	545	13.8×10^{-1}		13.2×10^{-2}	9.57	
15	521.5	42.0×10^{-2}	32.0×10^{-3}	23.7×10^{-3}	5.64	1.35
16	507	18.0×10^{-2}	15.6×10^{-3}	99.0×10^{-4}	5.50	1.575
17	496	60.0×10^{-3}		33.5×10^{-4}	5.58	
18	512	86.0×10^{-2}	78.0×10^{-3}	53.5×10^{-3}	6.22	1.47
19	496	15.3×10^{-2}	12.3×10^{-3}	87.0×10^{-4}	5.68	1.41
20	492	49.0×10^{-3}				
21	474	97.5×10^{-4}				
22	473	60.0×10^{-4}				

NOTE: ionizing electrons, 28 ev; electron current, 50 μa ; accel. volt, 7.5 KV
multiplier efficiency, $\gamma(\text{BeCl}_2)^+$, 214; $\gamma(\text{BeCl}_2)_2^+$, 202.

Table 2

BeCl₂ Isotope Intensities, BeCl₂, Be₂Cl₃, (BeCl₂)₂

t, °C	I ₇₉ ⁺	I ₈₁ ⁺	I ₈₃ ⁺	I ₁₂₃ ⁺	I ₁₂₅ ⁺	I ₁₂₇ ⁺
225-226	3.3 × 10 ⁻³	15.6 × 10 ⁻³	2.5 × 10 ⁻³	10.5 × 10 ⁻⁴	10.8 × 10 ⁻⁴	3.45 × 10 ⁻⁴
249-250	45 × 10 ⁻²	24.5 × 10 ⁻²	48 × 10 ⁻³	19.2 × 10 ⁻³	19.2 × 10 ⁻³	6.1 × 10 ⁻³
246-248	63 × 10 ⁻³	43 × 10 ⁻³	70.5 × 10 ⁻⁴	41.5 × 10 ⁻⁴	40 × 10 ⁻⁴	12 × 10 ⁻⁴
221-223	15.3 × 10 ⁻²	10.3 × 10 ⁻²	17.1 × 10 ⁻³	12.3 × 10 ⁻³	11.7 × 10 ⁻³	10.5 × 10 ⁻³
248	28 × 10 ⁻²	60 × 10 ⁻²	17.4 × 10 ⁻²	32 × 10 ⁻³	28 × 10 ⁻³	99 × 10 ⁻⁴
272	13.8 × 10 ⁻¹	87 × 10 ⁻²	15 × 10 ⁻²	90 × 10 ⁻²	86 × 10 ⁻²	30 × 10 ⁻²

I ₁₂₉ ⁺	I ₁₅₈ ⁺	I ₁₆₀ ⁺	I ₁₆₂ ⁺	I ₁₆₄ ⁺	I ₁₆₆ ⁺	
7 × 10 ⁻⁴	6.6 × 10 ⁻⁴	7.8 × 10 ⁻⁴	3.3 × 10 ⁻⁴			Mo cell 28 ev
13.5 × 10 ⁻⁵	14 × 10 ⁻³	18.4 × 10 ⁻³	91.5 × 10 ⁻⁴	18 × 10 ⁻⁴		Mo cell
33 × 10 ⁻⁴	13 × 10 ⁻⁴	16 × 10 ⁻⁴	8 × 10 ⁻⁴			Mo cell
11 × 10 ⁻⁴	87 × 10 ⁻⁴	10.5 × 10 ⁻³	47 × 10 ⁻⁴	10 × 10 ⁻⁴		Cu cell
5 × 10 ⁻²	23.7 × 10 ⁻³	29 × 10 ⁻³	14.1 × 10 ⁻³	30 × 10 ⁻⁴		Cu cell
	13.2 × 10 ⁻²	17.1 × 10 ⁻²	84 × 10 ⁻³	18 × 10 ⁻³	14 × 10 ⁻⁴	Cu cell

Table 3
Second Law Sublimation Enthalpies for BeCl_2 (g)

Temp. Range °K	$\frac{\text{BeCl}_2 \text{ (g)}}{\Delta H_{\text{gas}}^0} \text{ kcal/mol}$	$\frac{(\text{BeCl}_2)_2 \text{ (g)}}{\Delta H_f^0} \text{ kcal/mol}$	Experimental Method	Reference
450-545	38.9 ± 2.4	41.8 ± 3.5 (a) -31.3 ± 3.1 (b)	Knudsen-Mass Spect.	This paper
460-504	33.1		Torsion-Effusion	(1)
461-543	33.7	35.8	Knudsen-Mass Spect.	(1)
440-600	33.1 ± 0.5		Knudsen-gravimetric and Torsion-Effusion	(2)
623-683		36.0 ± 1	Transpiration	(3)
638-673	35.6		Manometric,	(4)
677-753	33.3		"Bell Method"	
524-568	34 ± 1	44 ± 1	Knudsen-Mass Spect.	(5)
573-753	32.05 30.68		Transpiration- Cl_2 gas	(6)

NOTES: (a) Reaction: $2\text{BeCl}_2 \text{ (s)} = (\text{BeCl}_2)_2 \text{ (g)}$
(b) Reaction: $2\text{BeCl}_2 \text{ (g)} = (\text{BeCl}_2)_2 \text{ (g)}$

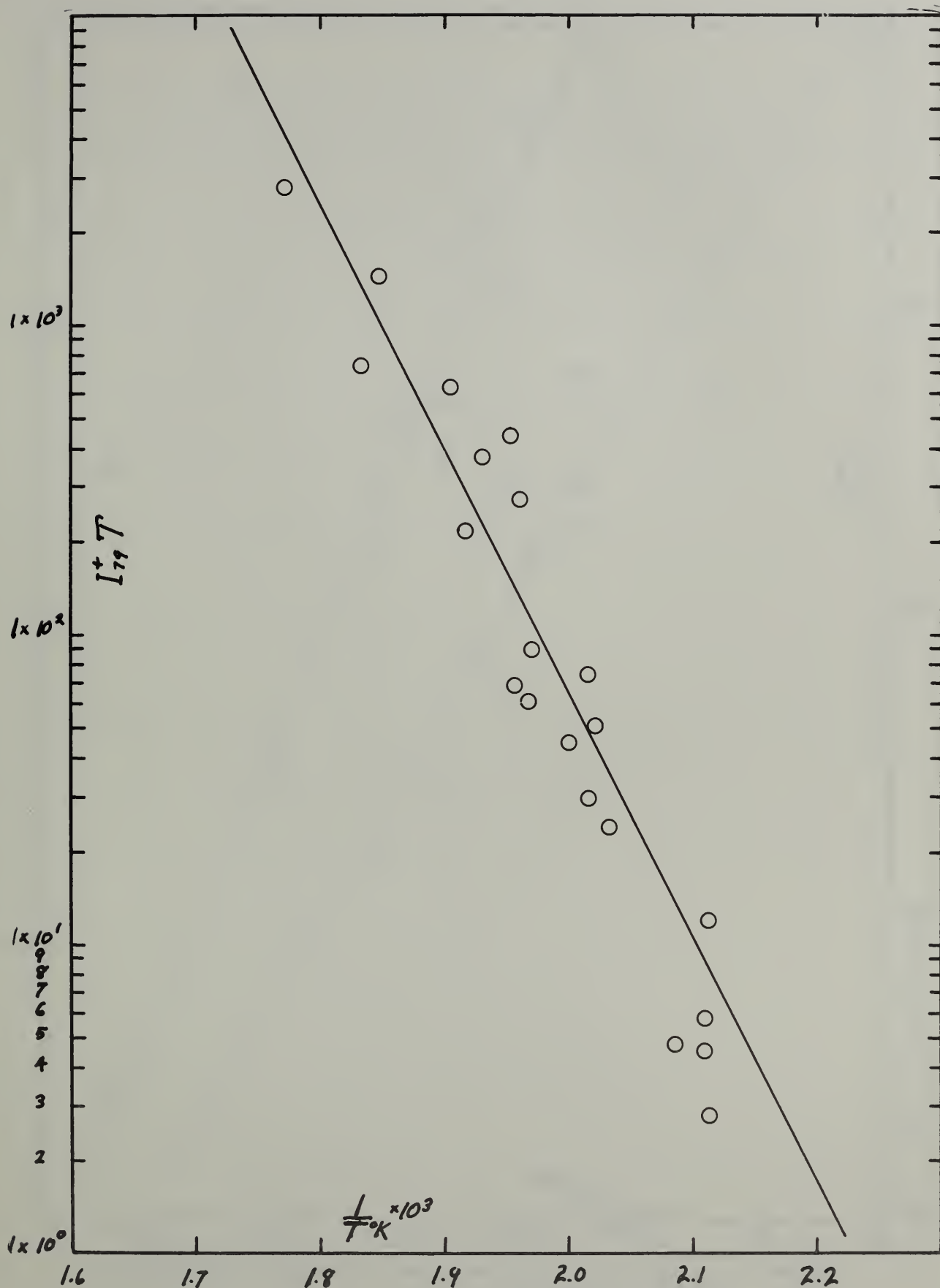
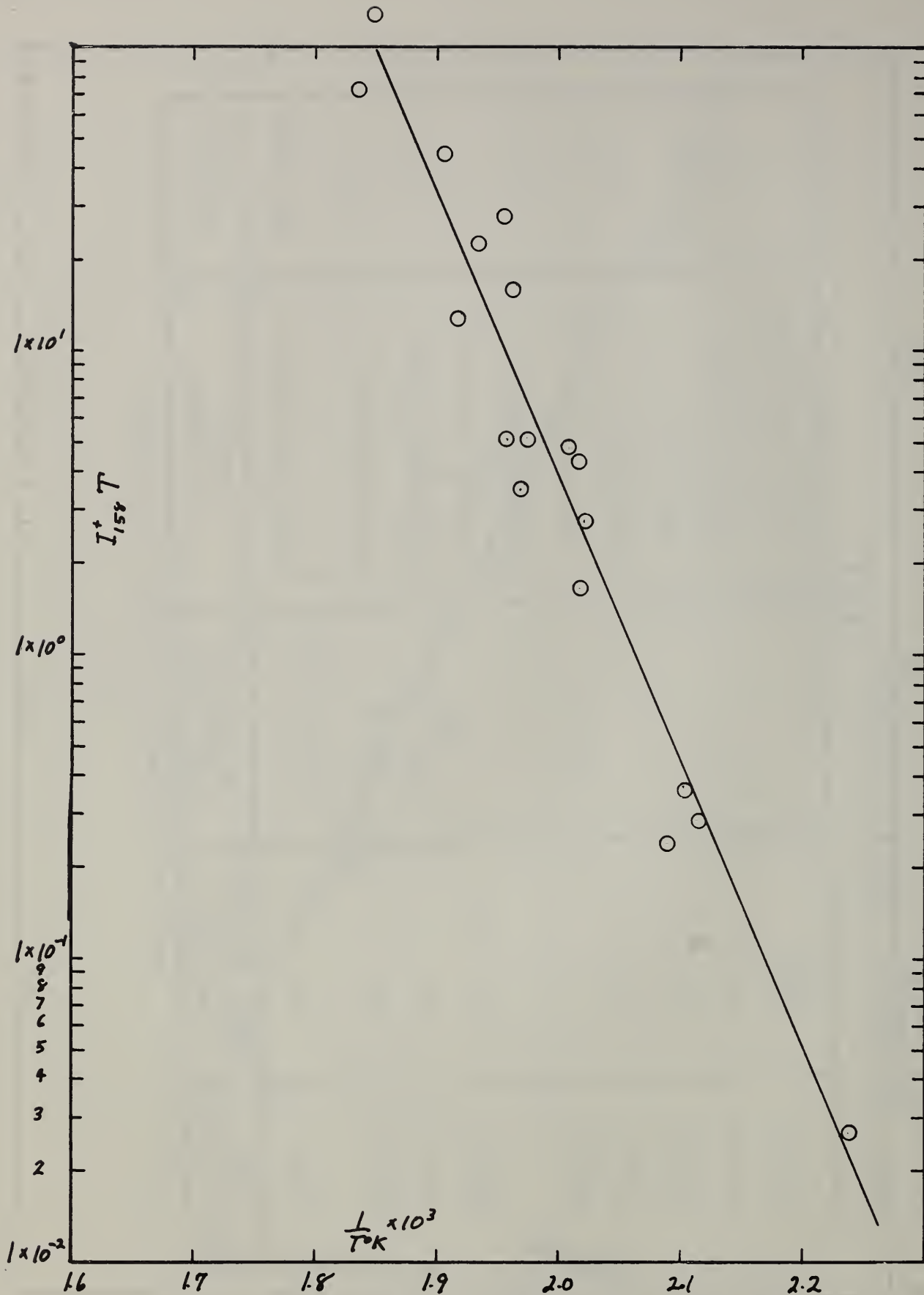


Figure 1: $\log I_{79}^+ T$ vs $1/T$ plot for the data of $\text{BeCl}_2(\text{s}) = \text{BeCl}_2(\text{g})$,
 $\Delta H_{13}^0 = 37.8 \text{ kcal/mol}$.



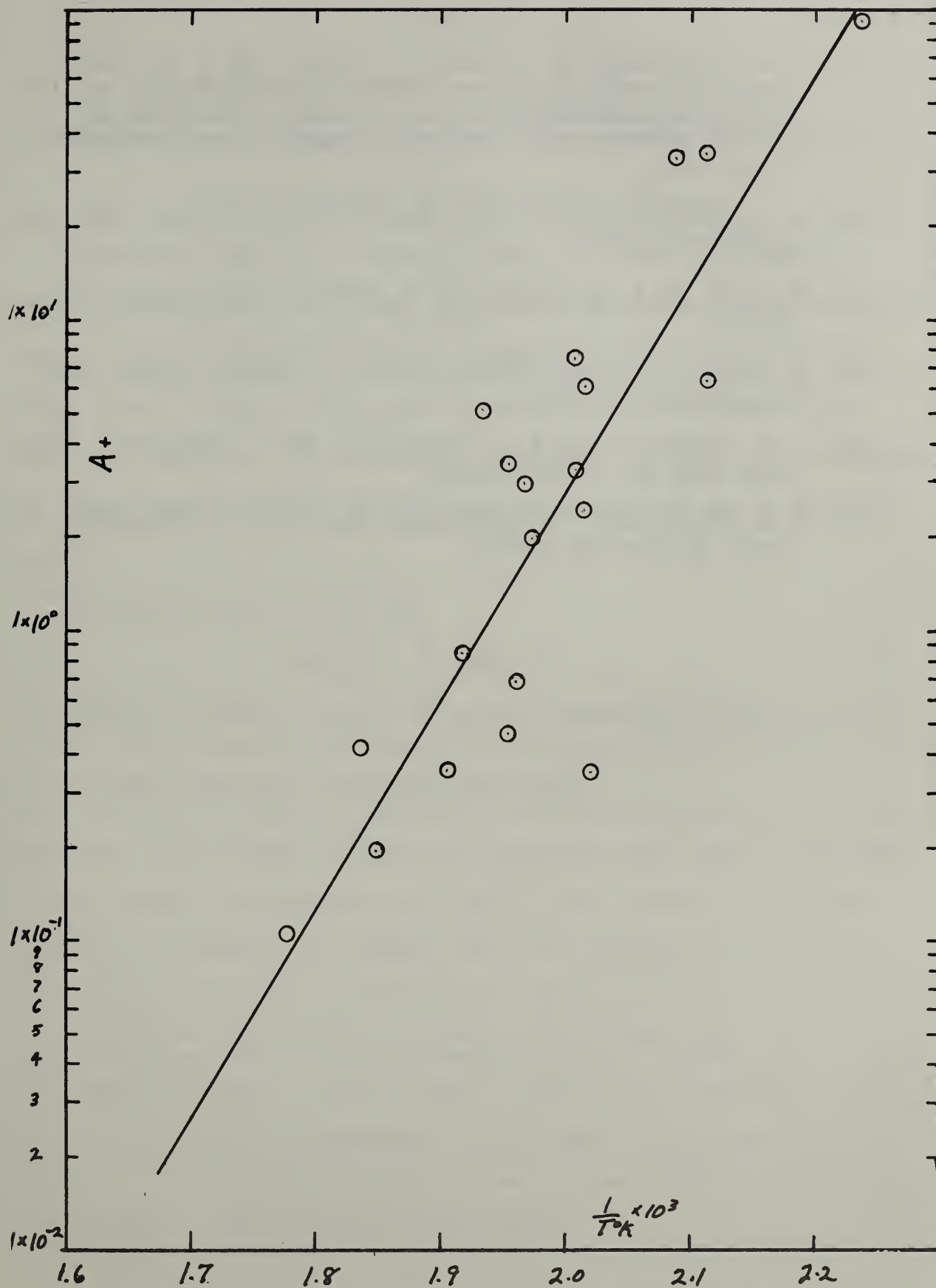


Figure 3: $\log A_+$ vs $1/T$ plot for the data of $2\text{BeCl}_2(\text{g}) = (\text{BeCl}_2)_2(\text{g})$,
 $\Delta F_{613}^\circ = -30.7 \text{ kcal/mol.}$

References:

- (1) D. L. Hildenbrand, L. P. Theard, E. Murad, and F. Ju, Final Technical Report - Investigation of Thermodynamic Properties of Rocket Combustion Products, Secondary Publication No. U-3068, Aeronutronics, Ford Road, Newport Beach, California, April 1965.
- (2) M. A. Greenbaum, R. F. Yates, and M. Farber, J. Phys. Chem. 67, 1802-1805 (1963).
- (3) K. C. Ko, M. A. Greenbaum, and M. Farber, *ibid.* 71, 254-258 (1967).
- (4) W. Fischer, T. Petzel, and S. Lanter, Z. Anorg. Allgem. Chem. 333, 226-234 (1964).
- (5) L. N. Ryabchekov and H. F. Tikhinskii, Fiz. i Metalloved. Akad. Nauk SSSR 10, 635-637 (1960).
- (6) I. N. Sheiko and V. G. Feshchenko, Ukrainskii Khimicheskii Zhur. 28, 478-483 (1962).

Chapter 7

REVISION OF CHAPTER 4 of NBS REPORT 9500, "THE VAPOR PRESSURE, VAPOR DIMERIZATION, AND HEAT OF SUBLIMATION OF ALUMINUM FLUORIDE, USING THE ENTRAINMENT METHOD"

Ralph F. Krause Jr. and Thomas B. Douglas

The above Chapter was revised in view of another investigation made available since the original version was prepared. Along with this recent work the comments of several readers invited us to review the weight given to other studies used to derive the recommended values reported previously. The approach to interpret our data was essentially unaltered; nevertheless we submit herewith an improved set of derived results.

The adopted value of ΔS^0 for



was revised according to Snelson's¹ infrared spectrum of AlF_3 by matrix

¹ A. Snelson, publication pending (June 1967).

isolation. He observed the spectra of saturated AlF_3 vapor in matrices of neon, argon, and krypton, which were in good agreement with those observed by Linevsky²; but Snelson noted that frequency shifts in his

² M. J. Linevsky, Space Sci. Lab. Rept., Philadelphia (Nov. 30, 1964).

three matrices showed a regular trend. Following the procedure described in an earlier paper³, he estimated the gas phase frequencies from the

³ A. Snelson, J. Phys. Chem. 70, 3208 (1966).

values that he observed in the neon matrix to be $\nu_2 = 300$, $\nu_3 = 965$, and $\nu_4 = 270 \text{ cm}^{-1}$ with a probable accuracy of 10 cm^{-1} . This improved set of frequencies along with another recent work by Douglas and Ditmars⁴, whose high-temperature heat content of $\text{AlF}_3(\text{c})$ was discussed

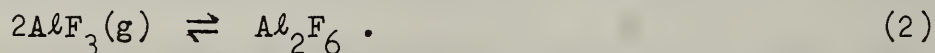
⁴ T. B. Douglas and D. A. Ditmars, J. Res. Nat. Bur. Std. 71A, 185 (1967).

in the above chapter, was used to revise the previously reported JANAF Table⁵ value of $\Delta S^\circ(1)$ to become $43.0 \pm 0.4 \text{ eu}$ at 1225°K . This new value

⁵ D. R. Stull et al, JANAF Thermochemical Tables, Dow Chemical Co., Midland, Mich. (Sept. 30, 1965).

agrees to 0.1 eu with the JANAF value only because the above two new pieces of superior data produce changes which fortuitously nearly cancel.

Using the method employed in the above Chapter, our entrainment data, P and dP/dT of reaction 1 at 1225°K , were combined with published values of two other properties to make the four necessary to define the following reaction besides reaction 1,



P was considered as the sum of the ideal monomeric and twice the dimeric vapor pressure. For the purpose of this revision the above revised $\Delta S^\circ(1)$ and Büchler's⁶ mass-spectrometric value of $2\Delta H^\circ(1) + \Delta H^\circ(2) = 86 \pm 3 \text{ kcal}$

⁶ A Büchler, Arthur D. Little Rept., Cambridge, Mass. (Sept. 30, 1962).

at 1000°K were assumed to be the other two properties. Figure 1 indicates hypothetical values of $\Delta H^\circ(1)$ and $\Delta G^\circ(2)$ which are simultaneously in

agreement with our precise entrainment data and reasonable choices of $\Delta S^{\circ}(1)$ and $2\Delta H(1) + \Delta H^{\circ}(2)$. Table I lists the results derived from the adopted values of the latter two and compares them with several values resulting from previously published investigations. Although Porter and Zeller⁷ reported a value of $\Delta H^{\circ}(2)$ which depends upon $\Delta S^{\circ}(2)$ assumed by

⁷ R. F. Porter and E. E. Zeller, J. Chem. Phys. 33, 858 (1960).

analogy with other halides, their measurement of $\underline{P_d/P_m}$ may be represented independently of this assumption by

$$\Delta G^{\circ}(1) + \Delta G^{\circ}(2) = -RT \ln (P_d/P_m). \quad (3)$$

Our evaluation of the extent of dimerization implicit in our entrainment data substantiates Porter and Zeller's mass-spectrometric measurement.

When our entrainment data is compared with several other vapor pressure investigations, which are enumerated in the above Chapter, the consistency of our points contrasts with the scattering of most of the others. In view of the precision of our data we believe our $\Delta H^{\circ}(1)$ is more reliable than those previously reported.

Table I. Thermodynamic Values for Reactions 1 and 2

T(°K)	Property	Previous Work	This Work ^a
1225	$\Delta H^{\circ}(1)$ kcal		67.0 \pm 0.4
	$\Delta S^{\circ}(1)$ eu		43.0 \pm 0.4 ^b
	$\Delta G^{\circ}(2)$ kcal		-7 \pm 1
1000	$2\Delta H^{\circ}(1) + \Delta H^{\circ}(2)$ kcal	85.8 \pm 3	68.1 \pm 0.4
	$\Delta H^{\circ}(1)$ kcal	67.3 \pm 3	
	$\Delta H^{\circ}(2)$ kcal	-48 \pm 4	-50 \pm 3
	$\Delta S^{\circ}(2)$ eu	-32 \pm 3	-35 \pm 3
	$\Delta G^{\circ}(1) + \Delta G^{\circ}(2)$ kcal	8.6 \pm 0.6	9 \pm 1

^a Derived by assuming $2\Delta H^{\circ}(1) + \Delta H^{\circ}(2) = 86$ kcal at 1000°K.

^b References 1, 4, and 5.

^c Reference 6.

^d Reference 7. See eq 3 for conversion of observed $\underline{P_d/P_m}$, whose uncertainty was taken to be twice its standard error.

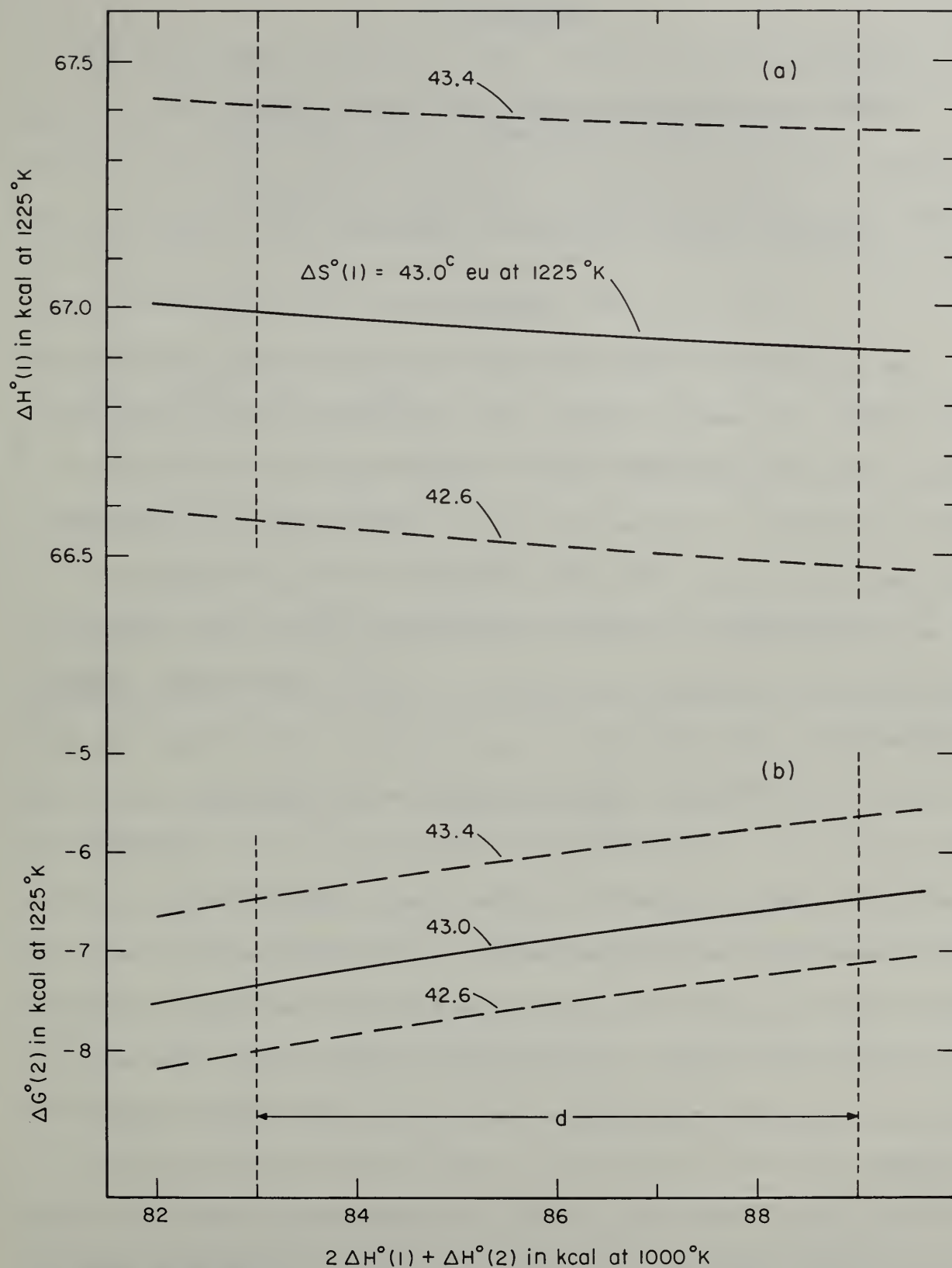


Figure 1. Hypothetical values of (a) $\Delta H^\circ(1)$ and (b) $\Delta G^\circ(2)$ calculated from P and dP/dT of this work and selected values of $\Delta S^\circ(1)$ and $2\Delta H^\circ(1) + \Delta H^\circ(2)$. A possible, constant error of 1 deg in our observed T would contribute 0.05 kcal to $\Delta H^\circ(1)$ and $\Delta G^\circ(2)$.

^c References 1, 4, and 5.

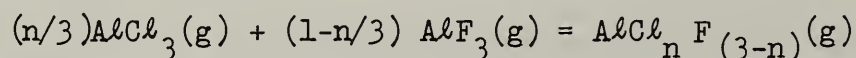
^d Reference 6.

HEATS OF FORMATION OF GASEOUS MIXED-HALIDE MONOMERS BY
THE CONCURRENT ENTRAINMENT OF AlCl_3 AND AlF_3 ¹

Ralph F. Krause Jr. and Thomas B. Douglas
National Bureau of Standards, Washington, D.C. 20234

ABSTRACT

The enhancement of the volatility of AlF_3 by the concurrent entrainment of AlCl_3 was measured between 1196 and 1256°K. When the flow of chloride vapor was generated with an average range of 2.4% at 373 or 394°K, the amount of sublimed fluoride was observed to be from 1.7 to 7.4 times that expected from its entrainment in an inert medium at the same temperatures. The vapor mixture saturated with the fluoride was considered to include the formation of the two mixed-halide monomers as defined by



where \underline{n} is 1 or 2. A correction for the formation of the 22 possible mixed-halide dimers besides the two pure dimers from the above reactants was estimated from the published values for the dimerization of each halide alone. An iterative method was used to fit the observed entrainment data by least squares to derive ΔH° of either of the above two reactions along with its estimated uncertainty to be 1.0 ± 0.5 kcal at 1225°K.

¹ This work was supported by the Air Force Office of Scientific Research under Contract No. ISSA-65-8.

INTRODUCTION

The mixed-halide monomers of AlCl_3 and AlF_3 have been commonly postulated, but no experimental work has heretofore indicated their existence, let alone giving information as to their properties. Several investigators^{2,3,4,5,6} have similarly estimated values of ΔH°_f of both

² D.L. Hildenbrand, ASTIA Document 233467 (Sept. 30, 1959).

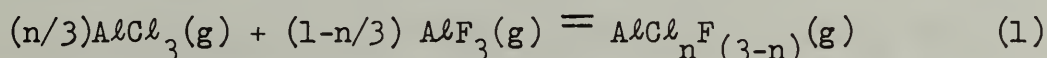
³ R.R. Koppang, C.M. Sherwood, and G.S. Bahn, Marquardt Corp., Van Nuys, Calif. (Oct. 1959).

⁴ C.B. Henderson and R.S. Scheffee, Atlantic Research Corp., Alexandria, Va. (Jan. 1960).

⁵ J.S. Gordon, ASTIA Document AD231995 (Jan. 1960).

⁶ D.R. Stull et al, JANAF Thermochemical Tables, Dow Chemical Co., Midland, Mich. (Aug. 1966).

$\text{AlClF}_2(\text{g})$ and $\text{AlCl}_2\text{F}(\text{g})$; besides using the published ΔH°_f of both $\text{AlCl}_3(\text{g})$ and $\text{AlF}_3(\text{g})$, the JANAF Tables⁶ had assumed ΔH° of both of the following two reactions,

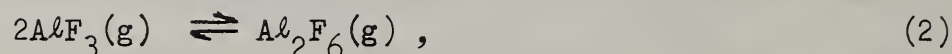


where n is 1 or 2, to be zero. A comparison of the estimated uncertainty of ± 20 kcal in ΔH°_f of the mixed-halides with that of ± 0.5 and ± 2.0 kcal in ΔH°_f of $\text{AlCl}_3(\text{g})$ and $\text{AlF}_3(\text{g})$, respectively, reflects the large uncertainties in ΔH° of eq 1.

Dimerization of a halide alone can contribute to the total vapor pressure observed by the entrainment method. Considering that $\text{Al}_2\text{F}_6(\text{g})$ is known from mass-spectrometry, a recent work⁷ in this laboratory

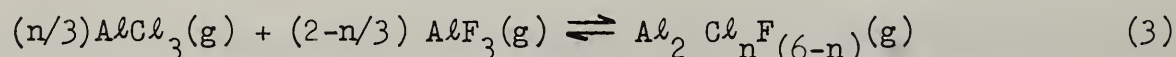
⁷ R.F. Krause Jr. and T.B. Douglas, publication pending (May 1967).

evaluated its mol percent in the saturated vapor, whose dimerization is shown by



to be 4.6 ± 1.4 at 1225°K . As reviewed in the JANAF Tables⁶, the chloride dimerization, analogous to eq 2, had been measured by several investigators between 628 and 944°K . Below its sublimation temperature near 460°K the saturated vapor of AlCl_3 is predominantly dimeric; but an extrapolation of the published dimerization values to 1225°K yields an apparently negligible 0.03 mol percent of dimer in pure chloride vapor whose partial pressure is 0.02 atm, near the upper limit of that employed in this work.

The AlCl_3 - AlF_3 gaseous system may contain an even larger proportion of dimers than indicated by the previously mentioned dimerization of each halide alone. Although there is no information on the mixed-halide dimers, their contribution may be postulated by considering their formation as demonstrated by the following reaction,



where $\underline{n} = 0, 1, 2, \dots, 6$, and by assuming their structure to be the same as the well known $\text{Al}_2\text{Cl}_6(\text{g})$. Even appreciable amounts of trimers and higher polymers might be possible; but only monomers and dimers, each behaving as an ideal gas, will be assumed. In fact the total number of physically distinguishable dimers that can be formulated is so great, namely 24 , that even a more arbitrary assumption will be involved: grouping the properties of many of them together before attempting an evaluation of our data.

CONCURRENT ENTRAINMENT

The experimental procedure in this work consisted of flowing argon gas through one vapor cell, where the chloride vapor was generated at 373 or 394°K, and passing the mixture through another vapor cell with the saturated vapor of AlF_3 at 1196 to 1256°K. The two sublimed halides were condensed separately downstream while the carrier gas was collected in a tank.

Some modification of the entrainment apparatus described in an earlier work⁷ was made to accommodate the AlCl_3 vapor. Otherwise the flow of argon, the high-temperature furnace, its temperature measurement, and the nature of holding the AlF_3 sample in a vapor-cell at one end and condensing its sublimate at the other end of the same composite Pt/10% Rh tube remained unchanged. After a weighed sample of AlCl_3 was loaded into a stainless steel-316 cell under dry box conditions preceding a succession of experiments, its vapor was generated by using either the saturated vapor of water or of tetrachloroethylene at barometric pressure. The stream of chloride vapor was passed through stainless steel-316 tubing, which was surrounded by an oven to keep the vapor 25 to 50 deg above its generated temperature. Special precautions were maintained to keep the flowpath clean and dry. Provisions were available to condense the chloride vapor in one of two glass traps which were held in a dry-ice/acetone bath. Trap 1 was positioned before the fluoride vapor cell to measure the entrainment of AlCl_3 independently of AlF_3 , and trap 2 was placed after, to measure the chloride entrainment in the mixed-halide system. Since the chloride vapor had some distance to flow from its

vapor cell to the fluoride vapor cell and another distance from the latter to trap 2, there being a total elapse of nearly 2% of the total flow time, some fluoride would be sublimed independently before a mixed-halide system could be attained. This problem along with another, which was to account for the chloride vapor remaining in the flowpath, was corrected by a subsequent flow of argon without the chloride. The amount of fluoride sublimed in a concurrent flow can be shown to be closely approximated by the difference of that observed in total and that calculated for this subsequent flow of argon.

The sample of AlF_3 , whose analysis was previously reported⁷, was contained in two, successive Pt/10% Rh boats, which were weighed before and after each experiment to measure the observed total of sublimed fluoride. As reported in the previous work, a diffusion study of the geometry of the fluoride vapor cell and its negligible weight loss for several experiments at zero gas flow indicated no correction for diffusion. The possibility of the chloride forming a solid solution with the fluoride can be shown to be negligible. Besides, a test for chloride in the fluoride sample after several concurrent entrainments was negative; and while exposed to room air, the fluoride sample maintained constant weight to 0.1 mg to show that it was not hygroscopic. The anhydrous, crystalline sample of AlCl_3 was chemically analyzed in duplicate to have 20.24% Al and 79.69% Cl while its theoretical proportions are 20.235% and 79.765%, respectively. Traces of Fe (<0.01%), heavy metals (<0.001%), SO_4 (<0.005%), and that not ppt by NH_4OH (<0.16%) were certified by the producer.

Generally, the deposits in trap 1 indicated that the chloride partial pressure in its vapor cell, corrected to a standard boiler temperature, was greater than that calculated from the deposit in trap 2. The chloride vapor generated in its boiler cell was observed to be less saturated with successive flows. A plot of the chloride pressure from trap 1 versus the boiler load was considered a measure of this unsaturation. The points of trap 2 whose chloride deposit was determined by chloride titration were found to be less than the above plotted values by 2.2 to 4.6% in the case of generating the chloride vapor at 373°K, whether or not the fluoride was present in its vapor cell, and by 0.2 to 1.7% in the case of generating the chloride vapor at 394°K. For any deposits in traps 1 a chloride titration corresponded to the weighed deposit within 0.1 to 0.3%; however, for those deposits in trap 2 generated at 394°K, the titrated deposit was from 1.5 to 1.8% less than the weighed deposit. In all cases including some blank runs, for which there was only Ar flow or no flow at all, the Pt/10% Rh composite tube itself, used to condense the sublimed fluoride, appeared to lose from 0.6 to 5.8 mg of its total 137g. A less likely possibility is that less fluoride was condensed than lost from the boats. Traces of both Pt and Fe were detected in a spectrochemical analysis of a trap 2 deposit while they were insignificant in one of a trap 1 deposit.

The mass \bar{y} of sublimed chloride concurrently entrained with the mass \bar{x} of sublimed fluoride was considered to be the mean of traps 1 and 2 with an average range of 2.4% as reported in Table 1. This mean was a compromise of whether the cause of the above discrepancy of traps 1 and 2

Table 1: Concurrent Entrainment of AlCl_3 and AlF_3 where \underline{v} is the flow of the gas mixture, $\underline{f^3}$ is the mass of AlF_3 sublimed in an inert medium, and \underline{x} is the mass of AlF_3 sublimed concurrently with the mass \underline{y} of AlCl_3 . Note that $\underline{f^3}$, \underline{x} , and \underline{y} were converted to units of partial pressure by assuming the vapor to be wholly monomeric.

Expt.*	T (°K)	\underline{v} (ml/min)	$\underline{f^3}$ (matm)	\underline{x} (matm)	\underline{y} (matm)	Range of \underline{y} (%)
1	1196.1	117.1	1.576	4.323	2.72	2.8
2	1214.9	112.5	2.463	5.653	2.86	4.6
3	1236.5	119.9	4.045	7.610	2.77	2.2
4	1252.2	118.1	5.736	9.764	2.88	2.5
5	1199.6	74.8	1.714	12.68	19.5	1.7
6	1215.8	76.6	2.516	15.05	19.4	1.5
7	1237.5	75.3	4.138	19.61	20.4	1.8
8	1256.6	75.7	6.315	23.21	19.3	1.8

* Chronological order: 2, 4, 3, 1, 7, 5, 8, and 6.

occurred before or after the fluoride vapor cell. If the Pt/10% Rh composite tube were implicated, the chloride vapor would have come in contact with equivalent portions of the tube before and after the fluoride cell.

PRELIMINARY ASSUMPTION

The enhanced volatility of AlF_3 by the concurrent entrainment of AlCl_3 may be interpreted for a first approximation by considering only the formation of mixed-halide monomers as shown in eq 1. A second approximation which will be discussed later will also consider the formation of all the possible dimers.

In general, the equilibrium constant \underline{K}_p for any reaction of eqs 1 and 3 at any \underline{T} over the temperature range of our experiments can be shown to be very closely approximated by

$$\underline{K}_p = \exp (\Delta \underline{S}_T^{\circ} / R - \Delta \underline{H}_T^{\circ} / RT) , \quad (4)$$

in which $\Delta \underline{H}^{\circ}$ and $\Delta \underline{S}^{\circ}$ are defined at $\underline{T}' = 1225^{\circ}\text{K}$ and for which $\Delta \underline{C}_p^{\circ}$ was assumed from the equi-partitional heat capacities of the species involved. Also, it will be convenient to deal not with \underline{K}_p but with \underline{k} of a reaction such that at any \underline{T}

$$\underline{K}_p = \underline{k} \Pi \sigma^{-1} \quad (5)$$

where σ is the symmetry number of a given molecule.

The equilibrium partial pressure \underline{P}_n of either mixed-halide monomer $\text{AlCl}_n\text{F}_{(3-n)}$ may be expressed according to eqs 1 and 5 as

$$\underline{P}_n = 3 \underline{k}_n \underline{c}_f^{n(3-n)} \quad (6)$$

where \underline{f}^3 is the vapor pressure of $\text{AlF}_3(\text{g})$ and \underline{c}^3 is the equilibrium partial pressure of $\text{AlCl}_3(\text{g})$. The value of \underline{f}^3 at any \underline{T} of this work was

assumed for the purpose of this preliminary assumption to be equal to that observed in an earlier entrainment measurement,⁷ which was not corrected for dimerization. If all the gaseous species containing fluorine were decomposed to AlF_3 in a system of constant volume and likewise, those containing chlorine, to AlCl_3 , then the mass \underline{x} of sublimed fluoride and the mass \underline{y} of sublimed chloride may be expressed as

$$x = f^3 + 2k_1cf^2 + k_2c^2f \quad (7)$$

and

$$y = c^3 + k_1cf^2 + 2k_2c^2f, \quad (8)$$

where \underline{x} and \underline{y} are converted to units of partial pressure. Here we have two equations and three unknowns, \underline{c} , \underline{k}_1 , and \underline{k}_2 for any one experiment; so a least square method was applied to all the experiments.

Values of $\Delta H^0(n)$ for the reactions of eq 1 were derived from eqs 7 and 8 by an iterative method using a digital computer programed in BASIC⁸. Since these reactions have no change in the degree of

⁸ J.G. Kemeny, T. E. Kurtz, BASIC, Dartmouth College (1965).

association, $\exp(\Delta S^0(n)/R)$ was assumed to be $\Pi\sigma^{-1} = 3$. Combining this with eqs 4 and 5 gives

$$\Delta H^0(n) = -RT \ln k_n. \quad (9)$$

Hypothetical values of \underline{k}_n were substituted into eqs 7 and 8 for all the experiments to give a hypothetical \underline{y} for each experiment; the difference in the observed and calculated \underline{y} led to $\sum(\Delta y/y)^2$ as shown in Table 2.

A selection of $\Delta H^0(n)$ can be made by considering whether any $\sum(\Delta y/y)^2$ is a reasonable approach to that indicated by traps 1 and 2. We believe

Table 2: Preliminary least square determination of $\Delta H^\circ(n)$ of eq 1 at 1225°K by assuming eqs 7 and 8 without correction for dimerization and $\Delta H^\circ(2) = \Delta H^\circ(1)$ of eq 1.

$\Delta H^\circ(n)$ (cal)	$\sum (\Delta y/y)^2 10^4$	$\Delta H^\circ(n) = -300 \text{ cal}$		
		Expt.	c^3 (matm)	$(y_{\text{obs}} - y_{\text{calc}})/y_{\text{calc}}$ (%)
-800	1350	1	0.328	3.0
-700	899	2	0.246	4.4
-600	540	3	0.151	2.8
-500	277	4	0.118	0.6
-400	112	5	6.72	0.3
-300	47	6	5.84	-0.9
-200	86	7	5.15	-2.7
-100	228	8	3.70	-1.6
0	477			
100	832			
200	1295			

that any set of hypothetical $\Delta H^{\circ}(n)$ must be disregarded if $\Sigma(\Delta y/y)^2 10^4$ exceeds 120, which corresponds to our estimate of the uncertainty in y to be an average deviation of about 4%. Uncertainties in f^3 , x , and T were believed to be negligible compared to that in y . To make a convenient presentation of the calculations listed in Table 2, we have given only those results where $\Delta H^{\circ}(2)$ was assumed to be $\Delta H^{\circ}(1)$, shown later to be reasonable.

DIMERIZATION CORRECTION

The preceding first-approximation is convenient but not realistic in view of the published information on the dimerization of each pure halide alone, which was discussed above. The following second-approximation shows the effect that an estimate of the formation of dimers has upon the evaluation of $\Delta H^{\circ}(n)$ of eq 1 from our entrainment data. In so doing it is convenient to consider that both x and y may be exemplified by

$$x = x_m + x_d \quad (10)$$

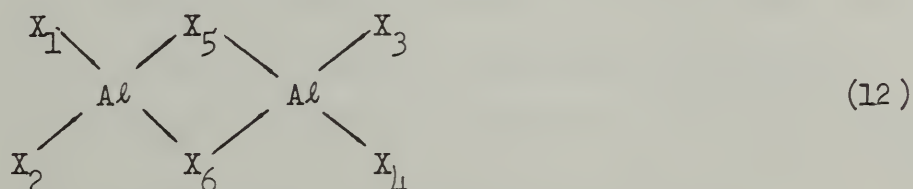
where m refers to monomer and d to dimer.

The value of f^3 which had been employed in eqs 7 and 8 for the preliminary assumption was corrected for dimerization, which was defined by the published values⁷ of ΔH° and ΔS° of eq 2. Equation 4 was combined with the fact that in general the vapor pressure P calculated by assuming the vapor to be wholly monomeric in an entrainment measurement can be shown to be very closely approximated by

$$P = P_m + 2P_d \quad (11)$$

The substitution of this resulting f^3 in eqs 7 and 8 now define x_m and y_m respectively.

Earlier we referred to 24 physically distinguishable dimers in the $AlCl_3-AlF_3$ system in which only 2 have been shown to be pure-halide dimers. The chemical composition of any dimer may be deduced from eq 3. The various mixed-halide dimers, some of which have a common composition, can be realized by assuming that any dimer has the same structure as the well-known chloride dimer:



The two bridge-bonded halides 5 and 6 are in a plane perpendicular to that containing the four end halides. The identity of each possible dimer \underline{d} , its symmetry number, and its bridge-bonded halides are shown in Table 3.

The equilibrium partial pressure of each dimer, shown in the last column of Table 3, was derived from the familiar expression for the \underline{K}_p of its formation described in eq 3. As shown in eq 5, \underline{K}_p is taken to be related to the symmetry of the species involved and for the reactions in eq 3 becomes

$$K_p = 36 k_d / \sigma_d \quad (13)$$

Properties common among several dimers were grouped together to make it practical to pursue an estimate of each \underline{k}_d . Although several alternative sets of assumptions were tried, assuming that \underline{k}_d was dependent on the halide content of the bridge-bonds was found to be the most plausible.

Table 3: Possible dimers in the $\text{AlCl}_3 - \text{AlF}_3$ system where K_0 and K_b are equilibrium constants for dimerization of AlF_3 and AlCl_3 , respectively, K_b is defined by eq 14, c^3 is partial pressure of $\text{AlCl}_3(\text{g})$, and f^3 is partial pressure of $\text{AlF}_3(\text{g})$

d	Formula	X-Position	σ	Bridge Halides	Partial Pressure at T
1	Al_2F_6		4	2F	$K_0 f^6$
2	Al_2ClF_5	1	1	2F	$4K_0 c f^5$
3	"	5	2	Cl, F	$2K_b c f^5$
4	$\text{Al}_2\text{Cl}_2\text{F}_4$	1,2	2	2F	$2K_0 c^2 f^4$
5	"	1,3	2	2F	$2K_0 c^2 f^4$
6	"	1,4	2	2F	$2K_0 c^2 f^4$
7	"	1,5	1	Cl, F	$4K_b c^2 f^4$
8	"	1,6	1	Cl, F	$4K_b c^2 f^4$
9	"	5,6	4	2Cl	$K_6 c^2 f^4$
10	$\text{Al}_2\text{Cl}_3\text{F}_3$	1,2,3	1	2F	$4K_0 c^3 f^3$
11	"	1,2,5	1	Cl, F	$4K_b c^3 f^3$
12	"	1,3,5	1	Cl, F	$4K_b c^3 f^3$
13	"	1,4,5	2	Cl, F	$2K_b c^3 f^3$
14	"	1,4,6	2	Cl, F	$2K_b c^3 f^3$
15	"	1,5,6	1	2Cl	$4K_6 c^3 f^3$
16	$\text{Al}_2\text{Cl}_4\text{F}_2$	1,2	2	2Cl	$2K_6 c^4 f^2$
17	"	1,3	2	2Cl	$2K_6 c^4 f^2$
18	"	1,4	2	2Cl	$2K_6 c^4 f^2$
19	"	1,5	1	Cl, F	$4K_b c^4 f^2$
20	"	1,6	1	Cl, F	$4K_b c^4 f^2$
21	"	5,6	4	2F	$K_0 c^4 f^2$
22	$\text{Al}_2\text{Cl}_5\text{F}$	1	1	2Cl	$4K_6 c^5 f$
23	"	5	2	Cl, F	$2K_b c^5 f$
24	Al_2Cl_6		4	2Cl	$K_6 c^6$

At least approximate values of ΔH° and ΔS° are available to define the dimerization of each pure-halide alone; so it is natural to seek a simple relation among the K_p of the other dimerization reactions in terms of these two. From eq 13 the K_p of the dimerization of the fluoride, where $n = 0$ in eq 3, may be defined as $K_0 = 9k_0$; likewise, the K_p of the dimerization of the chloride, where $n = 6$ in eq 3, as $K_6 = 9k_6$. We assumed that for any dimer with two bridge-bonded fluorines (F,F), $k_d = k_0$; and for any dimer with (Cl, Cl), $k_d = k_6$. In order to include those possible dimers with (Cl, F), we defined an arbitrary parameter b such that the K_p of eq 3 to form any such dimer could be estimated according to

$$K_p = 4K_0^{(1-b)} K_6^b / \sigma_d. \quad (14)$$

Later we shall see what effect reasonable choices of b have upon this dimerization correction.

The contribution of all the possible dimers to the observed mass \underline{x} of sublimed fluoride or to the observed mass \underline{y} of sublimed chloride for a given experiment at temperature \underline{T} may be obtained by adding the products of each term in the last column of Table 3 and a factor which denotes either the moles of AlF_3 or $AlCl_3$, respectively, required to form one mole of the stated dimer. Simplifying leads to the relationships

$$x_d = 2f(c+f)^3 [f(c+3f) K_0 + c(c+5f) K_b + 2c^2 K_6] / 3 \quad (15)$$

and

$$y_d = 2c(c+f)^3 [2f^2 K_0 + f(5c+f) K_b + c(3c+f) K_6] / 3. \quad (16)$$

Expressions for \underline{x} and \underline{y} can be obtained from eq 10 and the corrected versions of eqs 7 and 8. In addition the total mol fraction $\underline{\Sigma N_d}$ of all the dimers may be obtained by adding all the terms in the last column of

Table 3 to give

$$\Sigma P_d = (f^2 K_0 + 2cfK_b + c^2 K_6)(f+c)^4, \quad (17)$$

which is related to the observed sum of \underline{x} and \underline{y} by

$$x + y = \Sigma P_m + 2\Sigma P_d, \quad (18)$$

similar to eq 11.

DERIVED VALUES

The least square method used to solve eqs 7 and 8 in the preliminary assumption was also applied to the corrected version. Again hypothetical sets of $\underline{\Delta H}^0(n)$ were substituted for all the experiments to give a hypothetical \underline{y} for each experiment, from which were calculated $\Sigma(\underline{\Delta y}/\underline{y})^2$; however, besides the parameter \underline{c} , the role of another parameter \underline{b} , defined above in eq 14, had to be considered. Also, the uncertainty in \underline{K}_0 was found to have some effect while that in \underline{K}_6 was nil.

As shown in Table 4A, an arbitrary choice of $\underline{b} < 0.2$ appears incompatible with what we expect to be the uncertainty in \underline{y} , and our data afford no limiting value of $\underline{b} > 0.2$. These results were made by assuming $\underline{\Delta H}^0(2)$ to be $\underline{\Delta H}^0(1)$, and for a given value of \underline{b} only those hypothetical $\underline{\Delta H}^0(n)$ were selected that corresponded to a least value of $\Sigma(\underline{\Delta y}/\underline{y})^2$. Since a choice of \underline{b} near $\frac{1}{2}$ has little effect, the remaining calculations were made with this value.

The value of \underline{K}_0 used in eqs 15 and 16 was reported in our earlier work⁷ to be mainly dependent upon the parameters \underline{s} and \underline{h} . The former is any variation of the assumed value of $\underline{\Delta S}^0$ of sublimation to form $AlF_3(g)$ and the latter is any variation of the assumed value of $\underline{\Delta H}^0$ of sublimation

Table 4: Effect of various assumptions on a least square determination of $\Delta H^\circ(n)$ of eq 1 at 1225°K by assuming eqs 15 and 16 and the published values for the dimerization of AlCl_3 and AlF_3 .

A. Assuming values of \underline{b} , which is defined in eq 14, and $\Delta H^\circ(2) = \Delta H^\circ(1)$ of eq 1.

\underline{b}	$\Delta H^\circ(n)$ (cal)	Least Square
0	4500	418
0.2	1500	96
0.4	1050	64
0.5	1000	58
1.0	950	60

B. Assuming values of \underline{K}_0 , which is the equilibrium constant for the dimerization of AlF_3 , to be defined by \underline{s} and \underline{h} ; $\underline{b} = 1/2$; and $\Delta H^\circ(2) = \Delta H^\circ(1)$ of eq 1.

\underline{s} (eu)	\underline{h} (kcal)	$\Delta H^\circ(n)$ (cal)	Least Square
-0.4	-3	2200	157
	0	1600	124
	3	1150	95
0	-3	1300	69
	0	1000	58
	3	750	55
+0.4	-3	750	34
	0	500	32
	3	400	28

(Table 4 continued on next page)

Table 4 (cont.)

C. Assuming values of $\Delta H^\circ(1)$ and $\Delta H^\circ(2)$ of eq 1 and $b = 1/2$.

$\Delta H^\circ(1)$ (cal)	$\Delta H^\circ(2)$ (cal)	$\sum (\Delta y/y)^2 10^4$
800	-500	212
	0	84
	500	76
	800	124
	1000	176
900	-500	284
	0	105
	500	45
	900	74
	1000	91
	1500	225
1000	-500	389
	0	166
	500	59
	1000	58
	1500	145
1100	0	262
	500	114
	1000	72
	1100	74
	1500	117
	2000	234
1200	0	388
	500	206
	1000	127
	1200	121
	1500	136

to form $\text{Al}_2\text{F}_6(\text{g})$. Table 4B tabulates those $\Delta H^{\circ}(\text{n})$, which were selected as those in Table 4A, for given values of \underline{s} and \underline{h} whose assignments were the respective uncertainties. Although the least $\Sigma(\Delta y/y)^2$ for a given set of \underline{s} and \underline{h} becomes smaller as \underline{s} and \underline{h} are increased to their estimated limits, these lesser "least squares" should not be taken too seriously. The basis for any set of $\Sigma(\Delta y/y)^2$ are the observed \underline{y} ; and while we believe hypothetical $\Delta H^{\circ}(\text{n})$ must be discarded if $\Sigma(\Delta y/y)^2$ exceeds our estimated accuracy, the order of the lesser "least squares" can be changed by varying the observed \underline{y} within their uncertainty.

Finally the effect of assuming $\Delta H^{\circ}(2)$ to be $\Delta H^{\circ}(1)$ of eq 1 is shown in Table 4C. For any reasonable choice of $\Delta H^{\circ}(1)$ there corresponds a range of $\Delta H^{\circ}(2)$ near to and including that assigned to $\Delta H^{\circ}(1)$ such that there are reasonable $\Sigma(\Delta y/y)^2$; so we have found it convenient to report values of $\Delta H^{\circ}(1)$ and $\Delta H^{\circ}(2)$ and their uncertainties as $\Delta H^{\circ}(\text{n})$.

The results derived from the concurrent entrainment of AlCl_3 and AlF_3 to which we have applied the above interpretation is summarized in Table 5. Selections of hypothetical $\Delta H^{\circ}(\text{n})$ outside of those shown gave $\Sigma(\Delta y/y)^2$ which exceeded that estimated for the accuracy of this work.

ACKNOWLEDGMENTS

We thank E.K. Hubbard for her spectrochemical analyses and R.A. Paulson for his chemical analysis of Al in the AlCl_3 sample.

Table 5: Least square determination of $\Delta H^\circ(n)$ of eq 1 at 1225°K by assuming eqs 15 and 16, the published values for the dimerization of AlCl_3 and AlF_3 , $\underline{b} = 1/2$, and $\Delta H^\circ(2) = \Delta H^\circ(1)$ of eq 1.

$\Delta H^\circ(n)$ (cal)	$\sum (\Delta y/y)^2 10^4$	$\Delta H^\circ(n) = 1000 \text{ cal}$			
		Expt.	c^3 (matm)	$\sum N_d$ (%)	$(y_{\text{obs}} - y_{\text{calc}})/y_{\text{calc}}$ (%)
500	492	1	0.653	9.2	-4.7
600	332	2	0.499	9.0	0.4
700	210	3	0.312	8.8	3.6
800	125	4	0.242	8.8	4.4
900	74	5	8.08	13.9	0.2
1000	58	6	7.28	14.0	-0.6
1100	74	7	6.60	14.2	-0.9
1200	121	8	4.98	13.7	1.5
1300	197				
1400	301				
1500	431				

UNCLASSIFIED

Security Classification

DOCUMENT CONTROL DATA - R & D

(Security classification of title, body of abstract and indexing annotation must be entered when the overall report is classified)

1. ORIGINATING ACTIVITY (Corporate author) National Bureau of Standards Washington, D. C. 20234		2a. REPORT SECURITY CLASSIFICATION UNCLASSIFIED	
		2b. GROUP	
3. REPORT TITLE PRELIMINARY REPORT ON THE THERMODYNAMIC PROPERTIES OF SELECTED LIGHT-ELEMENT AND SOME RELATED COMPOUNDS			
4. DESCRIPTIVE NOTES (Type of report and inclusive dates) Scientific Interim			
5. AUTHOR(S) (First name, middle initial, last name) Thomas B. Douglas and Charles W. Beckett			
6. REPORT DATE 1 July 1967		7a. TOTAL NO. OF PAGES 128	7b. NO. OF REFS
8a. CONTRACT OR GRANT NO. ISSA-67-6		9a. ORIGINATOR'S REPORT NUMBER(S) NBS Report No. 9601	
b. PROJECT NO. 9750-01			
c. 61445014		9b. OTHER REPORT NO(S) (Any other numbers that may be assigned this report) AFOSR 67-2236	
d. 681308			
10. DISTRIBUTION STATEMENT This document is subject to special export controls and each transmittal to foreign governments or to foreign nationals may be made only with prior approval of the AFOSR (SRGL).			
11. SUPPLEMENTARY NOTES Tech, Other		12. SPONSORING MILITARY ACTIVITY AF Office of Scientific Research (SREP) 1400 Wilson Boulevard Arlington, Virginia 22209	
13. ABSTRACT This report presents a number of new thermodynamic properties resulting from recent NBS experimental studies and their interpretation, as well as descriptions of improved measuring techniques in two areas. Earlier NBS enthalpy measurements on the compound $\text{BeO} \cdot \text{Al}_2\text{O}_3$ (0° - 1200°K) are extended up to 2400°K , leading to the heat of fusion and the common thermodynamic properties well into the liquid range. The infrared matrix spectra of lithium fluoride and an alkali hydroxide (CsOH), with isotopic variations, have been obtained and interpreted, yielding the vibrational frequencies. Lithium fluoride is found as a previously unreported linear dimer (Li_2F_2), and the results for CsOH are consistent with and complement the earlier NBS microwave results for this molecule. Some preliminary mass-spectrometric data on beryllium dichloride are given. These data yield thermodynamic values for the reactions involving $\text{BeCl}_2(\text{c})$, $\text{BeCl}_2(\text{g})$, and $(\text{BeCl}_2)_2(\text{g})$. Thermodynamic values for the reactions involving $\text{AlF}_3(\text{c})$, $\text{AlF}_3(\text{g})$, and $(\text{AlF}_3)_2(\text{g})$, derived earlier using precise NBS entrainment data, are revised in the light of new published information. The volatility of AlF_3 is found to be markedly enhanced by the presence of AlCl_3 . After reasonable accounting for dimer formation, the data indicate the hitherto unobserved species AlF_2Cl and AlFCl_2 to be formed in the gas phase and each with a very small heat effect ($+1.0 \pm 0.5$ kcal per mol). Studies on the automation of temperature measurements complement previous studies on the automation of electrical-energy measurements--all designed to make low-temperature heat-capacity calorimetry fully automatic. The development of two refinements in oscilloscopic recording improve by at least tenfold the previous high-speed-measurement accuracy for determining specific heats and other properties at very high temperatures.			

DD FORM 1473
1 NOV 65

UNCLASSIFIED

Security Classification

UNCLASSIFIED

Security Classification

14. KEY WORDS	LINK A		LINK B		LINK C	
	ROLE	WT	ROLE	WT	ROLE	WT
.Thermodynamic properties						
$\text{BeO} \cdot \text{Al}_2\text{O}_3$						
Infrared matrix spectra						
Lithium fluoride						
Mass-spectrometric data						
Beryllium dichloride						
$\text{BeCl}_2(\text{c})$						
AlF_3						
AlCl_3						
CsOH						

UNCLASSIFIED

Security Classification

